The Thesis Committee for James Oscar Felan
Certifies that this is the approved version of the following thesis:

Shear Strength and Effects of HDPE Plastic Post-Tensioning Duct on a Prestressed Girder

APPROVED BY
SUPERVISING COMMITTEE:

Supervisor: _____

Oguzhan Bayrak

_____

Wassim Ghannoum

Shear Strength and Effects of HDPE Plastic Post-Tensioning Duct on a Prestressed Girder

by

James Oscar Felan, BSAE

Thesis

Presented to the Faculty of the Graduate School of

The University of Texas at Austin

in Partial Fulfillment

of the Requirements

for the Degree of

Master of Science in Engineering

The University of Texas at Austin

May 2013

Dedication

This thesis is dedicated to my mother.

Acknowledgements

To begin, I want it to be known that it was a privilege to continue my studies at the University of Texas at Austin Engineering School. I would first like to thank my wife, Beatrice for encouraging me to start the process in applying to graduate school to become a better engineer. Her sacrifice includes countless hours of taking care of our son, Matthew alone while I studied for the GRE and then while I studied throughout the program. In addition, I would like to thank my parents for instilling in me that education is a priority and should not be taken lightly. I can still remember my mother taking me to the library as a child and giving me assignments during the summer because I was bored. In addition, I can also remember my mother tutoring me throughout the years of my education but finally came to a stop when I took Statistics at UT. Now my mother just proof reads all my papers for grammatical errors. Thank you mom.

Prior to getting accepted in the UT Graduate Structural Engineering program, I had several meetings with Dr. Bayrak, Dr. Williamson and David Hohmann (former TxDOT Bridge Division Director) and those talks were encouraging and fact facing in the challenges that graduate school brings. However, I would like to thank those men for supporting me to get into the graduate program.

During the course work of the program, I met many students from all over the world and I humbled myself to learn from these individuals to become a better engineer. I would like to thank all those and a few names that come to mind are Kostas Belivanis, Dhiaa Al-Tarafany, and Candice Cong. In regards to the research, I am truly thankful for Andy Moore, Chris Williams, Josh Massey and David Wald. Those guys are sharp, organized and have a wealth of knowledge that they are willing to share. In addition, I

would like to thank Andrew Valentine, Blake Stasney, Dennis Fellip, Eric Schell, and Barbara Howard. I learned a lot from those in the Ferguson Structural Engineering Laboratory that I believe I will carry with me for the rest of my life.

I would like to thank all those who helped me in completing this thesis: Dr. Bayrak, Dr. Ghannoum, Andy Moore, Chris Williams, UT tutors and my mother.

Finally, I cannot say I completed this program and thesis on my own accord. There were many times I struggled and was discouraged, but it was through the power of God and his grace and love that I was given new strength, hope and placed into the lives of people who were able to help. Thank you God.

April 9, 2013

Abstract

Shear Strength and Effects of HDPE Plastic Post-Tensioning Duct on a Prestressed Girder

James Oscar Felan, M.S.E.

The University of Texas at Austin, 2013

Supervisor: Oguzhan Bayrak

The goal of the splice girder research project 0-6652 funded by the Texas Department of Transportation is to utilize the full potential of splicing prestressed TX girders continuously. The TX girder family of beams is cost effective alone due to their simple, repetitive fabrication, but to truly optimize their potential would be to span several beams together as one continuous unit. The weight and length restrictions allowed by trucks or barges limit the prestressed beam lengths. Therefore, splicing together prestressed beams becomes the solution to the transporting obstacle.

As a result, the prestressed girders will be more competitive to other bridge types such as steel I-girders, steel trapezoidal girders, cable-stayed bridges, and concrete segmental bridges. In fact, a prestressed/post-tensioned concrete bridge is preferred over steel designs in highly corrosive environments such as the coast or in snow regions where de-icing chemicals are used. In comparison, to a segmental box girder bridge, the post-

tensioned prestressed bridge has reduced complexity due to fewer segments and the number of reduced joints susceptible to corrosion.

The issue that arises with splicing prestressed beams is that in the process of connecting them together an opening must be made to install the post-tensioning (PT) steel strands. The openings are created by installing several steel or plastic circular ducts into the web region. Since the post-tensioning results in a reduction of the concrete web region, a modification is necessary to the shear capacity equation.

The experimental study performed at the Ferguson Structural Engineering Laboratory consisted of fabricating and testing two full-scale prestressed Tx46 girders. One girder contained a plastic post-tensioning duct with grout and steel strands installed in the web region. The other beam was a standard Tx46 beam fabricated without a duct. Both beams had a reinforced concrete deck installed with an overhang to model an actual bridge section. Furthermore, the purpose of the standard beam was to serve as a direct comparison to the beam with a duct and determine the actual reduction in shear capacity.

The research and findings will include the impact of the plastic duct in the Tx46 compared to the control beam. The failure loads of the test specimens will be compared to the current 2012 AASHTO code predictions for shear design. Also, revisions to the AASHTO code will be recommended if necessary.

The primary goal of this research was to improve the design and detailing of the skewed end-blocks commonly used in these beams. As U-beams had been in service for several decades without incident, it was anticipated that there would be little need for change in the design, and the findings of the research would involve a slight tweaking to improve the overall performance.

Table of Contents

List of Tables

List of Figures

CHAPTER 1

Introduction

1.1 OVERVIEW

The use of spliced girder bridges has gained momentum within various U.S. DOT's and there are several spliced-girder bridges currently in service. An example of a splice girder bridge under construction is shown in Figure 1-1. The bridge has a center span of 325-feet and is currently the longest spliced precast, prestressed concrete girder bridge in the United States. The Texas Department of Transportation (TxDOT) has gained interest in utilizing this technology because it allows longer spans while possibly using existing bridge girder forms. The potential for using existing girder designs and forms gives spliced girder bridges a cost advantage over other types of construction. Even if current standard girders need to be modified slightly, spliced girder bridges still have the potential to outcompete complex bridge types or steel bridges that are required for medium span lengths. In addition, since concrete is a durable material that protects the steel strands and reinforcement in corrosive environments, spliced girder bridges may have a maintenance cost benefit over steel bridges.

Figure 1-1 Route 22 Bridge over the Kentucky River, near Gratz, KY

Past research has demonstrated a reduction in shear strength due to the presence of post-tensioning ducts in I-girder webs. As a result, the effective web width resisting shear forces is reduced in design. Strength reductions can be large when the duct grout-material is less stiff than the surrounding concrete.

The Florida Department of Transportation, FDOT, has observed cracking along the tendon trajectory in spliced/post-tensioned prestressed bridges after being placed in service. The spliced bridges with cracking had HDPE (Plastic) ducts. Plastic (HDPE-High Density Polyethylene) ducts have a smoother surface than their steel counterparts, which reduces bond between the duct and surrounding concrete and enhances the splitting effect caused by transverse tensile stresses (Muttoni, 2006). Regardless, plastic ducts are often preferred over steel ducts in highly corrosive environments due to their resistance to corrosion.

Much of the experimental research on shear strength of girder webs with ducts was performed on small-scale compression panel tests. That research suggests that even grouted ducts reduce panel capacity from that of a solid panel without a duct (Muttoni, 2006). Furthermore, plastic ducts have been shown to generate a lower capacity compared to metal ducts. However, most of the past research was performed on panels containing plastic ducts with duct-to-web-width ratios that were low and not representative of the ratios seen in current typical spliced girder bridges. Such tests showed ducts generating low strength reductions. More testing is needed with realistic larger duct-to-web-width ratios.

Current code provisions, (AASHTO, Eurocode, and JSCE) are based on smaller scale concrete panel tests. The panel tests have been used extensively in research due to

their rapid assembly and low cost. However, full scale girder tests are needed extend panel results to girder shear capacity.

1.2 PROJECT OBJECTIVES

Before implementing splice girder bridges in Texas, TxDOT requires several issues to be resolved related to strength and serviceability.

The objective of this project is to evaluate the shear performance of post-tensioned I-girders when large ducts are present that would be used in spliced girder construction. Later projects will examine current standard girder splicing detail and provide recommendations for improvement of the splicing detail.

A series of panel tests were performed at The University of Texas at Austin within the scope of this thesis and are described in part in (Wald, 2012). Testing was also performed on two full-scale 30 ft Tx46 girders. One girder had no post-tensioning ducts while the other had a plastic duct. Tests were conducted up to shear failure and were aimed at investigating the effects of a duct containing post-tensioning strands and grout on shear strength and cracking. Girder tests results were also used to verify panel results and validate or disprove their applicability to full-scale girders. Girder tests results were compared with current code predictions of shear strength.

Although, the girders tested are not of same size as those that are planned for splice girder tests, they are large enough to do serve as transitional tests from panel tests to planned larger Tx62 full-scale tests.

1.3 ORGANIZATION

Chapter two discusses shear behavior and the research related to web shear-strength modifications required as a result of post-tensioning ducts in prestressed girder web regions. The research includes extensive experiments on small-scale panels with ducts and limited tests on existing full-scale prestressed girders with ducts.

Chapter three presents the experimental program. The chapter goes into detail of the test girder sectional properties and materials. A thorough description is presented of the fabrication of the Tx46 with plastic duct and the Tx46 control girder, followed by one of the test setup used of test the specimens.

Chapter 4 describes observations made during both tests of the Tx46 control girder and Tx46 with plastic duct girder. In addition, the results of the actual shear failures and the calculated shear resistances based on the AASTHO LRFD 2012 shear method are presented in this chapter.

Finally, chapter five discusses the results with conclusions from relevant concrete panel specimens with a plastic duct, the Tx46 control girder, and the Tx46 girder with a plastic duct. The discussion is followed by recommendations for future work.

CHAPTER 2

Literature Review

2.1 OVERVIEW

There has been much research completed on the effects of ducts in the web section of reinforced/prestressed concrete beams. A discussion on basic shear behavior in concrete and the theory behind the reduction in shear strength is included in this chapter. A synopsis of the past research that relates the effects of shear stresses with the presence of post-tensioning ducts in the concrete web region will follow and will then be expanded upon.

2.2 SHEAR BEHAVIOR

In bridge I-girders, high shear stresses can develop in the web regions. The cracks that occur in the web only are called “web shear cracks” (Brown, 2012). As shown in Equation 2-1, as B (web thickness) decreases, the shear stress increases. Figure 2-1 shows the relation between shear stress acting upon an I-beam cross-section and location along beam depth. Lower stresses occur in I-sections at the top and bottom flange due to the larger width compared to the web.

$$v = \frac{VQ}{IB}$$ ***Equation 2-1***

where:

ν = shear stress [ksi]

V = shear force [kips]

Q = moment area [in.^{3}]

I = moment of inertia [in.^{4}]

B = web thickness [in.]

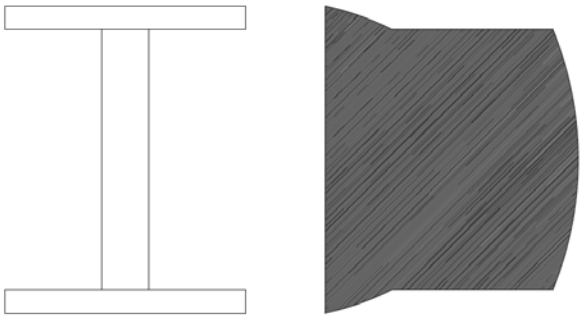

Figure 2-1 I-Beam cross section and diagram representation of the shear stress acting upon the depth

Figure 2-2 shows a typical tendon location within a bridge I-girder. When utilizing post-tensioning steel strands in a bridge I-shaped girder, there is a change in the material and therefore a lack of homogeneity at the location of the duct. To understand the behavior of shear in webs with post-tensioning ducts, research was performed on concrete panel specimens representing the web as illustrated through a section in Figure 2-2.

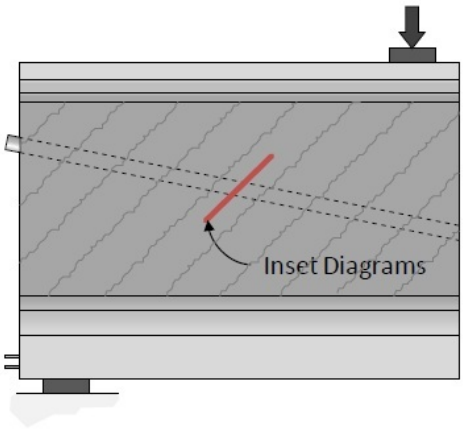

Figure 2-2 Tendon duct in the web region

The behavior of stress flow in the concrete does not follow the same pattern as a solid concrete section (Figure 2-3). As illustrated in Figure 2-3, with increased grout stiffness, there is an increased of portion of compressive stresses carried through the grout. on the other hand, when there is no grout, stress will flow around the void (Figure 2-3). In previous and recent concrete panel testing research, it was observed in the un-grouted specimen, tensile stresses occurred at the duct which caused splitting along the width (Wald, 2012).

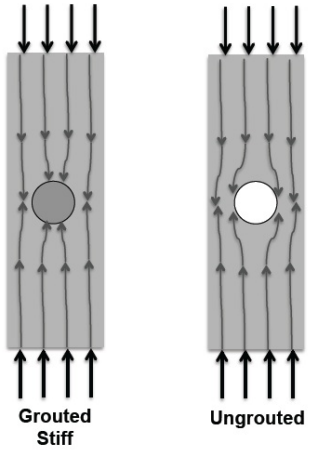

Figure 2-3 Compression field of concrete with and without grout

The tensile stresses locations can be seen below in Figure 2-4. Since compression stresses travel around the void, expansion occurs due to Poisson's effect and equilibrium, which results in tensile stresses transverse to the compression stress flow.

Stress flows caused by grouted or un-grouted ducts can reduce the shear strength of webs. Depending on grout stiffness and duct type a modification must be made to the shear strength of webs. Several code provisions address this modification and will be discussed in section 2.4.

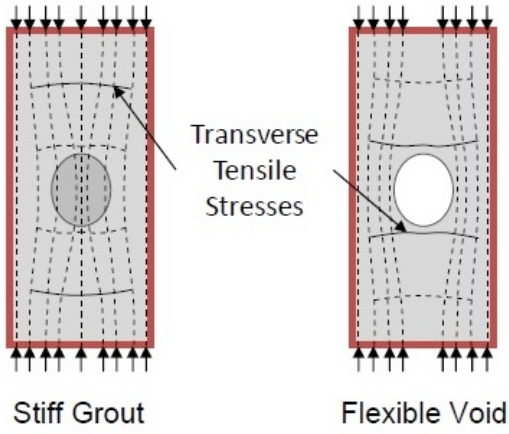

Figure 2-4 Tensile stresses occurring in panel tests (Muttoni et al., 2006)

Figure 2-5 shows the strut and tie model (STM) of the web region with the presence of ducting with and without grout. It can be observed from the STM models in Figure 2-5 (right) that tensile stresses develop that can cause splitting of the block. Such splitting cracks were seen in current research by (Wald, 2012). The same phenomenon is believed to be accentuated in plastic ducting due to the lack of bond developed between the plastic material and concrete (Muttoni, 2006).

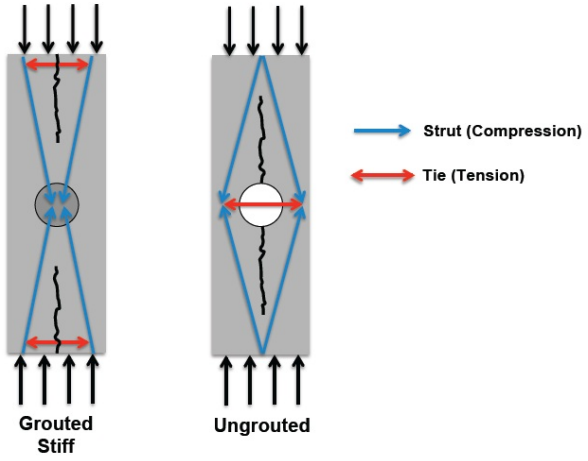

Figure 2-5 Strut and tie model (Wald, 2012)

2.3 SHEAR CAPACITY OF STRUCTURAL CONCRETE

Prior to discussing various codes it is important to elaborate on the shear behavior calculation method that the AASTHO LRFD, (AASHTO Design Specifications, 2012) utilizes because it will be referenced many times in the shear resistance calculation. AASHTO LRFD Bridge Design Specifications 2012 is based on the Modified Compression Field Theory, (MCFT, Vecchio, and Collins, 1986). The theory is based on a truss model consisting of struts and ties. The strut represents the compressive stresses at a calculated angle "Θ" of cracking that is resisted by concrete. The ties are the tensile stresses that develop the cracking and are resisted by steel stirrup reinforcement. The maximum strain to occur in the web and representing the tension chord of the truss model is the longitudinal strain ε_x (ACI 445R-99). The larger the longitudinal strain, the less shear stress is required to fail the web. The calculated strain value is limited 0.002, which is the yielding strain of the steel.

The MCFT also indicates that diagonally cracked concrete stress-strain behavior does not follow that of typical behavior of concrete cylinders (Collins, 1978). As a result,

the stress of cracked concrete follows a softened behavior due to the concrete resisting tensile stresses. Furthermore, the MCFT indicates that "tension stiffening" occurs in concrete. Tension stiffening is the result of cracked concrete still being able to resist tensile stresses.

Figure 2-6 shows a typical prestressed bulb-tee girder and illustrates the compressive strains, ε_2, acting in the direction of cracking representing the concrete struts. The strains labeled ε_1 acting in the transverse direction to the compressive strains are being resisted by the steel transverse reinforcement and by concrete tension stiffening effects.

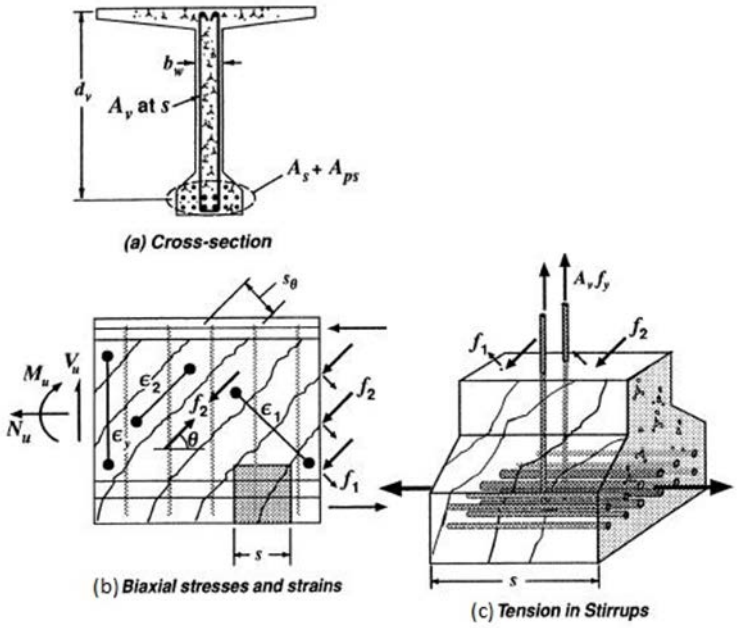

Figure 2-6 Typical prestressed I-Girder undergoing shear, moment and axial load (ACI 445R-99)

2.4 EFFECT OF DUCT TYPE ON SHEAR STRENGTH OF THIN WEBS

There has been significant research performed on small-scale panels that represent the web in a prestressed concrete beam. The ACI article on the "Effects of Duct Type on Shear Strength of Thin Webs" (Muttoni et al., 2006) published many findings on this topic. Below is a summary of their research that is relevant for this project.

To begin, the presence of a post-tensioning duct in the web of a prestressed beam results in a reduction in their load carrying capacity. Concrete compression struts are significantly affected by the interference of a post-tensioning tendon. There is a stress flow disruption since the material changes through the duct, which results in a change in stiffness. The reduction in stiffness is a result of the duct material, grout consolidation, and post tension strands.

Through testing by Muttoni et al., (Muttoni et al., 2006) it has been shown that with high density polyethylene (plastic) ducts, there is a significant reduction in panel compressive strength compared to steel ducts. In addition, the trajectory angle of the duct position has no effect to the shear strength.

To predict the shear failure capacity of concrete within a spliced region, small scale panel testing was performed. The results and variables associated with those test are shown in Table 2-2. To determine the web width reduction due to the presence of ducts is based on the reduction factor η_D shown in Equation 2-2.

$$\eta_D = \frac{Panel\ Failure\ Load}{Average\ Control\ Panel\ Failure\ Load} \qquad \textit{Equation 2-2}$$

However, to correlate the results of the test to specific criteria in a spliced beam a k factor had to be developed. The criteria includes duct material, grouted and un-grouted. Equation 2-2 cannot directly be used because it includes the term η_D which consists of several variables as mentioned above: duct material, grouted or un-grouted. Therefore, the development of the k factor starts with Equation 2-3 and Equation 2-4, which is based on prism/panel test research.

$$\boldsymbol{b_{eff} = b_w \cdot \eta_D} \qquad \textit{Equation 2-3}$$

Where:

b_{eff} = effective web width [in.]

b_w = gross cross-section web width [in.]

η_D = strength reduction factor accounting for duct presence

$$\boldsymbol{\eta_D = 1 - k \cdot \delta} \qquad \textit{Equation 2-4}$$

Where:

η_D – strength reduction factor

k – diameter correction factor

δ – ratio of the total duct section to the overall width of the web

When manipulating Equation 2-3 and Equation 2-4 relationship can be found between η_D and k, and is shown in Equation 2-5. As a result of the test performed, a correction factor can predict the reduction in the web thickness that should be used in determining the shear capacity based on the duct parameters. The summation term is to take into account if it is desired to design the ducting side by side.

$$b_{eff} = b_w - k \cdot \Sigma \Phi \qquad \textit{Equation 2-5}$$

Where:

b_{eff} = effective web width in the presence of duct material [in.]

b_w = gross cross-section web width [in.]

k = diameter correction factor based on material and if grouted

Φ = inside nominal diameter of duct [in.]

A summary of all the current code provisions required to reduce the web width when utilizing ducts that are grouted or un-grouted can be seen in Table 2-1.

Table 2-1 Diameter correction factor "k" in variuous code provisions

Code	**Year**	**K**		
		Empty	**Steel**	**Plastic**
AASHTO (General Shear)	2012	0.5	0.25	
AASHTO (Segmental)	2012	1.0	0.5	
ACI 318-11	2011	-	-	
Japan Society of C.E.	2002	0.5	0.5	
Eurocode 2	2002	1.2	0.5	1.2

To predict the shear failure capacity of concrete within a spliced region, small scale panel testing was performed by Muttoni et al (Muttoni, Burdet, and Hars, 2006). The results and variables associated with those test are shown in Table 2-2 and in Figure 2-7. Table 2-2 shows the dimensions of the duct diameter, grouted or not, angle of duct,

curing time and the results. All specimens are concrete panels measuring 23.6 x 23.6 x 4.9-inches.

Table 2-2 Panel specimen parameters and results (Muttoni et al., 2006)

	First series, laboratory panels												Second series, bridge panels			
Specimen	W1	W2	W3	W4	W5	W6	W7	W8	W9	W10	W11	W12	W21	W22	W23	W24
Duct	HDPE		None		Steel		Steel		HDPE		Steel 1967		Steel 1967		None	
	Injected		—		Injected		Empty		Injected		Injected		Injected		—	
$\varnothing_D$, in. (mm)	2.48 (63)	2.48 (63)	0 (0)	0 (0)	2.44 (62)	2.44 (62)	2.44 (62)	2.44 (62)	2.48 (63)	2.48 (63)	2.36 (60)	2.36 (60)	2.36 (60)	2.36 (60)	0 (0)	0 (0)
δ	0.50	0.50	0	0	0.50	0.50	0.50	0.50	0.50	0.50	0.48	0.48	0.45	0.45	0	0
Injected	Yes	Yes	—	—	Yes	Yes	No	No	Yes	Yes	Yes	Yes	Yes	Yes	—	—
f'_c, psi (MPa)	5278 (36.4)	5452 (37.6)	5250 (36.2)	5415 (37.3)	5076 (35)	5154 (35.5)	5352 (36.9)	5116 (35.3)	5434 (37.5)	5304 (36.6)	4984 (34.4)	5329 (36.7)	7818 (53.9)	6846 (47.2)	6962 (48)	6846 (47.2)
t, days	22	30	21	28	16	18	25	17	29	23	14	24 years	36 years	36 years	36 years	36 years
β, degrees	0	0	—	—	0	0	0	0	34	34	0	0	52	50	—	—
N_R, kips (kN)	386 (1718)	396 (1763)	607 (2700)	627 (2790)	501 (2228)	538 (2393)	248 (1103)	228 (1013)	389 (1733)	388 (1725)	413 (1838)	508 (2258)	464 (2066)	433 (1924)	719 (3200)	736 (3276)
N_{Rs}, kips (kN)	29 (129)	31 (139)	46 (203)	45 (202)	42 (187)	46 (205)	27 (120)	21 (91)	22 (100)	23 (100)	36 (161)	41 (181)	0 (0)	0 (0)	23 (102)	21 (94)
N_{Rc}, kips (kN)	357 (1589)	365 (1624)	561 (2497)	582 (2588)	459 (2040)	492 (2188)	221 (982)	207 (921)	367 (1633)	365 (1625)	377 (1677)	467 (2076)	464 (2066)	433 (1924)	696 (3098)	715 (3182)
$\frac{N_{Rc}}{b_w \cdot c}$, psi (MPa)	3072 (21.2)	3140 (21.6)	4829 (33.3)	5005 (34.5)	3946 (27.2)	4231 (29.2)	1900 (13.1)	1781 (12.3)	3158 (21.8)	3142 (21.7)	3242 (22.4)	4015 (27.7)	3720 (25.6)	3479 (24)	6117 (42.2)	6153 (42.4)
$\frac{N_{Rc}}{b_w \cdot c \cdot f'_c}$	0.58	0.58	0.92	0.92	0.78	0.82	0.35	0.35	0.58	0.59	0.65	0.75	0.48	0.51	0.88	0.90
η_D	0.63	0.62	1.00	1.00	0.84	0.89	0.38	0.38	0.63	0.64	0.71	0.82	0.54	0.57	0.99	1.01

Figure 2-7 shows a bar chart comparison of the results of η_D of various duct types with and without grout. The duct to width ratio, δ for all specimens was approximately 0.5. The figure shows the relationship of the reference specimen of a pure concrete specimen with no duct in W3, W4 compared to the other specimens with other variables. Specimens W5 and W6 are grouted steel ducts and having a slight reduction in strength compared to the control. The average strength reduction of steel duct specimen appear is shown to be 0.87. The plastic duct specimens are shown in panels W1, W2, W9 and W10 and have an average strength of 0.67 compared to the control. Finally, panels W7 and W8 are ungrouped steel duct specimens and were observed to have the lowest capacity of 0.38.

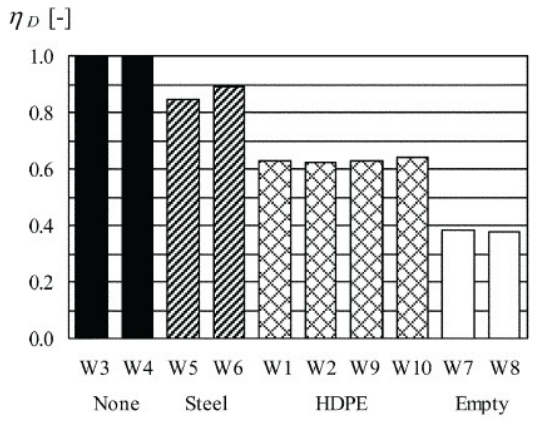

Figure 2-7 Effects of different duct types within a concrete specimen(Muttoni et al., 2006)

In addition, the article proposes code improvements for b_{eff}, the effective web width. To accurately model the failure in their panel testing research and they proposed a modification to the strength reduction in Equation 2-5. The k-factor as shown above in Table 2-1 is the variable that is recommended for revision and would change the current AASHTO code provisions. However, the proposed values from this article are correlated to "their" panel testing, which is not a true representative of actual full-scale beams and must match their specimen's parameters, web thickness, δ, f'_c, and f'_{gc}. Also, the web panel testing lacks the boundary condition effects from the restraints of the top and bottom flanges, which has the potential of decreasing the reduction in shear strength.

The article made a statement that can be compared to this research. It was stated that panels with HDPE ducts have a 37% loss in strength compared to the control panel without a duct as shown in Figure 2-7. Furthermore, based on their testing for their specimens, the author proposed the following strength reduction k-factor=0.8 for plastic ducts to fit their data.

2.5 SHEAR STRENGTH OF THIN-WEBBED POST TENSIONED BEAMS

Research performed by Fernandez Ruiz and Muttoni (2008) on full-size specimens taken from 1967 designed beams extracted from Switzerland. Five pre-stressed post-tension beams were tested with dimensions of 5 in. thick webs and 2.4-in. diameter tendons with a tendon to web ratio of 0.48. The beams had existing cracks and only had corrugated steel ducts. The goal of their research was to determine the actual strength of the post-tensioned webs and the interaction between the web cracking and the tendon. In addition, to accurately model the behavior, several shear stress field approaches and design codes were compared to actual results.

To model the field behavior and avoid flexure failure, the beams had an eccentric external axial force applied at both ends since the beams were spliced continuously. The beams were 16.5-feet in length, simply supported and had 2 point loads placed symmetrically about the mid-span. All beams failed by web crushing along the tendon profile. Figure 2-8 shows the cracking pattern and the concrete spalled in the web region to failed specimen SH3.

Figure 2-8 Failed specimen SH3 (Muttoni, et al., 2008)

Measured data indicated, the failed beam had vertical strains in the web larger than 5% indicating stirrup yielding. In addition, compressive strain developed in the top flange of the beams. By showing there is compressive strain in the top flange implies that there is a fraction of the total shear being resisted by it. This observation is important to differentiate between panel testing (web representation) and full-scale testing. It can

be deduced that the panel testing is not a true representation of the shear capacity since there are no top or bottom flanges or "boundary effects".

The following theories were analyzed to determine if they are suitable to model the actual behavior: Straight Stress Field, Deviated Stress Field, Discontinuous Stress Field, and Continuous Stress Field. Of those theories, the Continuous Stress Field was shown to be the best method to accurately predict the actual strength. In fact, the method predicted a value slightly higher than the actual, which is desirable. All methods were in agreement of one another in predicting a compression field angle of 19 to 20 degrees.

Their conclusions state the following: dimensioning of the web can be designed by "straight stress fields", Euro code 2 or AASHTO LRFD. The results are stated to be conservative. To check existing members, the same approach can be used. However, if the shear strength calculated is insufficient, then it is recommended to use "deviated stress field" analysis followed by "continuous stress field" as the final alternative for improved accuracy.

2.6 CODE PROVISIONS

2.6.1 AASHTO Bridge Design Specifications 6th Ed. 2012

AASHTO's design procedure is based on Modified Compression Field Theory. Guidelines from the code state shear capacity is calculated by Equation 2-6 with the maximum limit shown in Equation 2-7. The $0.25f'_c$ shear stress limit is the upper limit intended to ensure concrete in the web of the beam will not crush prior to yielding of the transverse reinforcement.

$$V_n = V_c + V_s + V_p \qquad \textit{Equation 2-6}$$

$$= 0.0316\,\beta\sqrt{f'_c}\,b_w\,d_v + \frac{A_v f_y}{s} d_v \cot\Theta + V_p$$

$$V_n = 0.25 f'_c\, b_v\, d_v + V_p \qquad \textit{Equation 2-7}$$

where:

V_n = shear load [kips]

V_c = concrete shear resistance [kips]

V_s = steel stirrup resistance [kips]

V_p = prestressed shear resistance [kips]

β = factor for concrete to transmit tension and shear [kips]

f'_c = concrete compressive strength [psi]

b_w = effective web width [in.]

d_v = effective shear depth [in.]

A_v = stirrup shear reinforcement area [in.^{2}]

s = stirrup spacing [in.]

f_y = yield stress of stirrup reinforcement [psi]

Θ = angle of compressive stresses [degrees]

The AASHTO 2012 shear strength code provision does include the prestressed shear resistance. If the prestressed strands were draped a vertical component force would be included in resisting the shear load. However in our testing the strands were kept horizontal with no vertical component to eliminate an additional variable in the research. AASHTO provisions do not differentiate between plastic and steel duct materials and there are two inconsistent requirements. The AASHTO provisions divide the use of ducting into General Shear and Segmental Shear as seen in the k-factors. A summary of

all the current code provisions required to reduce the web width when utilizing ducts that are grouted or un-grouted are shown in Table 2-1.

A spreadsheet prepared in Appendix I was prepared to perform an iterative calculation of the AASHTO LRFD 2012 shear method for the test specimen. Also, shown in Appendix I, are all the equations used for each cell and the corresponding AASHTO code equation.

2.6.2 AASHTO Bridge Construction Specifications 3rd Ed. 2010

In addition, the ducting within a prestressed beam must conform to the following AASHTO construction provisions:

AASHTO states "Plastic Ducts shall be considered and are highly recommended in saltwater environment or exposure to deicing chemicals. The plastic material shall be made of polyethylene or polypropylene and have a white coating on the outside shell with ultraviolet stabilizers" (AASHTO Bridge Constr. §10.8.3, 2010). This recommendation is specified to ensure the plastic material is durable in having a long life and not break down over time. When specifying a duct size, Table 2-3 shows the required plastic sizes in regards to nominal diameter and thickness.

Table 2-3 AASHTO LFRD Bridge Constr. §10.8.3. Duct thickness requirements for specific diameters

Duct Shape	**Duct Diameter [in.]**	**Duct Thickness [in.]**
Flat	any size	0.08
Round	0.9	0.08
Round	2.375	0.08
Round	3.0	0.10
Round	3.35	0.10
Round	4.0	0.12
Round	4.5	0.14
Round	5.125	0.16
Round	5.71	0.16

When determining the duct area to be used AASHTO Design provisions are followed and is as follows: the diameter shall be 0.25 in. larger than the nominal diameter of a single bar or tendon; for multiple bars or tendons the duct inside cross-sectional area shall be at least 2.0 times the net area of the steel, with the exception of utilizing the pull through method when inserted the strands into the duct and the duct area shall be at least 2.5 times greater than the area of the prestressing steel. In addition, the size of the duct shall not exceed 0.4 times the least gross concrete thickness at the duct. The last requirement was expanded upon in the panel program testing research performed by Wald (2012).

Several investigations are required and are as follows: the bonding characteristics of the polyethylene ducts to the concrete and the grout and the effects of grouting

pressure on the ducts and the surrounding concrete. In regards to the grouting pressure, it is shown in section 3.5.9.4 of this thesis how that method is performed.

When placing plastic ducts in the web and using longitudinal post-tensioning, the maximum support distance is not to exceed 2.0 ft. The ducting shall be supported by ties to the stirrups. At joints, the ducts are to be coupled with positive connections with no angle changes. To accommodate that requirement, a silicone adhesive sleeve is used with shrinking characteristics and is activated when heat is applied.

2.6.3 Japan Society of Civil Engineers-Standard Specifications for Concrete Structures-2002

Japanese code requirements in regards to ducts in the webs of prestressed concrete members state that the effective web width shall be reduced if the duct diameter is greater or equal to 1/8 the width of the web. If that requirement is met then the web shall be reduced by Equation 2-8 where all the terms are the same as Equation 2-3 except the ½ is the k-factor required by this code. The sigma term is listed to sum all the duct diameters within the same cross-section.

$$b_{eff} = b_w - \tfrac{1}{2} \Sigma \varphi \qquad \textit{Equation 2-8}$$

2.6.4 Eurocode 2: Design of Concrete Structures

The 2002 Eurocode 2 provisions in the design of concrete structures have several statements in regards to shear resistance with a web containing a duct. §6.2.3(6) states "the $V_{Rd,max}$ shall be calculated based on a nominal web thickness shown in Equation 2-9 when a web contains grout and the diameter, φ is greater than $b_w/8$". The code goes on to state the nominal web thickness should be calculated by Equation 2-10 for the

following scenarios of non-grouted ducts, grouted plastic ducts and unbounded tendons. The 1.2 factor is stated to account for the transverse tensile stresses that develop across the web and cause a splitting failure as opposed to a crushing failure as shown in the right of Figure 2-5. However, the provision goes on to state that if adequate transverse reinforcement is provided then the factor may be reduced to 1.0. A factor of 1.0 indicates the web is reduced directly by the dimension of the duct within the web.

$$b_{w,nom} = b_w - \tfrac{1}{2} \Sigma\varphi \qquad \textit{Equation 2-9}$$

$$b_{w,nom} = b_w - 1.2 \Sigma\varphi \qquad \textit{Equation 2-10}$$

2.7 NEED FOR RESEARCH

The purpose of this research project is to compare the shear behavior of a full-scale prestressed concrete girder (Tx46) with post-tensioning tendons utilizing plastic ducts to a Tx46 control prestressed beam and to verify current code provisions in light of those test results. As mentioned earlier, there has been significant research using scaled panel specimens representing the beam's web in shear. There has also been some research in full-size beam specimens to determine the actual shear capacity. However, the previous tests performed are not a true representation of what is desired to construct in today's practice. Specifically the duct diameter to web thickness was unrealistic. Furthermore, several state DOT's are interested in the results obtained using plastic ducts for the post-tensioning tendons to be used in highly corrosive environments such as in coast or snow conditions.

The panel test is a scaled down version of the web and does not include the top or bottom flanges, which have been shown to increase shear capacity. However, to verify panel testing trends, the results of panel testing to full-scale testing can be compared.

2.8 SUMMARY

In summary, an I-beam under loading develops higher shear stresses in the web region than the top or bottom flanges. To predict the shear strength of a prestressed concrete beam AASHTO LRFD general shear method follows a MCFT approach. The approach models the structure in terms of compression struts and steel ties. MCFT requires an iteration calculation of the compression angle of inclination and the longitudinal strain to predict the shear capacity. In the presence of a duct in the web region, compression stresses continue to flow through or around the duct depending if it's grouted and un-grouted. Higher tensile stresses develop if the duct is un-grouted. Furthermore, there is a reduction in compressive strength capacity due to the presence of a duct. To address the issue and incorporate it in the AASHTO LRFD general shear provisions, a k-factor was developed based on the following parameters, grouted, un-grouted and the Eurocode includes the duct material plastic or metal. The k-factor modifies the web width to an effective web thickness to fit the capacity strength of the past panel test research. More research was performed to better understand the behavior of ducts in other scenario's and determine trends and what works best in the field. However, the issue to be addressed in this research project is to determine the appropriateness of the k-factor from current code provisions in a full scale bulb-tee beam with a plastic duct.

CHAPTER 3

Experimental Program

3.1 OVERVIEW

Prior to testing full-scale girders, small-scale panel tests were performed. Findings derived from panel testing were used for the full-scale girder testing program. Panel design and testing frame fabrication are presented in the report titled "Development of a Testing Frame for Studying the Effects of Ducts on the Shear Capacity of Concrete Girders" by Schmidt (2011). Additional panel investigations are described in Wald (2012). An overview of the test frame and test specimens is presented in this chapter.

In order to better understand how the presence of a post-tensioning duct affects the shear strength of a prestressed girder it was necessary to test a girder at full scale. Therefore, two bulb-tee girders were constructed and tested at Ferguson Structural Engineering Laboratory (FSEL). The first of these two girders contained a post-tensioning duct and the failure of this specimen was compared against that of the second specimen which did not contain a duct.

Two 30-feet Tx46 prestressed bulb-tees girder specimens were fabricated in the Ferguson Laboratory and the process is described in this chapter. A 72-inch wide by 8-inch thick reinforced concrete deck was built composite with the girders. The girder with the post-tensioning duct had a 3-inch diameter HDPE (plastic) duct installed in the mid-height of the web. Both girders were fabricated at separate times starting with the Tx46 with the plastic duct in the winter of 2011 and the Tx46 control girder in the summer of 2012.

The girders were tested in a simply supported condition girder resting on two elastomeric bearing pads with a point load applied in the center until failure. The load and deflection responses were both measured throughout the test.

3.2 PANEL AND TESTING FRAME DISCUSSION

3.2.1 Panel Testing Program Discussion

The panel testing program consisted of one hundred fabricated concrete specimens with several varied parameters. The panels consisted of 5-inch, 7-inch and 9-inch thick rectangular sections with length and width of 24-inches by 24-inches. A typical set of fabricated panels can be seen in Figure 3-1. Panels had plastic and metal ducts with a nominal diameter measuring $2\frac{3}{8}$, 3, $3\frac{3}{8}$, and 4-inches. All panels had mild reinforcement representing the transverse steel. The arrangement of the through thickness reinforcement with respect to the ducts was also investigated. Furthermore, every set had at least two control panels with no variability to compare. Next the panels were compressed to failure by a testing machine designed and fabricated by students at the University of Texas at Austin Ferguson Laboratory. To ensure the accuracy of the testing machine, the first set of panels were replicates of the past research performed by Muttoni, et al. (2006). The panels that are referenced in this Tx46 research are the 7-inch thick web with the 3-inch plastic duct.

Figure 3-1 Concrete panels replicated the web of an I-Girder with a duct (Schmidt, 2011)

3.2.2 Testing Frame Discussion

The design and fabrication of a testing frame was required because no other compressive machine in the laboratory had the load capacity that was needed to crush the panels. It was estimated that a direct compression test of 2,000-kips was required to fail a 24" x 24" x 9" concrete panel, with f'_c of 10 ksi. Therefore a frame was fabricated to have two hydraulic rams that have the capability of applying 4,000-kips of load. A CAD drawing is shown below in Figure 3-2. Each component labeled of the testing frame is shown in Figure 3-3.

The testing frame is a self-reacting frame such that all forces are equilibrated within the frame. The frame consisted of four steel rods on each side (shown in yellow in Figure 3-2) which was required to resist the tension forces from the W14 x426 reaction girders (shown in blue). The reaction girders resisted the force produced by the two hydraulic rams and the force applied on the concrete panel specimen. An additional W14x426 reaction girder (shown in red) was utilized to uniformly distribute the applied

load produced by the two rams on to the concrete panel specimen. The material and dimensional design was thoroughly discussed in the report by Schmidt (2011) and Wald (2012).

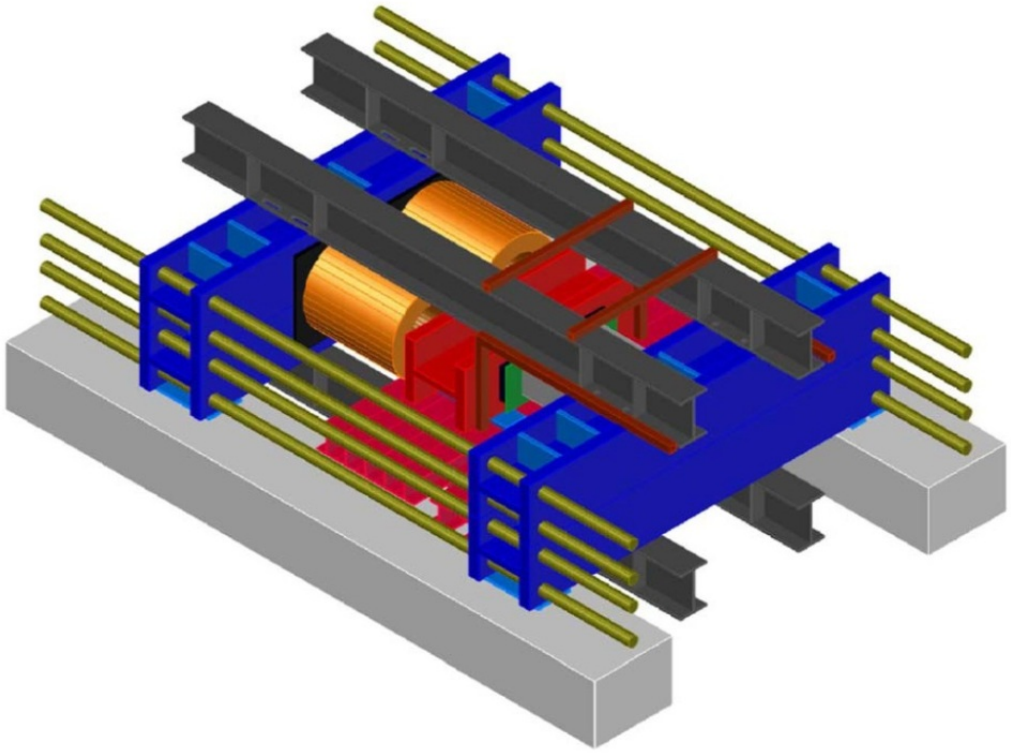

Figure 3-2 3D Compressive Concrete Panel Loading Frame (Schmidt, 2011)

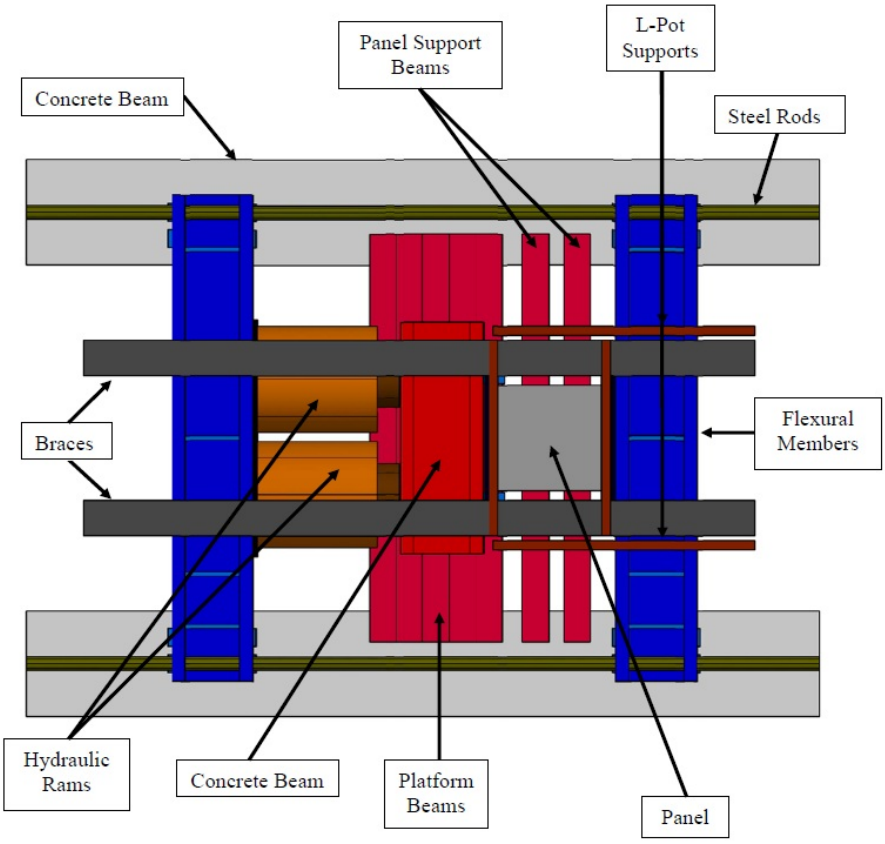

Figure 3-3 Top view of the loading frame with componet labels (Schmidt, 2011)

The results obtained from the concrete panel testing are presented and thoroughly discussed in the research performed by Wald (2012). The results that are relevant to this research in regards to a plastic duct with a 7-inch thick web are presented in Chapter 4 and are discussed with conclusions in Chapter 5.

3.3 TX46 TEST SPECIMEN DESIGNS

Both Tx46 girder specimens were fabricated identically with little to no deviation to the cross-sectional area, steel, presstresing strands, and concrete mix design and properties.

3.3.1 Tx46 Girder Sections

The two girders used in this testing program were based on the standard 46-inch deep version of the TxGirder series (Tx46). These girders were developed by the Texas Department of Transportation (TxDOT) circa 2005, but have been recently updated to include larger sections, which will be used for spliced post-tensioned girders. Although the Tx46's are too small to be used in most post-tensioned spliced girder applications, their shear behavior is similar to other large versions of the same girder series. The geometry of the standard Tx46 section is shown in Figure 3-4. The drawings for the full series of TxGirders currently in use as well as the section properties of the Tx46 can be found in Appendix A.

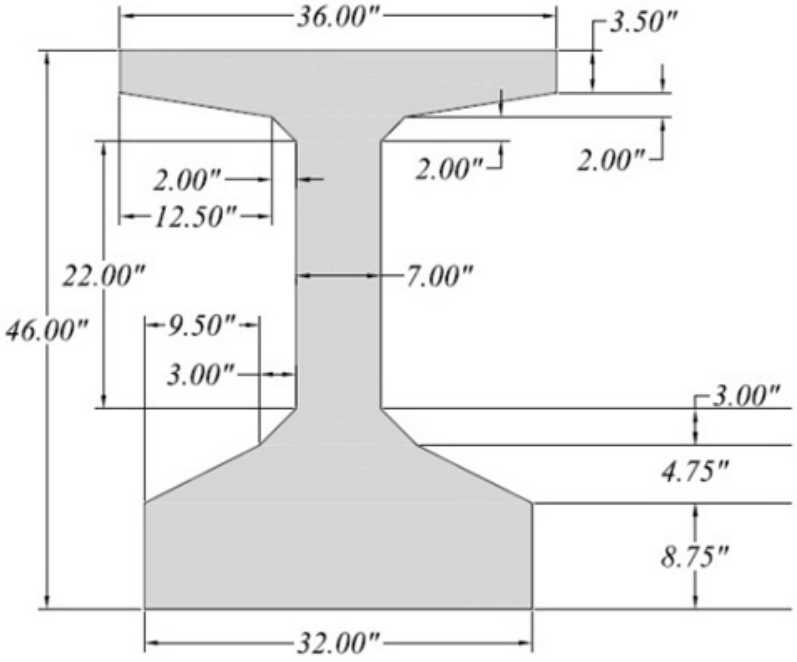

Figure 3-4 Tx46 Cross section dimensions

The girders contain several mild reinforcement arrangements depending on location. The purpose of each reinforcing bar will be discussed in the next few paragraphs. In Figure 3-5, Figure 3-7, and Figure 3-8 the location of each bar within the Tx46 cross-section and elevation is shown. The corresponding dimensions for each mild steel reinforcement bar and nomenclature is shown in Figure 3-6 .

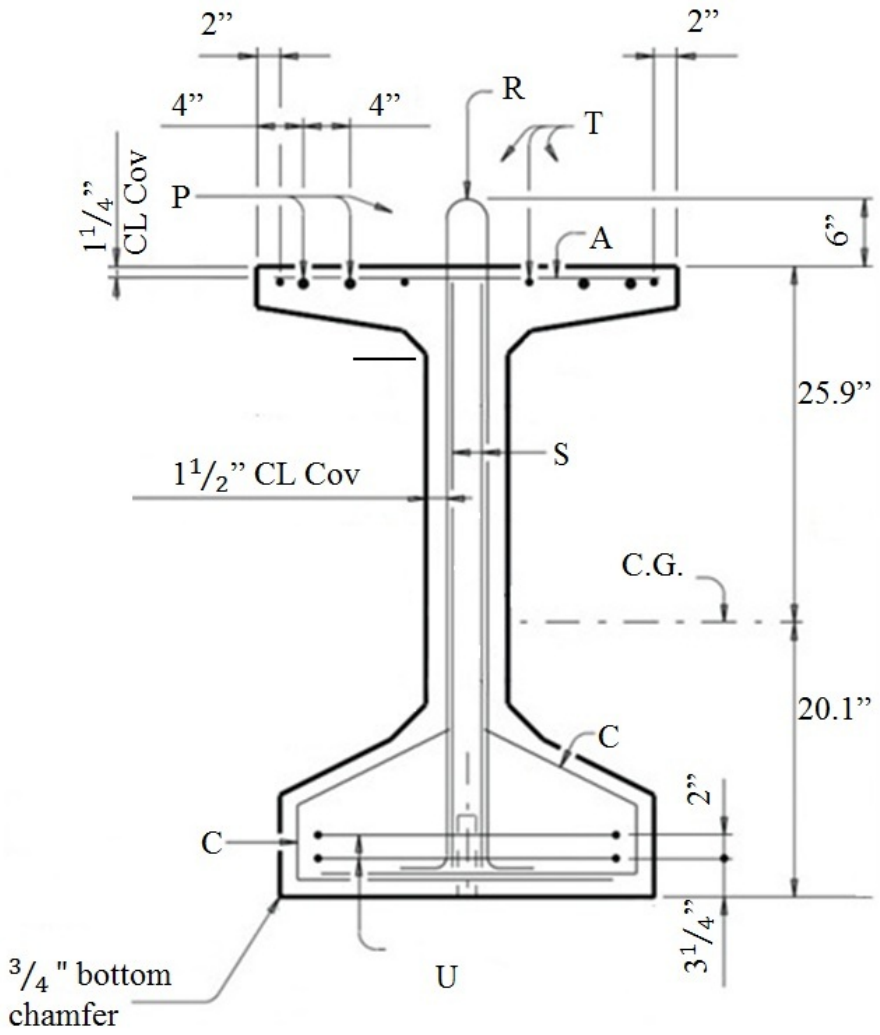

Figure 3-5 Tx46 reinforcement layout

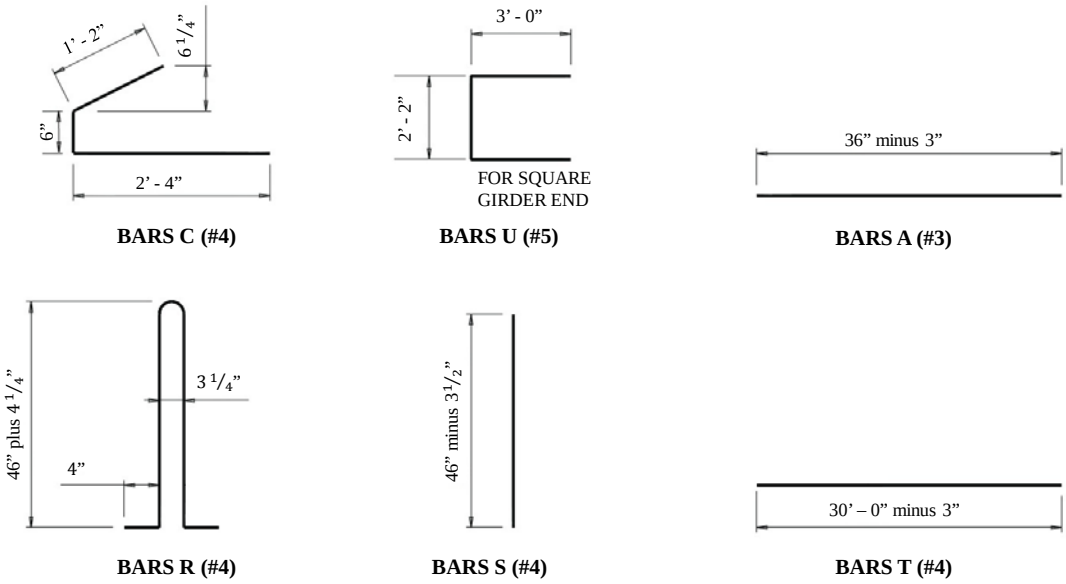

Figure 3-6 Girder Reinforcement nomenclature and Dimensions

Both girders utilized standard mild steel rebar for transverse reinforcement, (R bar). As shown in Figure 3-8, the end region of the first 3-feet, the R bars are spaced 3-inches apart and then transition to 6-inches for the remainder of the girder. The R bars also extend 6-inches above the girder's top flange to engage with the concrete deck and create a composite system as shown in Figure 3-5.

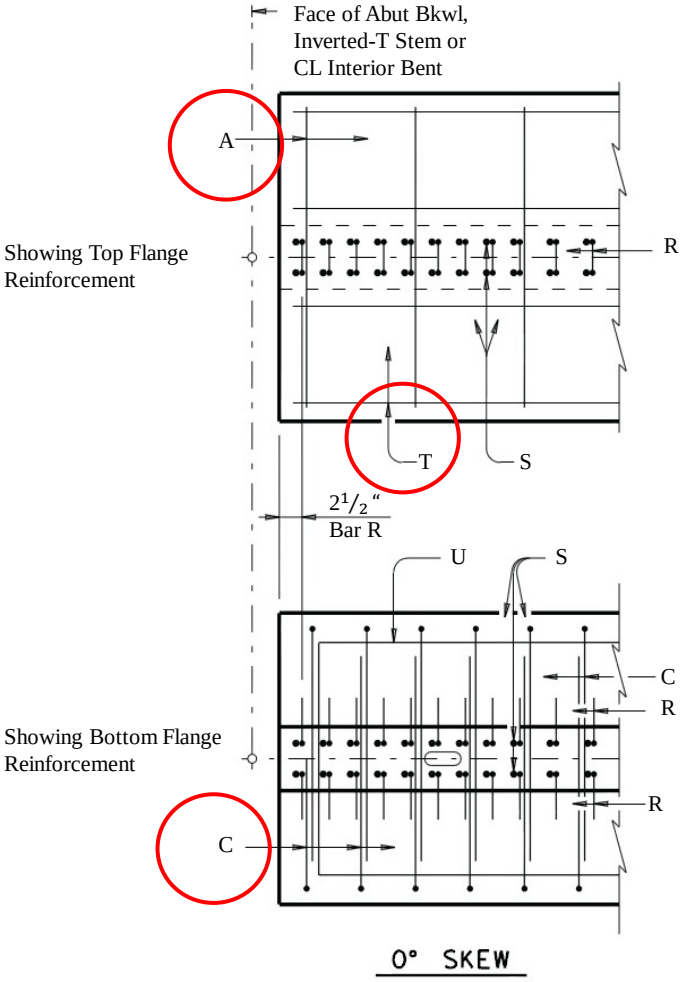

Figure 3-7 Plan view of the reinforcement to girder ends, top and bottom flange

The A and T bars are added for additional tensile reinforcement for the concrete. The bars are required for temperature, shrinkage and loading of the girder and are not for additional capacity. Since concrete cracks during curing, the tensile reinforcement reduces crack widths. During loading conditions the top flange A Bars prevent the concrete from spalling.

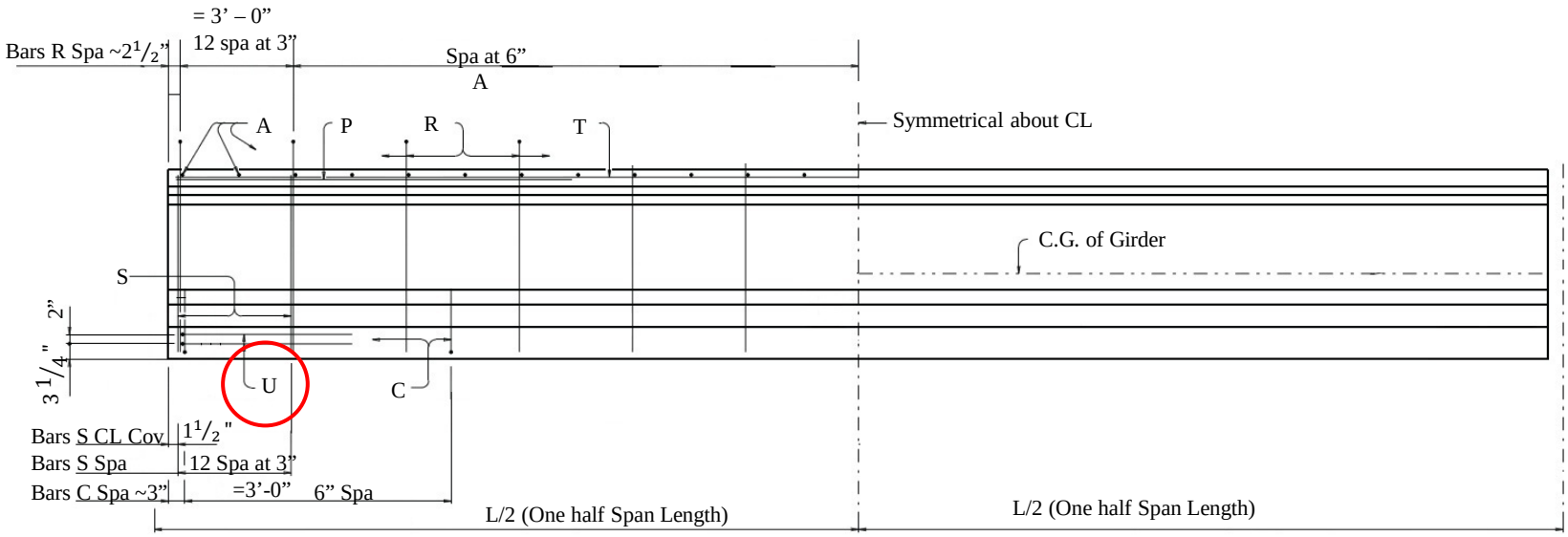

Figure 3-8 Girder elevation of reinforcement layout

As shown in the bottom of Figure 3-7 and in Figure 3-8, the first three feet of the end region of the Tx46 is heavily reinforced. To better show the image of Figure 3-8, the actual reinforcement built-up end is shown in Figure 3-9. The end region is composed of stirrups (R bars), confinement steel (C-bars) and a reinforcement (S-bars) for bursting stresses due to release of the prestressing strands (O'Callaghan, 2007). In addition, shown in Figure 3-9 at the bottom flange, there are two square No. 5 U Bars at both ends. The U Bars, C Bars and S Bars are required to prevent bursting in concrete from the release of prestressing steel strands (O'Callaghan, 2007). .

Figure 3-9 Image of the Tx46 reinforcement end region

3.3.2 Tx46 with a plastic duct

The plastic duct placement can be seen in Figure 3-10 and is shown as the opaque circular image at the mid-height of the web or at a center height of 27.5-inches from the bottom. Both Tx46 specimens followed the concrete cover requirements from AASHTO's provisions in Article 5.12.3. However, the Tx46 with a 3-inch nominal

diameter plastic duct has a cover requirement that is stated to be one-half the diameter of the duct. Therefore as illustrated in Figure 3-10 that requirement of 1.5-inches of cover is met. There are no code provisions in regards to the vertical placement of the duct and therefore the location was chosen based on having a simple constant height dimension for the length of the girder. However, there is a requirement in duct placement when there are ducts adjacent and when positive or negative flexure resistance is required. However, it has been proven in the research by Muttoni et al. (2006) that duct trajectory does not affect strength.

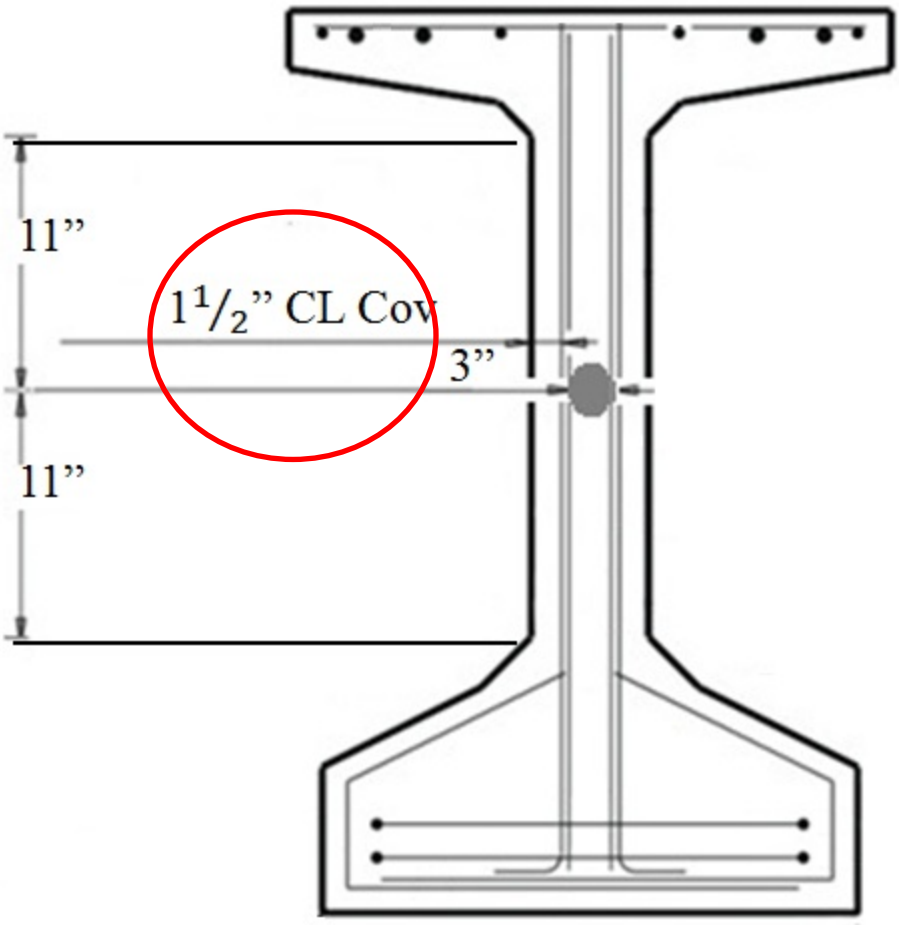

Figure 3-10 Tx46 with plastic duct cross section dimensions

3.3.3 Prestressing Strand Properties and Partial De-bonding

Both Tx46 specimens utilized 0.5-inch diameter low-relaxation prestressing strands with an ultimate strength of 270 ksi. The strand pattern followed TxDOT standards, in regards to cover and spacing, which meets AASHTO 5.10.3.3 guidelines. The AASHTO provision 5.10.3.3.1 states the center-to-center spacing for a 0.5-inch pretensioning strand is a minimum of 1.75-inches. The AASSHTO commentary states minimum spacing is to ensure adequate surrounding concrete for the strand to transfer their prestressing force and reduce the stress concentration to the concrete acting around the strand. As shown in Figure 3-11 the strands are spaced 2-inches apart.

The strand pattern and quantity was chosen to ensure that the girder would have adequate moment capacity that would allow for shear failure. As shown below in Figure 3-11, 48-½" steel prestressing strands were used. Appendix F shows that this flexure design produces a moment capacity of 7632 k-ft. Appendix F also shows the highest moment for the girder to resist in the Tx46 control girder which is composed of the self-weight, load frame and approximate point load required for shear failure.

The tensile capacity and the elastic modulus of the steel strands were not tested. The failure test was dependent on shear capacity and therefore the strands' assumed property strengths were used. All steel strands run horizontal and therefore it is unnecessary to obtain exact values for the strands tensile strength f_{pu} and E_p. The vertical component V_p in Equation 2-6 was not calculated because the strands were not harped.

To prevent excessive high compressive stresses at the bottom end region of the girder due to the prestress force and to also lower the tensile stresses at the top flange, the strands were partially de-bonded. A total of 16 strands were de-bonded for a length of 6-feet from the end face into the girder. A spreadsheet was created in determining the

amount of strands to de-bond and another one was created in determining the length. A description of these calculations can be found in Section 3.8 and the de-bonded strand elongations length calculation can be seen in Appendix D. The de-bonded strand placement can be seen in Figure 3-11.

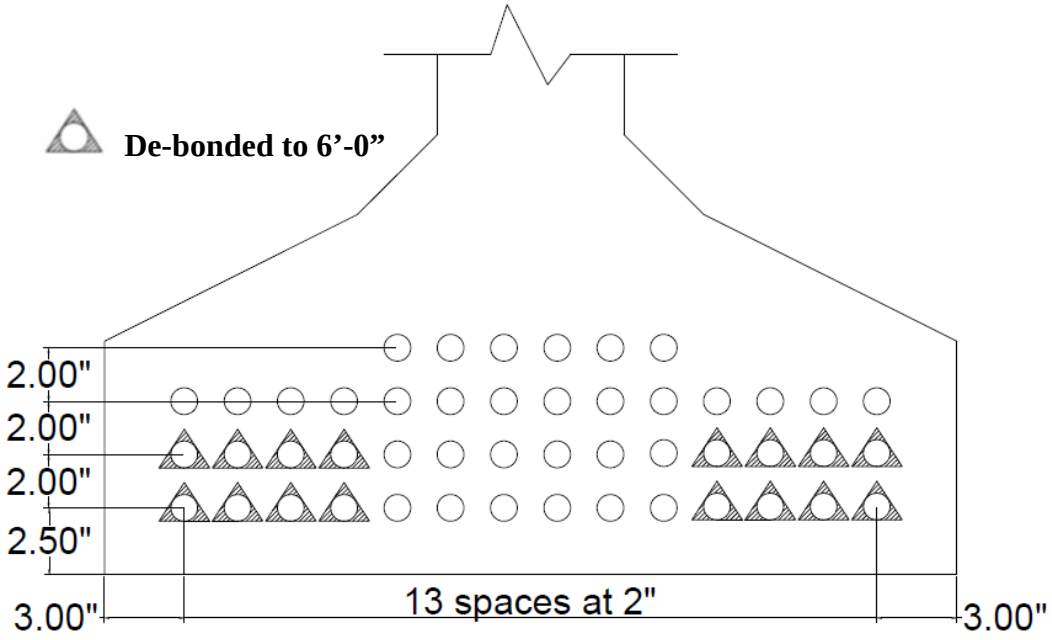

Figure 3-11 Prestressing strand pattern and debonding pattern with dimensions (48 total)

TxDOT allows a maximum of 75% of the strands to be de-bonded and 33% of the strands were de-bonded.

To partially de-bond the strands a plastic sleeve was wrapped around the steel followed by duct tape along the plastic length and just an inch passed the end. Figure 3-12 shows an image of a partially de-bonded strand.

Figure 3-12 Partially de-bonded steel strands

3.4 MATERIAL PROPERTIES

This section describes the physical properties of the transverse reinforcement, the concrete mix design, and the concrete and grout compressive strength. To accurately model the calculated shear resistance, it is essential to obtain the actual properties of the steel reinforcement yield strength and concrete compressive strength. Each sub section goes into detail of the testing method used, followed by the results.

3.4.1 Transverse Reinforcement Properties

Standard ASTM A370 tests were performed to determine the average yield stress and ultimate tensile stress of reinforcement. Figure 3-13 shows the stress strain graph from one of the transverse reinforcement bars. It can be seen in Figure 3-13, the bar followed an elastic-plastic behavior followed by hardening. Furthermore, it can be seen from the same figure that the yielding behavior is typical such that the bar exhibits a plateau of constant stress value with an increasing strain.

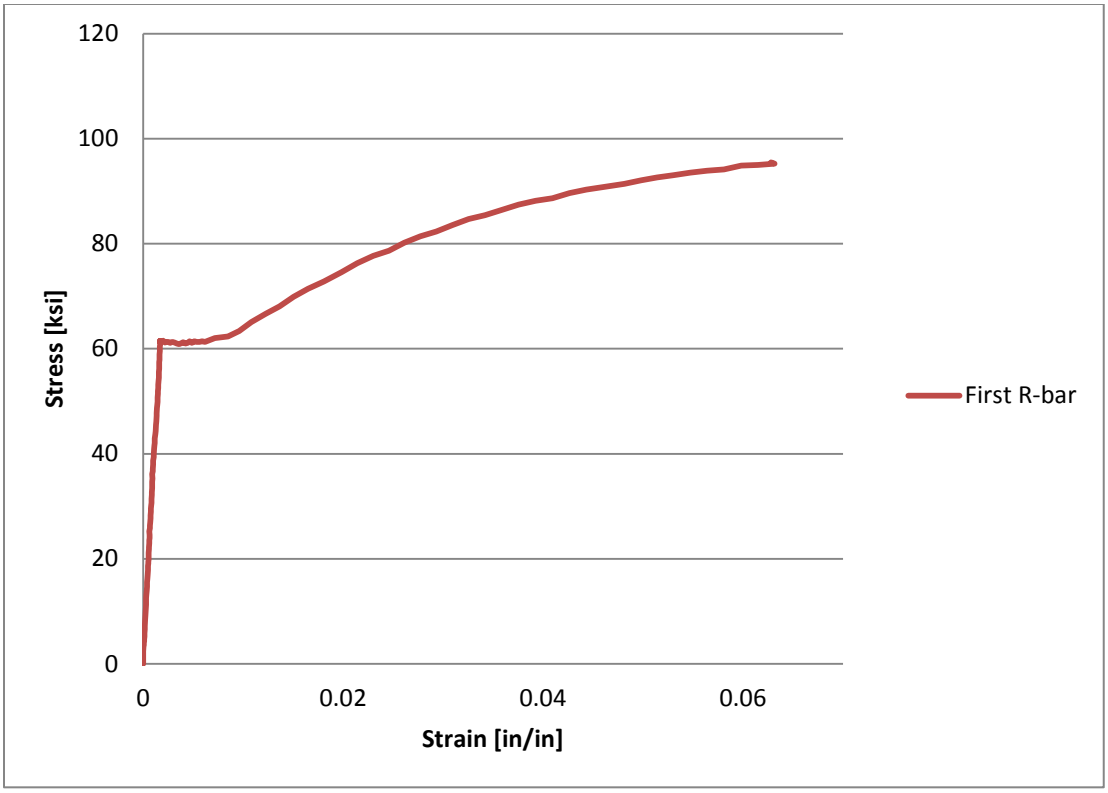

Figure 3-13 ASTM 370 Stress vs. Strain graph for the stirrups in the Tx46 w/plastic duct

Table 3-1 below shows the transverse reinforcement's average results of yield and ultimate stresses. As expected the yield strength was about 60 ksi, which indicates acceptable results. The stress strain graphs for the transverse reinforcement, "R-bars" used in the Tx46 control girder can be seen in the Appendix I.

Table 3-1 Transverse reinforcing bar properties

Girder	Type	Bar Size	f_y (ksi)	f_u (ksi)
Tx46 w/Plastic Duct	R – rebar	#4	61.6	98.1
Tx46 Control	R – rebar	#4	60.2	97.2

3.4.2 Concrete Properties

The concrete design mixtures of the two tested specimens can be seen below in Table 3-2. As required by Texas Department of Transportation, 25% fly ash (by weight of total cementitious material) was introduced in both precast concrete mixtures. In lieu of adding water, several ounces of super-plasticizer were used, to achieve the desired slump for workability.

Table 3-2 Concrete mixture design

Material	**Properties**	**Quantity**		
		Tx46 w/ Plastic Duct	**Tx46 Control**	**Units**
Cementitious Material	Alamo Gray Type III	600	600	*lb/yd³ concrete*
	Type F fly Ash	200	200	*lb/yd³ concrete*
Coarse Aggregate	½ in. Crushed Limestone	1385	1385	*lb/yd³ concrete*
Fine Aggregate	River Sand	1500	1500	*lb/yd³ concrete*
Water	-	180	180	*lb/yd³ concrete*
Water/Cement Ratio	-	0.23	0.23	*unit less*
Water-Reducer	Superplasticizer	**5**	**4**	*oz/hundred weight cement*
Desired Slump	-	8	8	*Inches*

The purpose of the ratios in the mix design was to achieve a high compressive strength concrete. A high strength concrete is desired for spliced girder design for several reasons. This type of bridge will have longer spans, which will require greater amounts of prestressing applied to resist positive moment. As a result, higher tensile and compressive stresses will occur due to the prestressing force. A higher concrete compressive strength would allow for higher limits of tensile and compressive stresses. In addition, there will be an increased modulus of elasticity due to the higher compressive

strength, which will reduce short-term and long-term deflections, (PCI Bridge Design Manual, 2004).

3.4.3 Concrete and Grout Compressive Strength

The concrete compressive strength was determined in accordance with ASTM C39. The compressive test was performed on the release day of the steel strands and also on the day of the girders' testing. The tests were performed on a concrete cylinder with a diameter measuring 4-inches and a height of 8-inches. The ends of the cylinders were capped with neoprene pads to fill any voids in the concrete. A typical ASTM C39 test is shown in Figure 3-14.

Figure 3-14 Concrete compressive test machine (O'Callaghan 2007)

Figure 3-14 shows a Forney concrete cylinder testing machine applying a force to the cylinder until a crushing failure occurred in the concrete. The compressive strength of the concrete f'_c was then determined by Equation 3-1. To determine the compressive

strength used in equation the average of three cylinder tests was obtained. Table 3-3 lists the average compressive strengths of concrete and grout during prestress transfer and the day of shear testing.

$$f'_c = \frac{P}{\pi D^2/4} \qquad \textit{Equation 3-1}$$

Where:

f'_c – Concrete Compressive Stress [psi]

P – Load [lbs.]

D – Diameter of cylinder [in.]

Table 3-3 Concrete & grout compressive strengths

Girder Compressive Strength	**Tx46 w/Plastic Duct** f'_c	**Tx46 Control** f'_c	**Units**
Release strength	6960	7460	*psi*
Day of Test	9700	8690	*psi*
Grout	8620	*N/A*	*psi*
Deck Compressive Strength	f'_c	f'_c	
Day of Test	9900	9950	*psi*

In regards to the grout, a high compressive strength, pumpable grout was obtained by following the Masterflow 1205 manufacture's specifications. To achieve a 28 day compressive strength greater than 8,000 psi, 1.95 gallons of water was mixed per 55 lbs. of grout. As a result the water to grout ratio is 0.30. To determine the compressive stress of the grout cement, ASTM C 942 test was performed. The test consisted of filling three 2-inch by 2-inch square cubes with grout in two layers of equal depth, shown in Figure 3-15. Figure 3-16 shows each layer of the grout impacted 16 times with a tamping rod.

Figure 3-15 Mold for cube grout specimens

Figure 3-16 Rodding the grout

3.5 TX46 GIRDER FABRICATION

Both Tx46 girders were fabricated within the 3.2 million pound prestressing bed at the Ferguson Structural Engineering Laboratory, shown below in Figure 3-17. The design and construction of the prestressing bed was part of thesis research work done by O'Callaghan (2007). The following section and sub-section detail the construction process of the test specimens.

Figure 3-17 FSEL High Capacity Prestressing Bed (O'Callaghan 2007)

3.5.1 Steel Prestressing Strand and Strand De-slacking

The fabrication process started by installing the prestressing strands in the bottom flange and utilizing two construction prestressing strands in the top flange to build and support the steel reinforcement cage. Then all the strands were de-slacked individually to 1.5 kip prior to the mild steel reinforcement installation. The purpose of de-slacking the bottom strands was to avoid any entanglement in the reinforcement or in the strands. Adding stress to the top construction top strands was essential because they support the

weight of the reinforcement and it was desired to prevent any sagging produced by the weight of the steel. This ensures the locations of the reinforcement are as specified. The de-slacking of the strands was done one by one with a Single Strand Jack and hydraulic pump. To produce a 1.5 kip force, the strands were stressed up to a specific pressure that was determined by dividing the force desired by the area of a single strand.

3.5.2 Reinforcement Cage Assembly

The design and location of the reinforcement follows that of the Tx46 standard design as shown in Appendix A. No deviation in the design was made during the fabrication in either girder. Once the prestress strands were installed, de-slacked and partially de-bonded, then came the assembly of the mild reinforcement. The reinforcement assembly began with the insertion of the transverse reinforcement, R bars. Next came the A bars tied to the stirrups, (R bars). No reinforcement was allowed to be tied to the prestressing strands because when stressed they would move the mild reinforcement out of place. The S bars were tied to the R bars at the end block only for the first 3-feet. The C bar installation used ½-inch rebar chairs to rest on and was tied to the stirrups with long ties. The U bars came next and were tied to the first stirrup at the end region and to the C bars along the U bar's length.

Once the reinforcement cage was assembled, the Tx46 with the plastic duct had an additional fabrication step compared to the Tx46 control. The extra step consisted of installing two 18-feet, 3-inch HDPE ducts placed in between the stirrups in the web section. The final length was corrected once the end forms were installed. The plastic duct was installed at mid height of the web and dimensions can be seen in Figure 3-10. The plastic duct was tied to the stirrups in the end region every six inches and then every

twelve inches, which meets the AASHTO LRFD Construction provisions. The completed reinforcement cage and the plastic duct can be seen in Figure 3-18. An up-close image of the plastic duct can be seen in Figure 3-19 and the dimensions of the material are in Table 3-4, where the material meets AASHTO LFRD Construction Requirements §10.8.3.

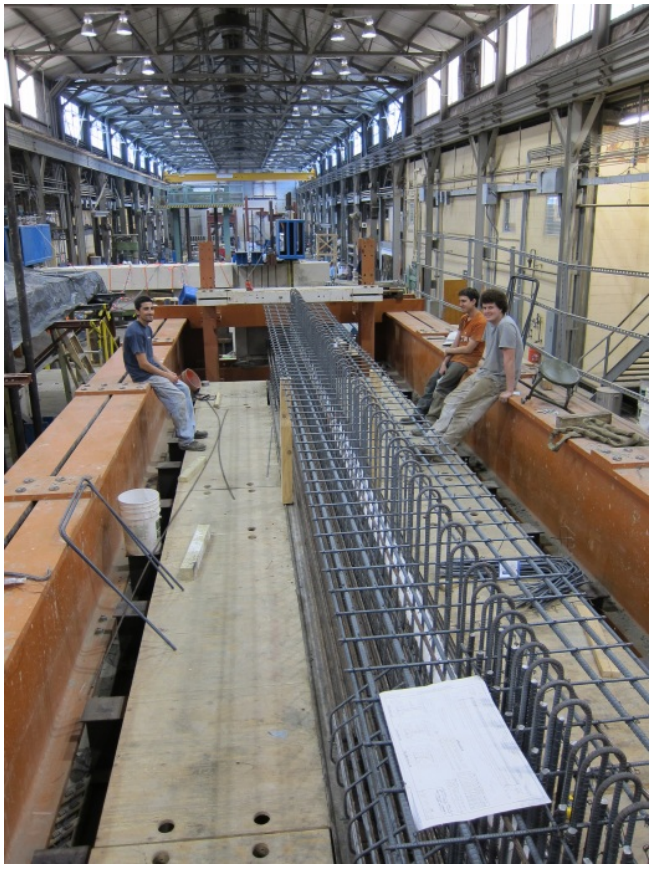

Figure 3-18 Completed reinforcement cage with installed HDPE duct

Figure 3-19 Image of the HDPE duct used

Table 3-4 Dimensions of the plastic duct used for the test

Nominal Diameter	Max Outside Diameter	Minimum Outside Diameter	Thickness
3”	3.5”	3.25”	0.125”

3.5.3 Formwork

The girder form is a prefabricated steel mold designed for a standard Tx46 girder. The form follows the specified dimensions of the bottom flange, web and top flange. Also the outside of the steel form has ridges for an external vibrator connection to properly consolidate the concrete. The width of the bottom flange rest on a smooth steel soffit. The end face of the form is a ¾” plywood with drilled holes that followed the prestress strand layout. The end face plywood was bolted on the forms and the edges were sealed with acrylic caulk foam at the strand joints to prevent concrete leaks. In addition, the form was installed after the cage assembly and before steel strand jacking for safety purposes in case the strands break.

3.5.4 Pre-tensioning the Steel Strands

Following AASHTO 5.9.3 “Stress Limitations for Prestressing Tendons” for Low Relaxation Strands, the strands were stressed to $0.75f_{pu}$. Following AASHTO Table 5.4.4.1-1 for a 0.5-inch low-relaxation strand f_{pu} is 270ksi and $0.75f_{pu}$ is 202.5 ksi. To achieve this stress, four 400-ton hydraulic rams applied force to the live end block and “stretched” the steel strands. The set up for jacking the bottom strands at live end is shown below in Figure 3-20. To ensure the stressing occurs as expected where no strands break or elongate excessively, several checks were performed. Equation 3-2 shows the predicted elongation of a single strand. Appendix C contains the spreadsheet of strand elongation calculations at various stages, which was then compared to the actual elongation during stressing. To obtain actual elongation values, the live end block had three linear potentiometers and measured the displacement of the end block. Three linear potentiometers were used to obtain an average for any uneven movement of the end block.

Figure 3-20 Pretensioning steel strand set up

$$\Delta = \frac{PL}{AE} \qquad \textit{Equation 3-2}$$

Where: Δ = elongation [in.]

P = average applied force [kips]

L = length of strand between end blocks [in.]

A = area of strand [in²]

E = Young's modulus of elasticity of steel prestressing strand [ksi]

(AASHTO 5.4.4.2 for strand: E_p = 28,500 ksi)

3.5.5 Prestressed Girder Concrete Cast

To avoid high ambient temperatures and fast curing of the concrete, both girder casts were done in the morning. Before casting the concrete into the Tx46 form, a slump test was performed. The desired slump of 8-inches was not achieved immediately and in lieu of adding water to the mix, superplasticizer was poured into the drum for a total of 5 oz. for the girder with the plastic duct and 4 oz. to the control girder. A high slump was desired to have good consolidation throughout the heavily reinforced Tx46 with a plastic duct.

As mentioned in Section 3.5.2 the plastic duct was tied to the transverse reinforcement every twelve inches in the testing region, which satisfies the 2-ft maximum spacing per AASHTO Bridge Construction provisions. However, to ensure the plastic duct remains in place at mid-height of the web throughout the girder during the concrete cast, two 0.5-inch strands were stressed as a construction support. Figure 3-21 shows the ¾-inch plywood end form with bolts connecting it to the side medal forms.

Figure 3-21 Stressing of strands in the plastic duct

Furthermore, the image shows a steel bracket bolted to the plywood form with strands pulled through the plastic duct and the bracket plate. The strands are held in place at both ends with chucks. Prior to the concrete girder casting the strands were stressed to 1 kip. Then once the concrete reached a f'_{ci} of 6376 psi, as shown in Table 3-5, the pretensioning strands and plastic duct construction strands were released.

As shown in Figure 3-22, the concrete was poured into the Tx46 form from an overhead bucket. Concrete was evenly poured in segments throughout the length followed by external vibrating. Several more passes went along the length of the concrete until it was flush with the medal form's top surface.

Figure 3-22 Concrete placement

During that time internal vibrators were used to obtain good consolidation of the concrete mix as shown in Figure 3-23. The top surface of the concrete was screeded level with a 2x4 block of wood and troweled the concrete surface smooth. The girder was then covered in plastic sheets to prevent excessive drying on the exposed surface to reduce plastic shrinkage cracking.

Figure 3-23 Concrete vibration for consolidation

3.5.6 Temperature Monitoring

To accurately match the concrete release and design strengths and because concrete has exothermic properties match-curing (Sure Cure) cylinders were utilized. Therefore, prior to casting the concrete girder, a thermocouple wire with a temperature sensor was installed onto the rebar reinforcement 5-feet from the end face. Figure 3-24 shows the insulated 4-inch by 8-inch match cure cylinders used. The rate of hydration can be correlated to concrete strength and since the girder contains more mass the rate of hydration occurs faster. Therefore, the girder reaches a compressive strength faster than

the cylinders. To match the heat, the thermocouple sends the temperature reading to the main computer controller, shown in Figure 3-25, which then increases or maintains the heat of the sure cure cylinders. The heat stays at a constant temperature due to the insulation surrounding the cylinder. The purpose for this system is to be notified of the exact time the concrete release strength has been obtained and therefore increases the efficiency of prestressed girder production. The temperature and approximate strength is then monitored on the main computer controller. When the strength is seen to achieve the release compressive strength f'_{ci}, three Sure-Cure cylinders are tested to verify their strength. At that time, the forms are removed and the steel strands are released.

Figure 3-24 Concrete cylinders being rodded

Figure 3-25 Main computer controller and surrounding Sure-Cure cylinders (Moore, 2010)

3.5.7 Prestress Strand Release

Once the concrete reached the compressive release strength f'_{ci} = 6376 psi, the pressure to hydraulic rams was slowly released. By gradually releasing the pressure in the rams, it allows for a uniform and static compression force to be applied to the bottom flange due to the prestressing force. An immediate release would introduce dynamic effects and would induce a larger force and possibly damage the concrete. The required and actual release strengths of f'_{ci} are shown in Table 3-5. The allowable stresses are obtained from AASHTO 2012 §5.9.4. Initially the Tx46 with the plastic duct f'_{ci} was 6040psi one day after the girder was cast and so the strands were not released. The f'_{ci}, was then adequate on day 2 as listed in Table 3-5.

To determine the needed f'_{ci}, it was based on the allowable tensile and compressive stresses and the stresses produced by the prestressing of the steel strands. The controlling stress is the tensile stress which would have required f'_{ci} of 13,080 psi. However, the girder was over designed in flexure capacity to ensure a shear failure. Therefore, the amount strands can-not be reduced to stay under the tensile limit and so it was exceeded, which caused cracking to the top flange of the girder. Since it was known

the girder will crack at the top, the needed f'_{ci} was then based on meeting the compressive stress limit. It was essential to meet the compressive stress limit to ensure the concrete will not burst or crush due to the prestressing strands.

Table 3-5 Allowable compressive and tensile stress and required release strength

Description	Max Compressive Stress $-0.65f'_{ci}$ [ksi]	Max Tensile Stress $0.24\sqrt{f'_{ci}}$ [ksi]	Needed f'_{ci} based on compressive stress limits [psi]	Actual f'_{ci} [psi]
Tx46 w/Plastic Duct	-4.145	0.868	6376	6960
Tx 46 Control	-4.145	0.868	6376	7460
f'_{ci} based on the limits	6.376	13.080		

A spreadsheet was developed to determine the top and bottom stresses based on the prestressing strands. To determine the maximum stresses through the length of the girder, Equation 3-3 and Equation 3-4 were utilized. Appendix E shows a graph with the results of the development of the compressive and tensile stresses throughout the girder. The results also take into account the 6-feet of de-bonding the strands at the ends, which reduced the compressive stresses at the end of the girder.

$$f_{top} = -\frac{P}{A_{gross}} + \frac{Pe_p(H-y_{btm})}{I_{girder}} - \frac{M_{sw}(H-y_{btm})}{I_{girder}} \qquad \textit{Equation 3-3}$$

$$f_{bottom} = -\frac{P}{A_{gross}} - \frac{Pe_p(H-y_{btm})}{I_{girder}} + \frac{M_{sw}(H-y_{btm})}{I_{girder}} \qquad \textit{Equation 3-4}$$

where: P = Prestress force from the steel strands [kips]

A_{gross} = Gross area of the concrete section [in.^{2}]

e_p= distance between the strands to the centroid [in.]

H = Height of the girder [in.]

y_{btm}= centroid of the girder with respect to the bottom [in.]

M_{sw}= Moment of the girder due to its self-weight [kip-in.]

I_{girder}= Moment of inertia of the girder [in.^{4}]

3.5.8 Concrete deck

The fabrication of the deck started at the end stage of the Tx46 girder cast. The top flange of the girder ultimately acts as the primary support in the decks formwork. Metal inserts were installed at the girder's top flange, shown below in Figure 3-26. The inserts allowed for threaded rods to be screwed into the inserts as shown in Figure 3-27. Grease was applied around the threading at the insert and rod connection as well the upper portion of the rod. The grease was applied to allow for removal of the rod and the grease is the bond breaker from the rod and concrete. The metal inserts will be permanently cast into the girder and will be used only once and the rods will be used over again since there is a plan for a simple removal.

Figure 3-26 Metal insert installed on the top flange of the girder

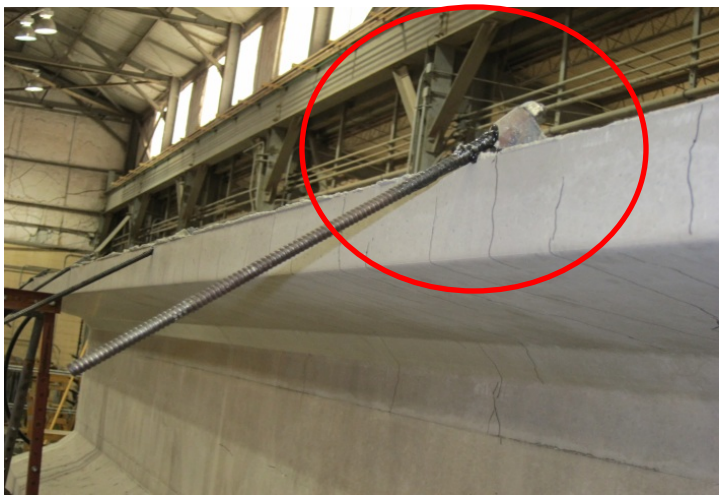

Figure 3-27 Threaded rods with grease screwed into the metal inserts

The rods then connect metal supports that brace the wood form and will hold up the concrete deck during the curing process. Figure 3-28 shows the metal brackets connected to the threaded rod with a base plate and nut. The bracket is needed since the concrete deck will overhang past the flanges of the girder by eighteen inches on both sides. To represent the girder in an actual bridge, an 8-inch slab deck is cast on the girder

with an effective width of 72-inches. Figure 3-29 shows an image of the wooden form that is supported by the brackets and will then support the future concrete deck flush with the top flange of the girder.

Figure 3-28 Metal brackets to support future form

Figure 3-29 Wooden form supported by brackets

In regards to the Tx46 deck, the wood platform and steel reinforcement can be seen in Figure 3-30 and is flush with the top flange of the girder. To form the deck, metal I-girders rest around the perimeter of the wood deck. The reinforced concrete deck is 6-ft wide and 8-inches thick.

Figure 3-30 Reinforcement, metal perimeter forms, and the wood platforms in preparation of the concrete deck cast

Figure 3-31 Tx46 w/plastic duct and reinforced deck ready for concrete cast

To move the Tx46 girder from the fabrication location to the testing area the following steps were taken. There were four PVC pipes that were placed into the deck form flush with the floor. These pipes allowed for a cylindrical void in the overhanging portion in the deck which allowed for an all thread screw to be inserted through and bolted. The bolts were then connected on the top surface of the deck to steel lifting loops. The loops then had lifting straps pulled through and were connected to the overhead crane.

Figure 3-32 shows the concrete cast of the deck and followed the same process as the concrete cast, which includes vibrating, screeding and hand troweling flush.

Figure 3-32 Concrete cast of the deck and vibrating for adequate consolidation

3.5.9 Grouting

To mimic the field practice of post tensioned girders, the plastic duct was grouted. Grout is commonly used to protect the steel strands. In addition, the grout acts as a very stiff material and allows for compression stress transfer (Muttoni, et. al., 2006).

Furthermore, based on panel test it has been observed that grouted ducts have higher capacity compared to an un-grouted duct. In this experiment, the plastic duct had twelve 0.5-inch steel prestressing strands installed into the duct and then was grouted following the established recommended procedures to ensure no air bubbles or voids. However, as in the panel program testing, the Tx46 with the plastic duct steel strands were not stressed. The following references utilized are (FDOT, 2002), (FHWA, 2004), (AASHTO Design, 2012) (AASHTO Construction, 2011) and (ASBI, 2012). The references indicate the procedure and tests required when grouting a post tensioned duct.

The laboratory had available a combined grout mixer and pump to thoroughly mix the grout and water. In addition, hand drills with connected mixer ends were used to obtain a fluid, un-clumped grout mix. The pump was used to inject the grout into the duct with two pressure gauges to indicate the flow pressure and sealed pressure.

3.5.9.1 Grout Vents

An intermediate mid length vent is recommended for ducts lengths greater than 150 feet or if there is a 20 inch change in elevation in the duct profile (FHWA, 2004). The Tx46 girder with a plastic duct is 30 feet in length. And although, the specimen tested does not have such lengths, an intermediate vent was installed to ensure no air voids remained in the plastic duct during grouting as shown in Figure 3-33. The vents were connected to the couples prior to connecting the side metal forms and before the concrete girder cast.

Figure 3-33 Plastic tube vent installed at the center of the girder

3.5.9.2 Duct Sealing

To ensure an adequate seal, the ducts had any dirt and oil wiped off and cleaned. To seal the cap for the specimen, a mold of the duct was made of grout approximately 4-5 inches in length and inserted and bonded with silicone adhesive and then had heat shrink sleeve installed as shown in Figure 3-34. An end plate was also constructed and connected to rods that were epoxy bonded into the girder's end face. An additional measure of "Gorilla" glue tape was added for a tertiary sealant measure. During the grout pumping process, a thin layer of grout seeped out, but the amount was small enough that no voids were formed within the duct.

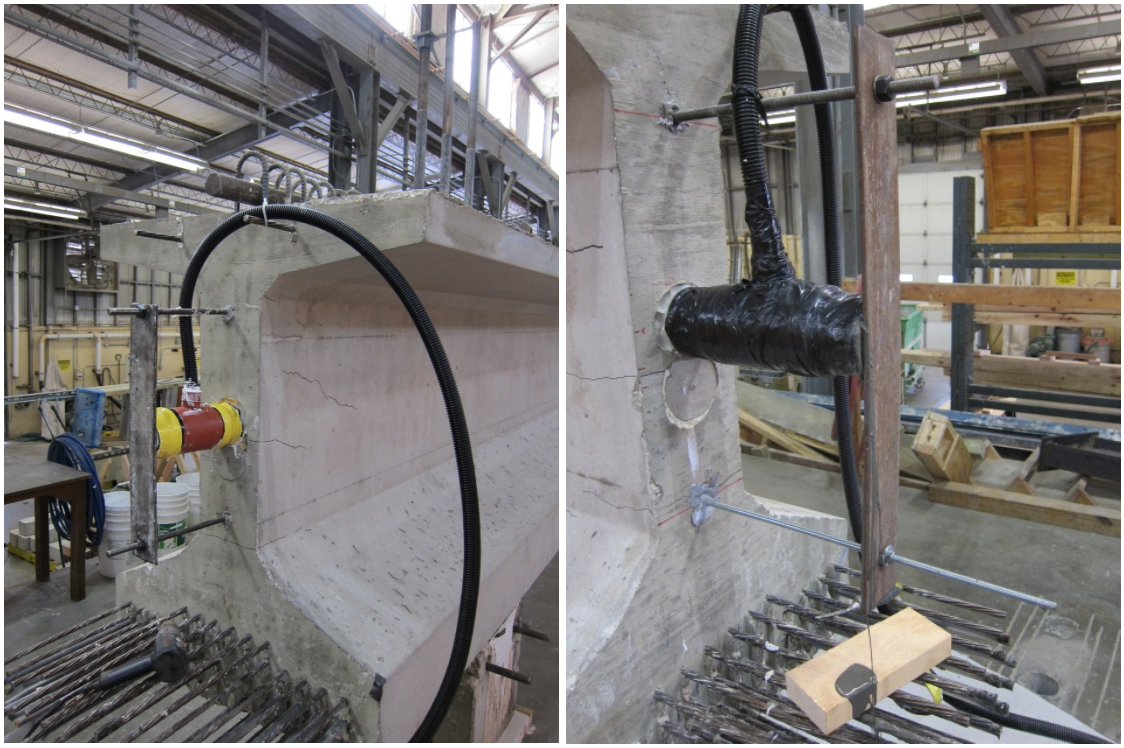

Figure 3-34 Actual sealed duct north and south end faces

3.5.9.3 Flow Cone Test

The flow cone test determines if the grout is fluid with no solids that would cause an uneven flow or even stop the flow during pumping (ASTM C939-10, 2011). The test procedure requires a 1725 ML of grout to be poured through a ½ inch inner diameter tube under 35 seconds. Figure 3-35 below shows a typical cross section to be used to perform the "flow cone test".

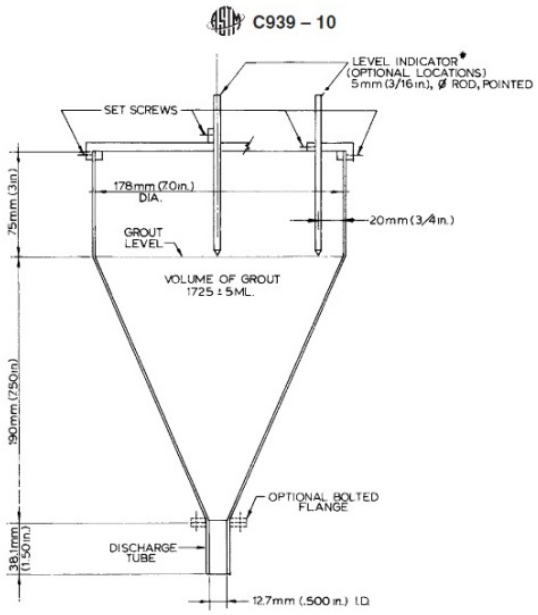

Figure 3-35 Cross section of flow cone for grout mix consistency

3.5.9.4 Specimen Grout Injection

The injection grout flow inlet pressure ranged from 30 psi to 50 psi and never exceeded 75 psi. Too much pressure increases the flow rate of the grout and would result in turbulent flow consisting of air voids and water (FDOT, 2002). Also an increased pressure would indicate a clog. To avoid air bubbles and voids the injection process required bleeding and burping. To bleed the system, 2 gallons of grout was discharged during the initial pumping as shown below in Figure 3-36. This discharge allows for good consistent grout. Once 2 gallons was reached the vent was sealed. The grout was continued to be pumped until full and the pressure read 75 psi, then locked and held for 2 minutes. At this time, a leak was found but quickly sealed. To remove any air bubbles entrapped in the system, the grout was burped, which is done by locking in the grout pressure to 10 psi for 10 minutes and opening and releasing the air/moisture from the

vent. The vents were then closed and the pressure of the grout was raised to 35 psi and locked.

Figure 3-36 Bleeding initial grout to remove air voids out of the grout

3.5.9.5 Grout Compressive Strength

Finally, during the grout injection process, cube specimens of the grout were taken. By following Masterflow water to grout ratio specifications the grout cube strength reached a compressive greater than 8000 psi at 28 days as shown in Table 3-3.

3.6 TX46 GIRDER TESTING PROGRAM

This section describes in detail the support materials, the method in obtaining the load and deflection responses and a description of the applied point load. As mentioned earlier the test setup of Tx46 girder consisted of a simply supported condition. The

girders rested on two elastomeric bearing pads and the load was applied at the center of the girders.

3.6.1 Support Conditions

The bearing conditions of the test simualted a simply supported condition; elastomeric steel reinforced bearing pads were used for that purpose. By using such a pad it allows for movement in the horizontal direction and releases rotations. Table 3-6 shows the dimensions of the bearing pad based on the TxDOT standard that is adequate to support a Tx46 prestressed girder with a 0^0 skew angle. However, due to the future testing of Tx62 girders, larger elastomeric pads were required. Therefore, the pad dimensions are 9 x 21-inches. The actual elastomeric pad used in the test can be seen in Figure 3-37.

Table 3-6 TxDOT Elastomeric Bearing Data, June 2007

Elastomeric Bearing Data Table						
Bent Type	Girder Type	Bearing Type	Girder End Skew Angle Range	Pad Size Lgth x Wdth	Pad Clip Dimensions	
					"A"	"B"
Abutments, Inverted-T and Transition Bents with Backwalls	Tx46	G-1-"N"	0° thru 21°	8" x 21"	------	------
	Tx62	G-5-"N"	0° thru 21°	9" x 21"	------	------

Figure 3-37 Actual 9" x 21" elastomeric bearing pad used in testing

3.6.2 Deflection

To measure the deflection six linear potentiometers (L-Pots) were used, on both faces of the girder at the supports and as well as under the point load at the center. The location of the potentiometers at the supports is shown in Figure 3-38 . Metal plates were attached to the bottom surface of the girder's bottom flange with a hardener and resin. The L-Pot was then placed in contact with plate and would measure the change in movement of the plates, shown in Figure 3-39. The reason for six L-pots was to take the average of both sides of the L-Pots at each location in case there was any rotation during loading. Then the difference was taken between the center deflection and at the supports to remove the deflection of the elastomeric bearing pads. The data deflection obtained from the "L-Pots", will be shown in the "Results" section of Chapter 4.

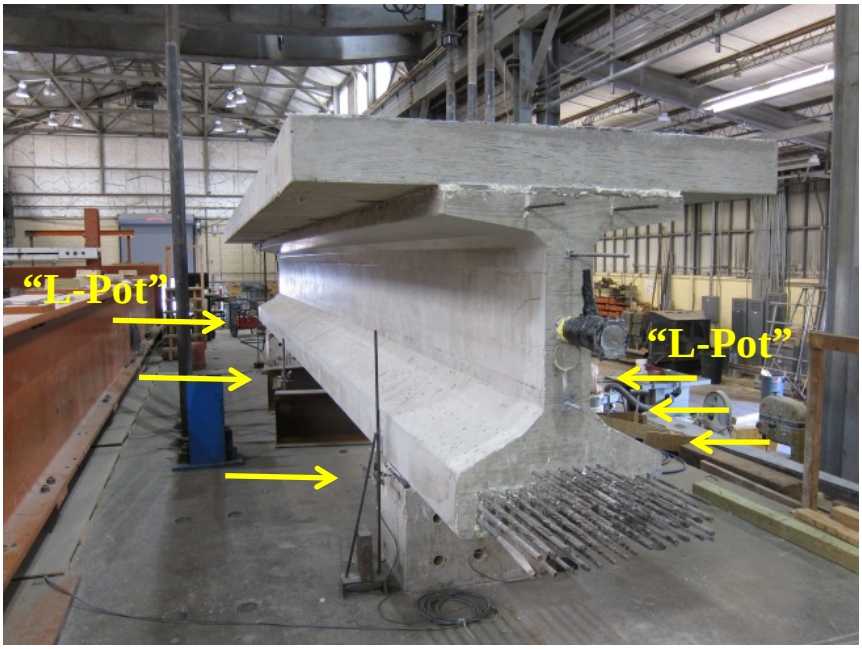

Figure 3-38 Set-up of the "L-Pots" at the supports and center of the girder on both faces

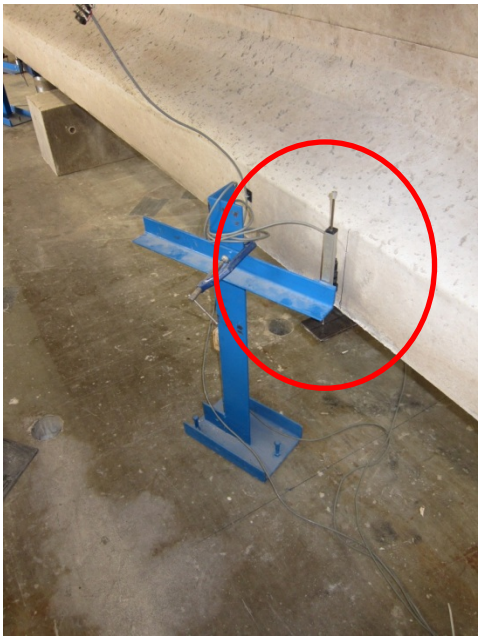

Figure 3-39 Up close image of the "L-Pot"

3.6.3 Loading

Figure 3-40 shows a CAD image of the testing configuration. Then Figure 3-42 and Figure 3-43 show the actual test set up of the Tx46 with the plastic duct and the Tx46 control respectively.

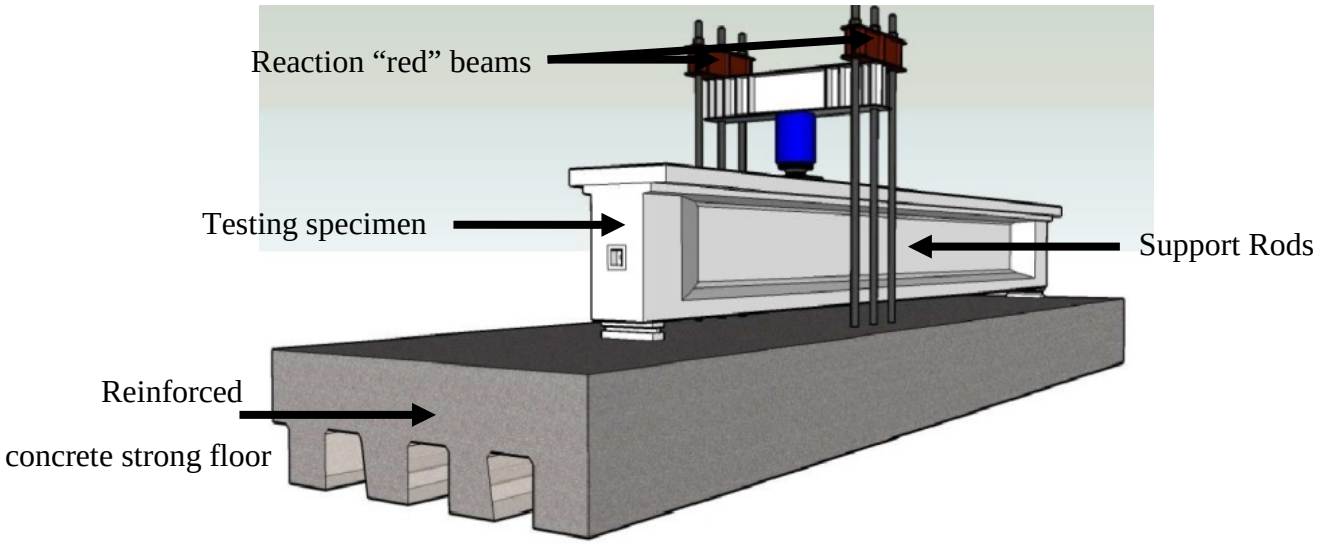

Figure 3-40 Typical CAD image of the test set up

To obtain accurate results and fail the girder in shear, a point load was the simple choice and is shown in Figure 3-41.

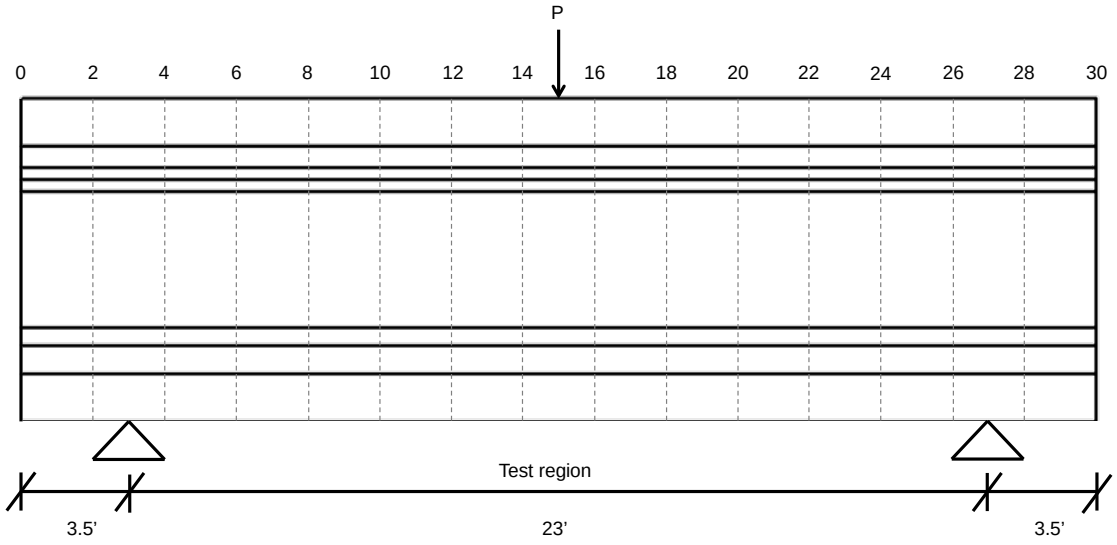

Figure 3-41 Test region contains transverse reinforcement spaced at 6-inches

The configuration consists of a reinforced strong floor base with approximately 4-inch hole openings to the ground floor. The openings allow for steel rods to be placed through and balance equilibrium from the force outputted by the point load. In regards to the Tx46 with a plastic duct, six rods were used in total, three on each side. Prior to testing the Tx46 control, a Tx62 with a plastic duct was tested in shear and required larger reaction beams, (colored in red Figure 3-40). As a result of changing out the reaction beams, only four rods were used, with two on each. Therefore, the load frame changed and increased the weight acting on the Tx46 control.

The strong floor was designed to support 800 kips of force (O'Callaghan 2007). The rods then support two beams (colored in red in Figure 3-40), which in turn reacts against the steel blue beam, and it is transverse to the testing specimen. The blue beam then reacts against the hydraulic ram. The ram has a 2-million pound capacity. The ram was then connected to a pump that forces a hydraulic fluid pressure to extend the ram and apply load onto the girder. In addition, the ram was connected to a pressure transducer that outputs the results and converts the value to a force applied from the ram.

To ensure a level smooth force subjected on the girder, a square area of 26-inch by 24-inch by approximately 1-inch thick of hydro-stone was poured onto the girder directly and was formed by perimeter of 2x4 blocks of wood. Spherical plates then rested on the hydro-stone and another was connected to the ram to produce a point load onto the girder.

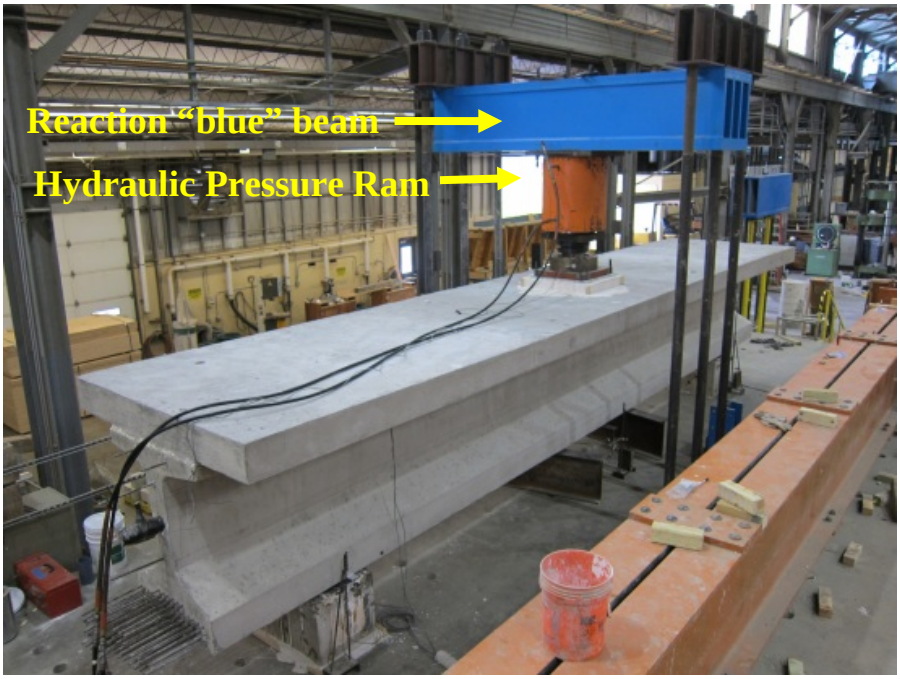

Figure 3-42 Actual set up of the test Tx46 w/Plastic Duct

Figure 3-43 Actual set up of the test Tx46 Control

3.7 SUMMARY

In summary, the research began with an investigation of small-scale concrete panel specimens that represent the web portion of the bulb-tee girder. A testing frame was designed and fabricated at FSEL to fail these concrete panels under compressive loading. The panel specimens consisted of many variables with most relevant configurations to the full-scale tests having7-in. thickness and containing plastic ducts.

Two full-scale girders were constructed and tested. One of the girders has a post-tensioning plastic duct and the other was the control. The design of the full scale specimens followed the design of the Tx-Girder series. To ensure a shear failure to determine the girder’s actual shear capacity the girder was overdesigned in flexure. Initially, compressive and tensile stresses within the girder exceeded allowable AASHTO

limits. To reduce the compressive stresses the girder required de-bonding and then only the tensile limits were exceeded.

The girder tested contained a 3-inch plastic duct placed mid height of the web region. The plastic duct was grouted and contained twelve non-stressed prestressing stands. The test performed was a point loaded simply span set up. The test measured the applied loading and deflection that was required to fail the girder.

CHAPTER 4

Test Results

4.1 INTRODUCTION

Prior to discussing the results to the girder testing, results of the concrete panel testing performed at the University of Texas at Austin Ferguson Laboratories will be discussed. Panel tests investigated many test variables that are useful to interpreting the effects of post-tensioning ducts.

Test results are presented and discussed in this chapter for the Tx46 girders. Reported test results include notes on the cracks and other commentary noted prior to the test, during the test and at failure. In addition, images of the crack orientation are illustrated in several figures. The results that will be presented are a shear vs. deflection diagram, tables of the calculated shear resistance with respect to various k-factors, followed by a graph of calculated shear with the corresponding k-factors. Lastly, there are two graphs of the Tx46 control and Tx46 with the plastic duct comparing the shear resistance and the total shear applied throughout the length of the girder.

4.2 OVERVIEW OF PANEL TESTING PROGRAM

The objective of the small scale panel research was to determine the effects of duct material, duct size, reinforcement placement, with and without grout. Although a full description of panel testing program is outside of the scope of this thesis the major findings are as follows:

- Well-distributed and efficiently placed through thickness reinforcement that extends through the member thickness above and below the duct improves crushing capacity
- The compressive strength of a plastic ducted panel is significantly less than that of a steel ducted panel
- The reduction in the strength of a plastic ducted panel is due, in large part, to the low bond between a plastic duct and the surrounding concrete
- Results of several concrete panels with a 7-inch thick web and plastic duct diameters of 2-3/8, 3 and 3-3/8 inches are shown in Table 4-1 (Wald 2012).

Table 4-1 Comparison of the 7-inch thick panel with the 3-inch plastic duct diameter results to Tx46 w/duct girder (Wald, 2012)

Specimen	$f_{concrete}$ [ksi]	f_{grout} [ksi]	[in.]	Nominal δ	η_D
P7-8	10.62	4.86	2.375	0.339	0.43
P3-3	9.39	5.29	3	0.429	0.37
P3-4	9.39	5.29	3	0.429	0.36
P3-6	9.39	5.29	3	0.429	0.35
P4-5	8.17	4.66	3	0.429	0.39
P9-3	10.19	6.25	3	0.429	0.35
P8-3	11.16	5.98	3.375	0.482	0.28

The two variables which hold the most significance in the girder testing program are at the presence of through thickness reinforcement and the reduction in strength between plastic and a steel ducted panel is due to the low bond between the plastic duct and the surrounding concrete. The first variable, the influence of through thickness reinforcement, is avoided in this girder testing program by supporting the duct externally

as is explained in Section 3.5.5. The second variable, the reduction in strength due to a plastic post-tensioning duct, is the primary variable explored in the Tx46 shear tests and will be discussed in more detail in the following sections.

4.3 TX46 GIRDER SHEAR TEST OBSERVATIONS

Prior to applying any load, all initial cracks were marked in black. Initial cracks were due to the release force from prestressing of the strands which caused tensile cracks in the top flange and spalling effects at the end region.

The girders were simply supported with a 3.5-feet overhang and point loaded at mid-span. The test configuration is shown in Figure 4-1 and the actual test set up is shown in Figure 4-2. Both test performed well by failing in shear with no unexpected issues. The girders were both loaded in 100 kip increments with all new and existing cracks marked or extended to the corresponding load written in kips.

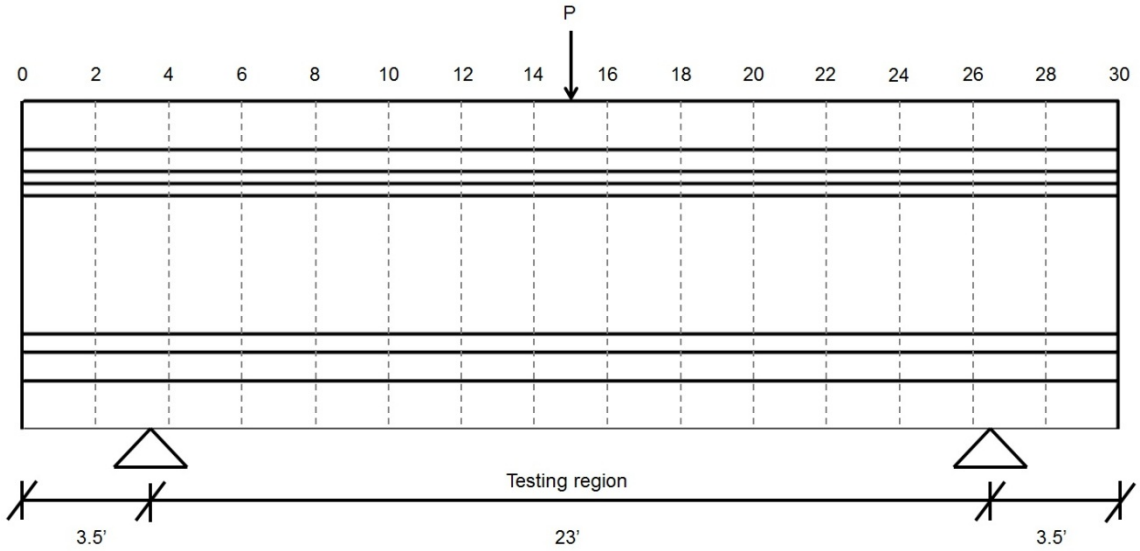

Figure 4-1 Elevation view of the testing configuration

Figure 4-2 Actual test set up of the Tx46 control

4.3.1 Shear Test Observations of the Tx46 Control

As mentioned all release cracks were marked; the majority of these were found to be along the top flange transverse to the length of the girder as shown in Figure 4-3 with the actual girder on the left and an image of the cracks highlighted on the right. The top cracks indicate flexure cracks from the prestressing inducing a cambering effect. In addition, initial cracks were found at the end region of the girder.

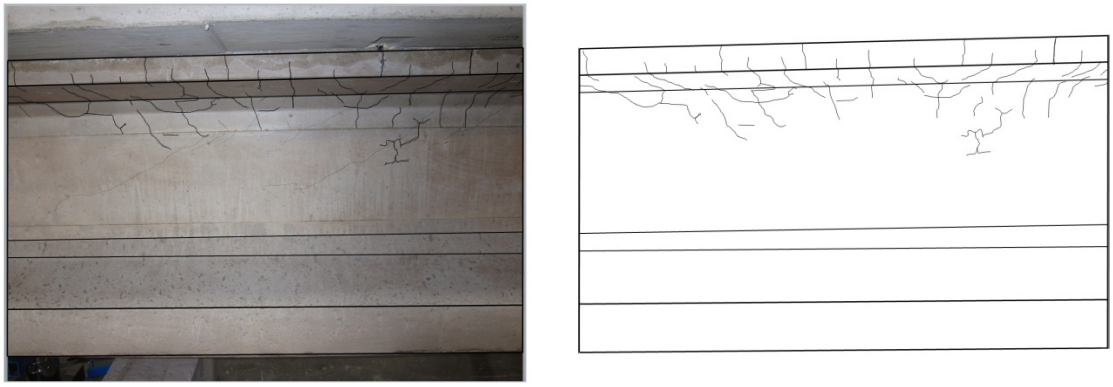

Figure 4-3 Elevation view of Tx46 control initial cracks to the top flange and highlighted cracks

Shear cracking initiated at 150-kips of applied load. The crack formation was in the web region, near the supports and traveled diagonally towards the applied load. At a shear of 200-kips, cracks extended to the bottom flange and began traveling along the length of the bottom flange to web interface towards the end of the girder. This crack direction became more apparent when the shear loading reached 250-kips. At 250-kips to 300-kips the diagonal cracks grew until they extended from the top to bottom flange as shown in Figure 4-4.

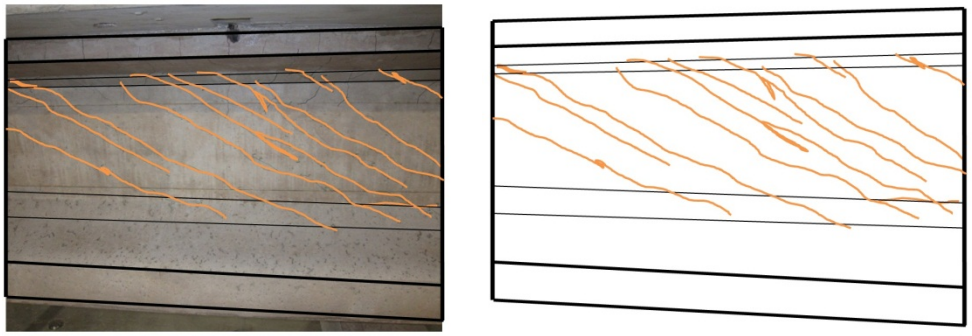

Figure 4-4 Highlighted images of Tx46 Control with cracks at 300-kip shear load

Approximately at a shear of 390 kips a popping sound was heard from the girder. The sound most likely indicated the initiation of prestress strands anchorage failure. Cracks continued to travel diagonally towards the bottom flange at 400 kips nearly reaching the bottom face of the girder. Flexure cracks appeared in the bottom flange at the shear load of approximately 450 kips. At 500 kips in shear, the cracks traveled across the transverse length of the bottom flange. The girder failed at a shear of 513 kips; the bottom flange concrete at the strands split apart as shown in Figure 4-5. The measured length of the split concrete is 6-feet from the south end, exactly at the location of the de-

bonded strands, most likely indicating a shear induced anchorage failure. The underside of the bottom flange is shown in Figure 4-6.

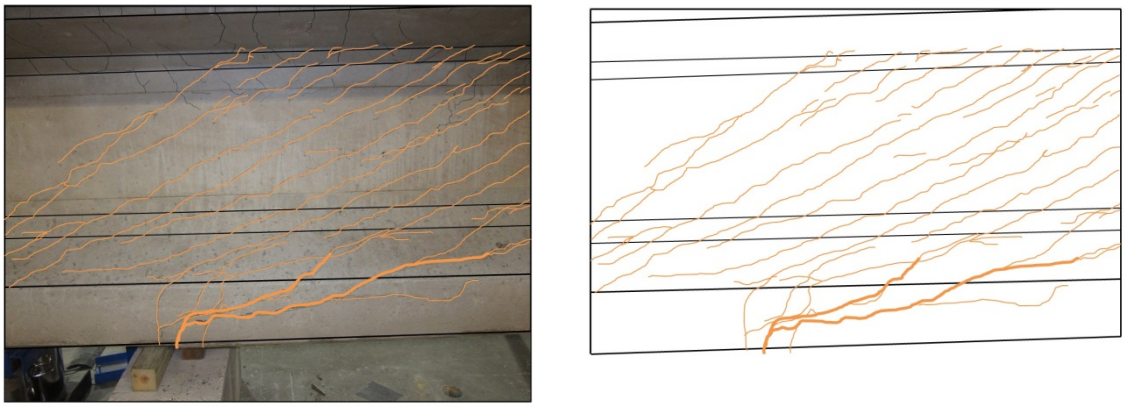

Figure 4-5 Failed elevation view of the Tx46 control with highlighted cracks

Figure 4-6 Underside view of the bottom flange Tx46 control and highlighted cracks

4.3.2 Tx46 with Plastic Duct Testing Observations

The Tx46 with the plastic duct as stated previously had all initial release cracks marked prior to applying load. Cracks were found around the duct area on the end face and on the end region of both faces on each ends. Cracks were also observed on the top flange edge face traveling to the web. The top flange cracks start approximately above the supports but are more repetitive around 6-feet into the girder.

A thorough investigation of cracks began at a shear loading of 100 kips but no cracks were found. Then at 150 kips in shear, the first cracks were noted in the web at the same height as the post-tensioning duct. Theses cracks were diagonal and were considered to be shear cracks, but they did not come with the "popping" sound that typically accompanies initial shear cracking in pretension girders. The cracks were spaced at regular 8-inch intervals and began at the support and continued until around 2-feet from the load point. At a shear of 250 kips, a loud pop was heard from the girder but there was no visual damage to correlate with the sound.

Throughout the testing, three cracks were measured to be 0.01-inches in width at a shear of 250 kips. At 325 kips in shear, two of the three crack widths grew to approximately 0.013-inches and one stayed constant. At 350 kips of shear loading, all three cracks were measured to be 0.01-inches. This reduction in crack width was likely due to faulting along the cracks. No flexure cracks were found on the bottom flange throughout the entire loading. The girder then failed by web crushing at an applied shear load of 443 kips.

All diagonal cracks occurred only in the web region. Also spalling and delamination of the web concrete observed at the height of the duct. An image of the

failure is shown in Figure 4-7. Few cracks were observed within 1-foot of the load point and were not seen anywhere in the overhanging region beyond the support.

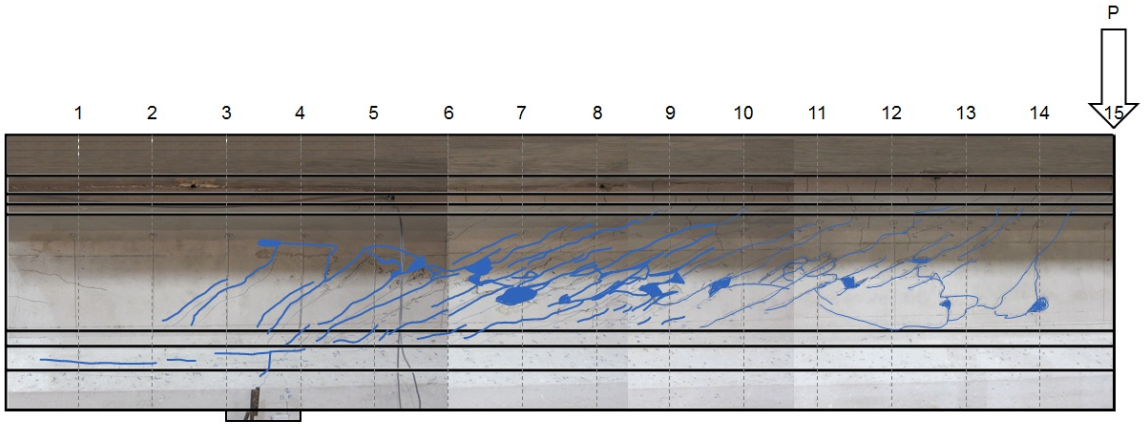

Figure 4-7 Image of the Tx46 w/Duct (North West face) with crack highlighted in color

Figure 4-8 shows a clear visual of the cracks orientation and location throughout the northwest half of the girder. As shown in Figure 4-8 all cracks are oriented with a diagonal inclination with the direction from the support towards the point load.

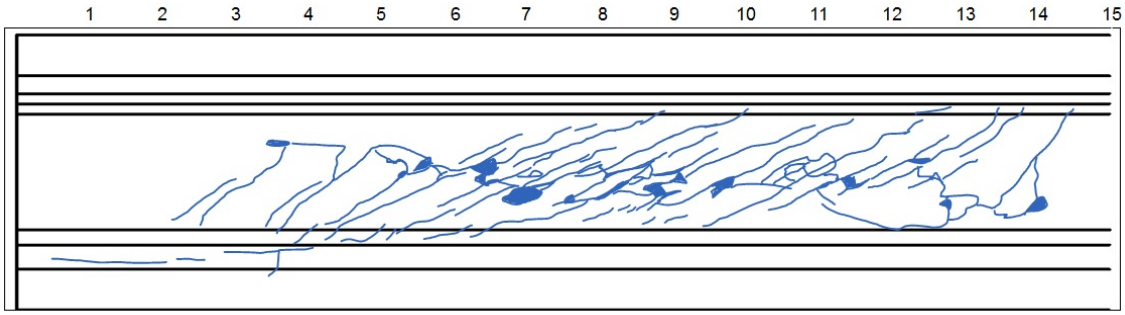

Figure 4-8 Outline of the Tx-46 w/Duct (North West face) with only dimensions and highlighted damage

4.4 TX46 RESULTS

The failure load to induce web crushing of the Tx46 girder with the plastic duct was 465 kips. The shear failure of the Tx46 control girder was 533 kips. The shear vs. deflection plot during testing is illustrated in Figure 4-9. Note that the shear applied does not pass through the origin. Shear was induced earlier prior to testing due to the self-weight of the girder and load frame weight. As it is shown in the plot of Figure 4-9 the Tx46 with the plastic duct failed at a lower shear and was stiffer than the Tx46 control. The Tx46 control f'_c was less than the Tx46 with the plastic duct f'_c, which would make the Tx46 plastic duct specimen stiffer than the other. As a result, there is less stiffness in the Tx46 control allowing for more deflection.

4.5 RESULTS

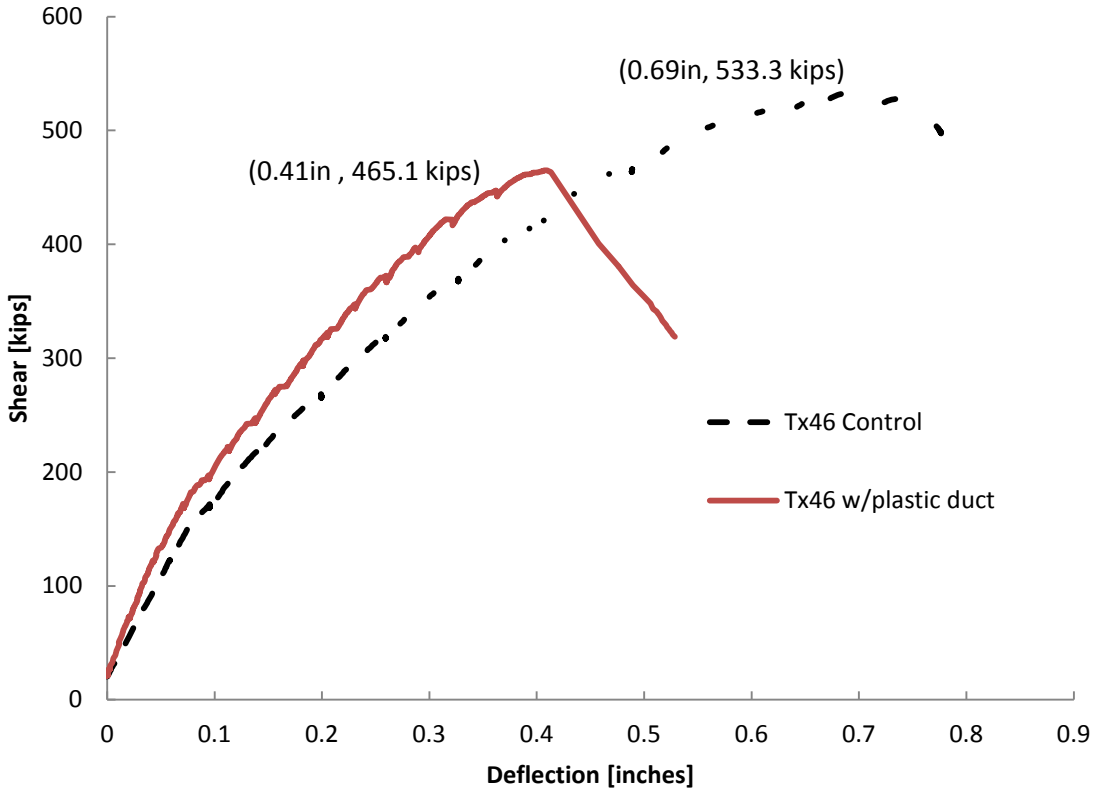

Figure 4-9 Graph of applied shear vs. deflection

4.5.1 Calculated Shear Resistance and Shear Applied at Failure

The nominal shear resistance of the member is calculated following AASHTO LRFD 2012 General Procedure §5.8.3.4, as shown in Equation 4-1. An excel spreadsheet was created and utilized to perform the calculation with iterations between θ, β, and ε_s to determine the critical section distance at which concrete web crushing will occur. The spreadsheet input and results are shown in Appendix F. Listed in Table 4-3 and Table 4-3 is a summary of the calculated shear capacities of the Tx46 control and Tx46 with plastic duct with the various k-factors as referenced in Section 2.4.

It is shown in Table 4-2, that the Tx46 control ratio V_{test}/V_n is 1.02. Therefore, the AASHTO 2012 LRFD general shear resistance estimate was nearly the same as the actual shear required for failure.

As for the Tx46 with plastic duct, the ratio values of V_{test}/V_n listed in Table 4-3 indicates that shear capacity is not accurately predicted until a k-factor of 1 is used. The specified AASHTO 2012 general shear k-factor of 0.25, results in an un-conservative V_{test}/V_n ratio of 0.90. Furthermore, the AAHTO 2012 provision for segmental shear design specifies a k-factor of 0.5 and again results in an un-conservative V_{test}/V_n of 0.93. Therefore, the AASHTO 2012 LRFD general shear k-factor provision does not fit the shear failure value in the test performed for the Tx46 with a 3-inch plastic duct and 8-inch deck.

Table 4-2 Tx46 control shear resistance calculation

Tx46 Control Summary , $\boldsymbol{V_{test}}$ ***= 533.3 [kips]***							
k	b_v*[in]*	*Vc[kips]*	*Vs[kips]*	*limit*	*Vn[kips]*	*% Reduction*	V_{test}/V_n
0	7	166.1	358.6	0.2	524.7	0.00%	1.02

Table 4-3 Tx46 w/plastic duct shear resistance calculation with various k-factors

Tx46 with Plastic Duct Summary, $\boldsymbol{V_{test} = 465.1[kips]}$							
k	$b_v[in]$	$V_c[kips]$	$V_s[kips]$	*limit*	$V_n[kips]$	*% Reduction*	V_{test}/V_n
0	7	173.7	357.9	0.2	531.7	0.00%	0.87
0.25	6.25	156.5	358.5	0.2	515.0	3.14%	0.90
0.5	5.5	139.0	359.0	0.2	498.0	6.33%	0.93
0.75	4.75	121.2	359.6	0.2	480.8	9.57%	0.97
1	4	103.2	360.3	0.3	459.9	13.51%	1.01
1.2	3.4	91.2	362.6	0.3	390.9	26.48%	1.19
1.4	2.8	78.2	365.0	0.3	321.9	39.45%	1.44

From the data in Table 4 3, a graph is plotted of the calculated nominal shear resistance, V_n vs. the various k-factors and is shown in Figure 4 10. In addition the graph includes the actual shear required to fail the girder and is labeled as Vtest. From the graph it is illustrated that at the intersection of the V_n to Vtest the k-factor is approximately 1. The significance of this intersection is that this is also the value at which the calculation of nominal shear resistance V_n, shown in Equation 4-1 changes to limit of AASHTO's 2012 LRFD stress limit shown in Equation 4-2.

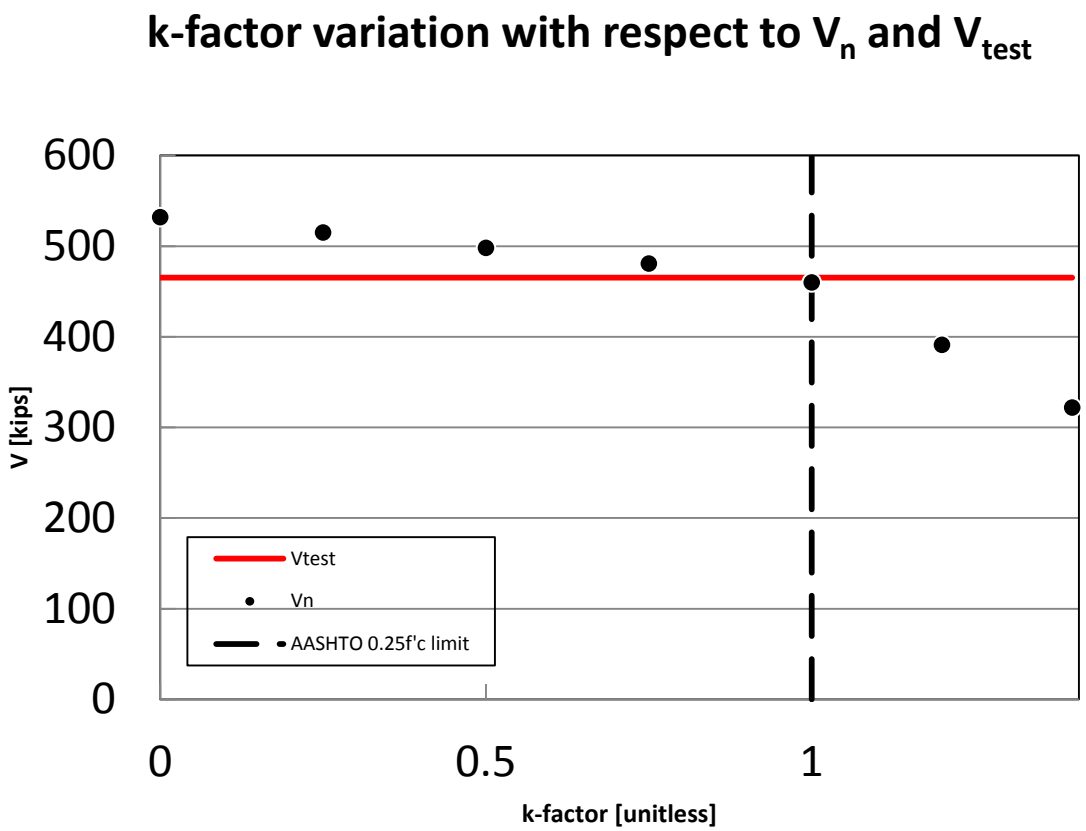

Figure 4-10 Tx46 with plastic duct graph of shear vs. k-factor

$$V_n = V_c + V_s + V_p \qquad \textit{Equation 4-1}$$

$$= 0.0316\,\beta\sqrt{f'_c}\,b_w d_v + \frac{A_v f_y}{s} d_v \cot\Theta + V_p$$

$$V_n = 0.25\, f'_c b_v d_v + V_p \qquad \textit{Equation 4-2}$$

As the k-factor increases, shown in Figure 4-10 the calculated shear resistance V_n decreases and produces a more conservative result when compared to the tested strength of the girder. At the stress limit, V_n is significantly affected by the k-factor which affects the b_v term. Prior to the $0.25f_c$' limit in Equation 4-2 the calculated nominal shear resistance, V_n does not vary much with respect to the k-factor since the calculated shear

capacity includes a V_s term. The "% Reduction" column provided in Table 4-3 quantifies this change in calculated shear resistance with respect to a k-factor. The significant change in reduction is due to V_s no longer included in Equation 4-2 and with the change b_v due to the k-factor applied the calculated shear resistance is affected.

4.5.2 Tx46 Comparison of the actual shear failure to the shear resistance

The graphs shown in Figure 4-11 and Figure 4-12 is a visual comparison of the actual shear at failure to the calculated shear resistance. The figures illustrate the shear vs. the distance within the girder starting with the far end traveling to the center, which is also the location of the applied shear load. Figure 4-11 represents the control girder and Figure 4-12 represents the girder with the plastic duct.

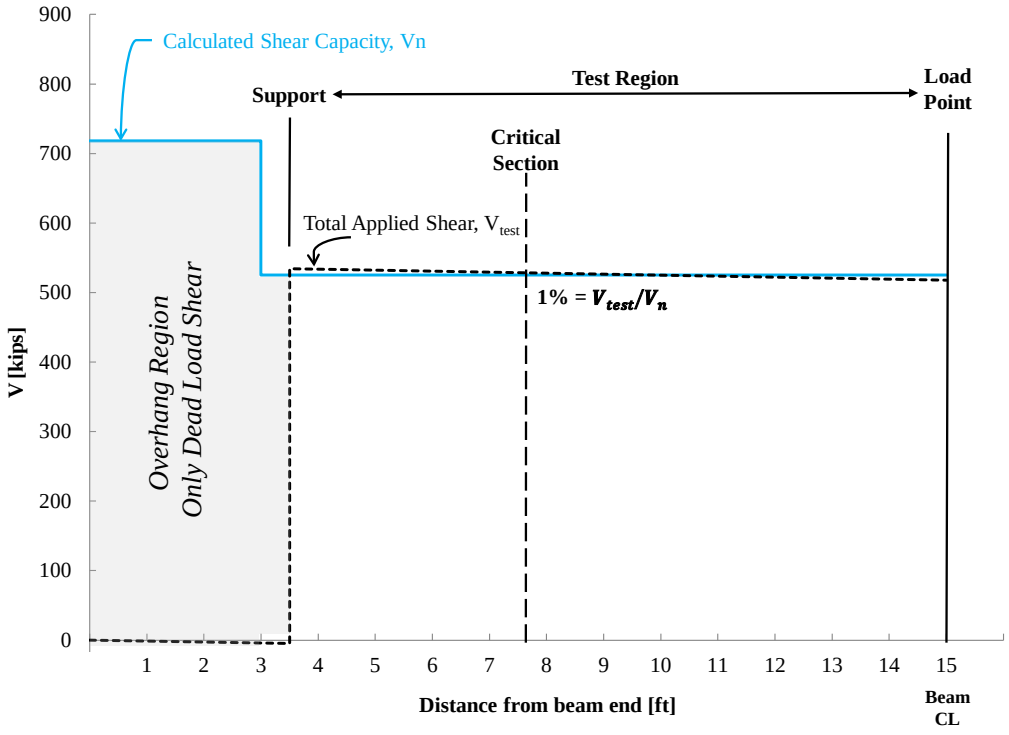

Figure 4-11 Tx46 control comparison of the actual shear failure to the shear resistance

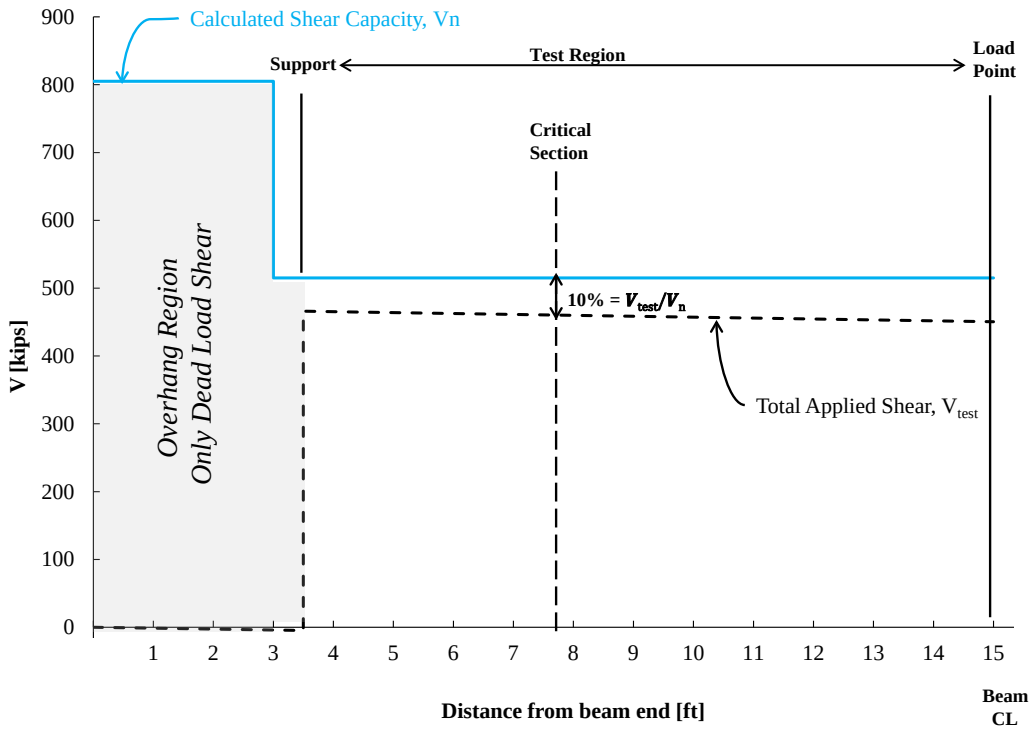

Figure 4-12 Tx46 w/plastic duct comparison of the actual shear failure to the shear resistance with a K-factor of 0.25

The applied shear acting on the girder consist of the girder and deck self-weight, test frame weight, steel rod weight, and the applied shear load. The only shear acting on the girder from the end of the girder at 0-feet to the support at 3.5-feet is the girder self-weight and the shear negative slope is due to the girder self-weight.

Both girders had an approximate critical section location calculated of 51.9-inches from the support or 7.825-feet from the girder's end face. The critical section is the approximate location of failure. The critical section is where the comparison is made of the actual shear failure load to the calculated shear resistance.

4.5.2.1 Tx46 Control Comparison

The control girder steel shear reinforcement follows the Tx46 standards as shown in Appendix A. The first 3-feet of the girder end has more transverse reinforcement spaced at a closer distance, which increases the shear resistance to 718 kips. The shear resistance did increase to a higher value due to the increase in transverse reinforcement, but was limited by Equation 4-2. As result, there is an increased shear resistance within the end of the girder compared to the remaining interior section of the girder. The test region of the girder spans from the support spaced 3.5-feet from the end. The remainder of the girder's nominal shear resistance past 3-feet is 525 kips and does not change within the test region.

As it is shown in Figure 4-11 of the control girder, the nominal shear resistance, of 525 kips was calculated to be lower than the actual shear failure of 533 kips, which is a 1% difference. Therefore, the AASHTO LRFD shear strength calculation method produced an accurate and slightly conservative value for shear resistance.

4.5.2.2 Tx46 with Plastic Duct Comparison

In regards to the girder with plastic duct illustrated in Figure 4-12, its nominal shear resistance is 515 kips. The value of 515 kips for shear resistance was reduced by the k-factor of 0.25 to account for a plastic duct with grout as specified in AASHTO general shear provisions. The k-factor modified the web width to an effective web width of 6.25-inches. The shear failure load was 465 kips at the critical section. Therefore, the AASHTO LRFD calculated shear resistance did not prove to be conservative and the girder failed at a shear 10% lower than predicted. Furthermore, the calculated shear resistance without applying a k-factor as shown in Table 4-3 is 532 kips. The calculated

shear resistance is 13% greater than the actual load at which shear failure occurred in the girder. By applying an increasing k-factor to modify the web the shear resistance does approach the actual shear failure as shown in Table 4-3.

4.6 SUMMARY

Tests were performed on small scale panels under compressive loading and two full-scale girders were tested to shear failure. The objective of the panel testing program was to determine the effects of duct material, size, reinforcement placement and grout. From the panel testing program the following results were obtained: the through thickness reinforcement above and below the duct improves capacity, panels with plastic ducts have less compressive strength than steel ducted panels, which can be attributed to the reduced bond between the concrete and the plastic. Finally, the average η_D for a 7-inch thick web concrete panel with a plastic duct is 0.35, or 65% shear strength capacity compared to the control panel.

In the transitional full scale testing of the Tx46 girders all crack were highlighted prior to applying any load. Both girders had flexural cracks in the center top flange region and at the ends upper region of the web and top flange prior to testing.

The Tx46 control girder began to exhibit shear cracking in the web at a shear load of 150 kips. Diagonally shear cracks continued to appear and extended from the web to the top and bottom flange interface. The girder failed at a shear of 533 kips in shear induced anchorage failure. Major cracks and a concrete split appeared in the bottom flange at the de-bonded strand location. The calculated shear resistance from AASHTO LRFD method is 525 kips a conservative 1% difference from the actual shear failure value.

In the shear testing of the Tx46 with the plastic duct, web diagonal cracks appeared at a shear of 150 kips. Web crushing failure occurred at a shear of 465 kips. The calculated shear resistance from AASHTO LRFD General Shear methods was calculated to be 515 kips with a k-factor of 0.25. Therefore, the research in this test indicates the AASHTO calculated shear strength resistance was 13% less the actual shear to cause failure. Furthermore, for this size specimen having a plastic duct with a nominal 3-inch diameter, using a k-factor of 1 produces a conservative calculated shear resistance of 460 kips.

CHAPTER 5

Discussion, Conclusion, Summary

5.1 SUMMARY

This chapter gives a summary discussion of the results with conclusions of the equivalent concrete panel test, the Tx46 control, and the Tx46 with a plastic duct.

5.2 PLASTIC DUCT PANELS AND TX46 WITH PLASTIC DUCT COMPARISON

As expected, the panel testing representing the web of a full scale girder is not a true representation. Table 5-1 has listed the results of 7-inch thick web with plastic ducting ranging in diameters from 2.375-inch to 3.375-inches. The specimens also have various details of hairpins and can be referenced from the research done by Wald (2012). The trend that can be observed in the test results in Table 5-1 of the panel testing show an increase in δ (duct ratio to web width) there is a decrease in η_D (ratio of the duct failure load to the control failure load).

Based on Table 5-1, Wald's thesis describes the drop of capacity within the panel in the geometric drawing shown in Figure 5-1. Due to the increased duct diameter, stresses will have to deviate around the duct resulting in a greater angle of compressive stresses. To resist such compressive stresses, greater tensile stresses are generated.

Table 5-1 Comparison of the 7-inch thick panel with the 3-inch plastic duct diameter results to Tx46 w/duct beam (Wald, 2012)

Specimen	$f_{concrete}$ [ksi]	f_{grout} [ksi]	[in.]	Nominal δ	η_D
P7-8	10.62	4.86	2.375	0.339	0.43
P3-3	9.39	5.29	3	0.429	0.37
P3-4	9.39	5.29	3	0.429	0.36
P3-6	9.39	5.29	3	0.429	0.35
P4-5	8.17	4.66	3	0.429	0.39
P9-3	10.19	6.25	3	0.429	0.35
P8-3	11.16	5.98	3.375	0.482	0.28
Tx46 w/ plastic duct	**9.70**	**8.60**	**3**	**0.429**	**0.86**

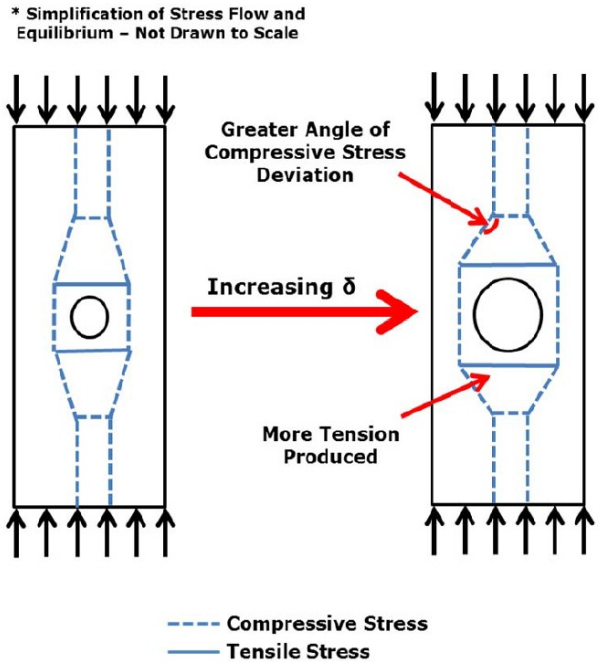

Figure 5-1 Behavior of panels with increasing δ (Wald, 2012)

From Table 5-1, the average η_D for the 7-inch thick panel with a 3-inch diameter plastic duct is 0.35. The value 0.35 indicates that there is a 65% shear strength reduction when utilizing a 3-inch plastic duct. However, for the full scale Tx46 beam with a 3-inch

plastic duct and an 8-inch concrete deck the η_D is 0.86, which corresponds to a 14% shear strength reduction. Therefore, there is a significant reduction in strength when performing small scale panel testing compared to full scale testing. Initially there was concern in the significant drop in compressive capacity in the plastic duct panels, but when testing an equivalent full scale girder with a plastic duct and a concrete deck the drop in capacity was not as significant. The dramatic differences could most likely be attributed to boundary effects from the top and bottom flanges and the compression induced from prestressing.

It can be concluded that the panel specimens are not a true representation of the girder behavior. The k-factors that are adjusted to predict the concrete crushing capacity of the panel with a plastic duct material, 3-inch duct diameter dimension, and 7-inch web thickness does not predict crushing capacity of equivalent Tx46 with a plastic duct.

5.3 TX46-CONTROL: CONCLUSION

The Tx46 control beam failed in a shear induced anchorage failure. The failure shear load was nearly the same as the calculated shear resistance. In addition, the shear resistance calculated was slightly lower than the actual shear failure value, confirming the conclusion. The AASHTO LRFD 2012 shear method is a conservative accurate calculation.

5.4 TX46-WITH A PLASTIC DUCT: CONCLUSION

When calculating the shear resistance for the Tx46 plastic duct based on the AASTHO LRFD General Shear provisions, an un-conservative shear capacity is obtained. When using the specified k-factor equal to 0.25 (General Shear) for a grouted plastic duct the V_{calc}/V_{test} ratio is 0.90, an un-conservative result. However, when

utilizing a K-factor of 1.0 the V_{calc}/V_{test} ratio is approximately 1.0. Therefore, it can be seen when using the Eurocode2 specified k-factor of 1.2 for a grouted plastic duct a conservative lower shear capacity is obtained for a full scale Tx46 with a plastic duct and an 8-inch concrete deck test specimen.

Moreover, a 14% reduction in the shear failure load was observed in Tx46 with a plastic duct compared to the Tx46 control beam for these specific testing parameters. Therefore, when utilizing a plastic duct there is a reduction in shear strength, but the drop is not as significant as in the small scale panel tests. Diagonal web cracks appeared at a shear loading of 150 kips, which was the same cracking shear loading as the Tx46 control.

5.5 FUTURE WORK

To understand the shear behavior of prestressed concrete beams with plastic ducts it is recommended to fabricate additional full scale girder specimens and compare results and trends. As part of the research required by TxDOT Project 0-6652, several shear tests on Tx62 specimens will be conducted to study the influence of a few primary experimental variables. Those experimental variables include the use a 3-inch plastic and metal duct and a control specimen with a seven-inch-thick web. In addition, another variable that will be introduced is the post-tensioning of steel strands in the web as the post-tensioning forces will most likely affect the shear strength of the girder. The results of these tests will be compared to panel test results and those of the Tx46 test with a plastic duct. From these comparisons, trends can be observed as well recommendations made for current AASHTO LRFD k-factor code provisions.

APPENDIX A

Texas Department of Transportation Standard TX Girders Series Drawings

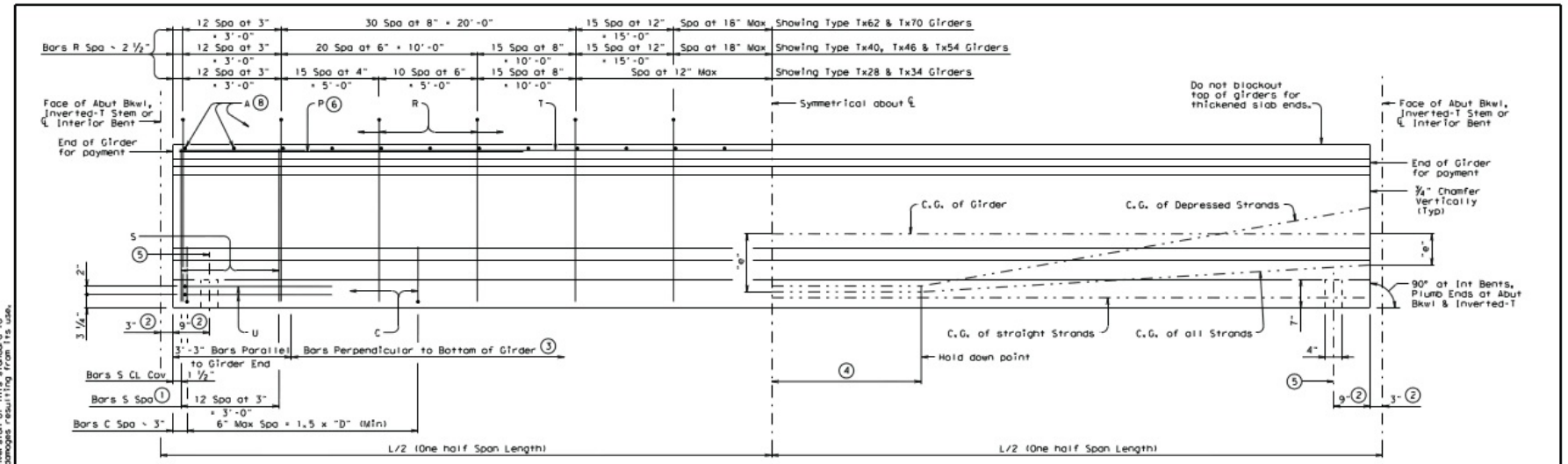

GIRDER ELEVATION

① Bundle with Bars R.

② Measured along ℄ Girder at Interior Bents; perpendicular to Abutment Bkwl or Inverted-T Stem.

③ The average of the top and bottom spacing of Bars R cannot exceed the required spacing.

④ L/20, but not less than 5'-0" (-0, +2").

⑤ ℄ 4" x 1 ½" Vertical Slotted Hole at doweled girder end (labeled (D) on Bridge Layout). Required for outside girder only or as shown on substructure details. Anchorage holes may be tapered (4 ¾" x 1 ⅜") at base. If holes are formed with sheet metal, forms may be left in place.

⑥ Bars P (#6 x 15'-0") are only required when "e" at girder ends exceeds 0.25 x "D". At the fabricator's option bars larger than #6 may be used. When L is less than 50 ft, Bars P are to be the same length as Bars T.

⑦ 1 ⅜" Clear Cover to Bars S.

⑧ Space Bars A at 6" Max for girders requiring overhang bracket hangers. Space at 12" Max for all other girders. Tie to Bars R as necessary. See standard IGMS for "Deck Forming Notes".

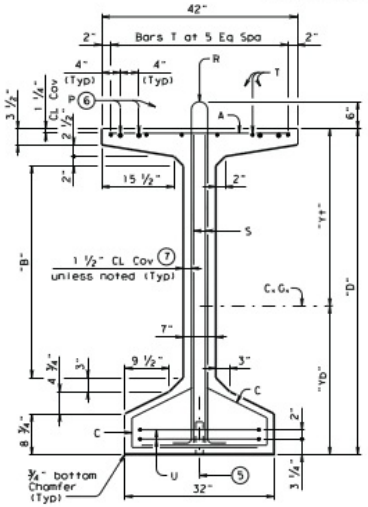

TYPE Tx62 & Tx70

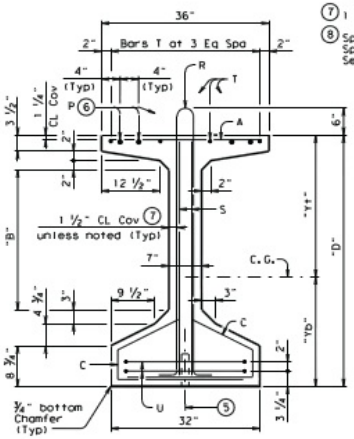

TYPE Tx46 & Tx54

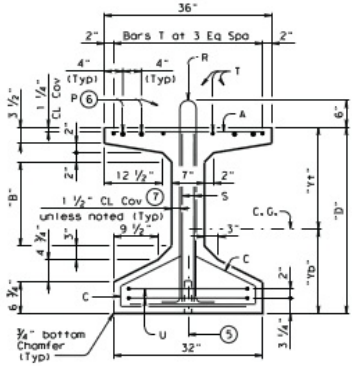

TYPE Tx28, Tx34 & Tx40

GIRDER DIMENSIONS AND SECTION PROPERTIES

Girder Type	"D" (In.)	"B" (In.)	"Yt" (In.)	"Yb" (In.)	Area (In.²)	"Ix" (In.⁴)	"Iy" (In.⁴)	Weight (plf)
Tx28	28	6	15.02	12.98	585	52,772	40,559	610
Tx34	34	12	18.49	15.51	627	88,355	40,731	653
Tx40	40	18	21.90	18.10	669	134,990	40,902	697
Tx46	46	22	25.90	20.10	761	198,089	46,478	793
Tx54	54	30	30.49	23.51	817	299,740	46,707	851
Tx62	62	37 ½"	33.72	28.28	910	463,072	57,351	948
Tx70	70	45 ½"	38.09	31.91	966	628,747	57,579	1,006

GENERAL NOTES:

Designed in accordance with AASHTO LRFD Specifications.

All concrete must be Class H. Provide Class HIHPC) if shown elsewhere in plans.

All reinforcing bars must be Grade 60.

An equal area of deformed Welded Wire Reinforcement (WWR) (ASTM A497) may be substituted for Bars A, C, R or T unless otherwise noted.

It is permissible for bars or strands to come in contact with materials used in forming anchor holes.

HL93 LOADING SHEET 1 OF 2

Texas Department of Transportation
Bridge Division

PRESTRESSED CONCRETE I-GIRDER DETAILS

IGD

File: Igdetail.dgn	Dsn: TxDOT	Ck: JAH	Dw: JTR	Ck: JAH
©TxDOT June 2007	DISTRICT	FEDERAL AID PROJECT		SHEET
REVISIONS 02/09 General Notes	COUNTY	CONTROL	SECT	JOB	HIGHWAY

DISCLAIMER:
The use of this standard is governed by the "Texas Engineering Practice Act". No warranty of any kind is made by TxDOT for any purpose whatsoever. TxDOT assumes no responsibility for errors or omissions in these standards or other formats or for incorrect results or damages resulting from its use.

LEVELS DISPLAYED PATHS

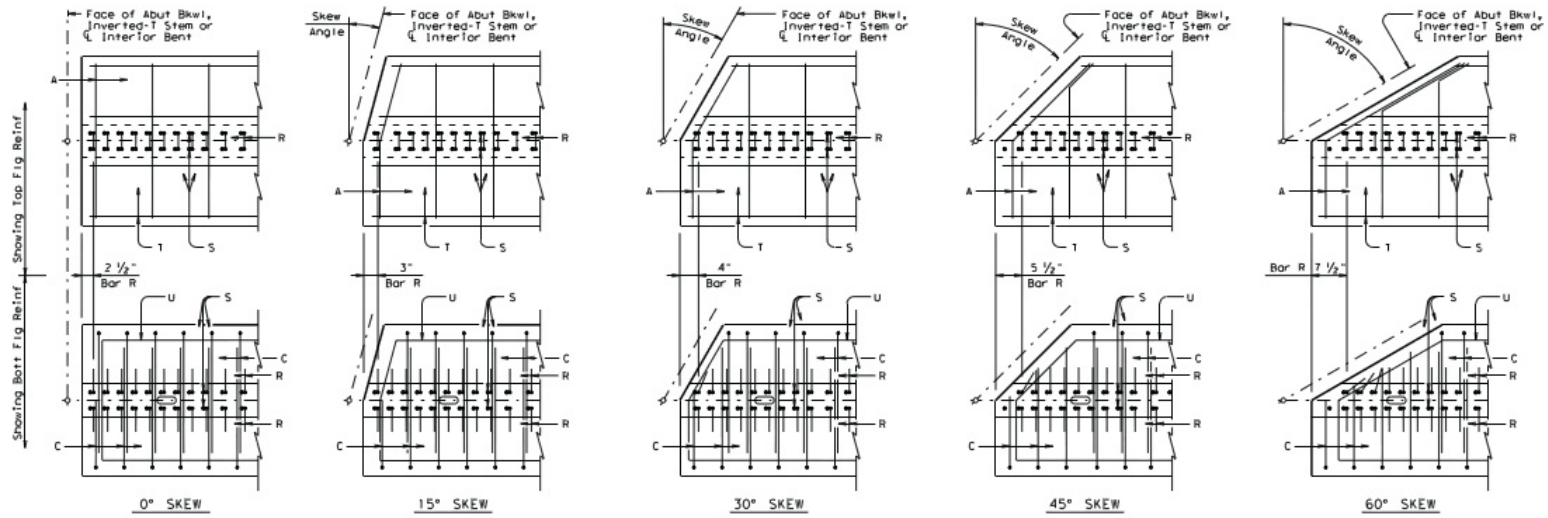

PLAN OF GIRDER ENDS (9)

(9) Reinforcing patterns shown are provided as guides to determine reinforcement placement in skewed ends. Place Bars S as close to girder end as cover requirements permit, which may prevent them to be bundled with Bars R.

(10) Bars may be cut or bent at skewed end as required.

(11) Increase as necessary for bars at skewed end.

(12) No portion of bar less than 10 ft.

(13) For Welded Wire Reinforcement (WWR) option, area of Bars R may be reduced in proportion to the increase in reinforcement yield strength over 60 ksi. Yield strength of WWR is limited to 75 ksi.

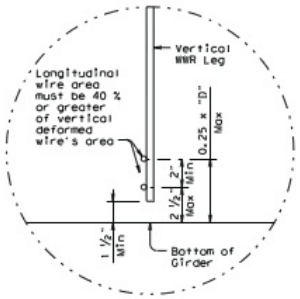

OPTIONAL WELDED WIRE REINFORCEMENT (WWR) DETAIL

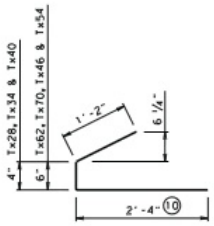

BARS C (#4)

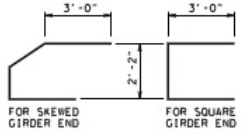

BARS U (#5)

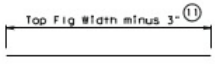

BARS A (#3)

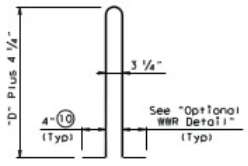

BARS R (#4) (13)

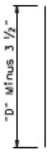

BARS S (#6)

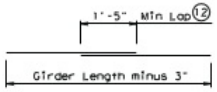

BARS T (#4)

HL93 LOADING SHEET 2 OF 2

Texas Department of Transportation
Bridge Division

PRESTRESSED CONCRETE I-GIRDER DETAILS

IGD

File: tgdstan1.dgn	Dsn: TxDOT	Ck: JAH	Dw: JTR	Ck: JAH
©TxDOT June 2007	DISTRICT	FEDERAL AID PROJECT		SHEET
REVISIONS 02/08 General Notes	COUNTY	CONTROL	SECT	JOB	HIGHWAY

APPENDIX B

Texas Department of Transportation Standard Elastomeric Bearing and Girder End Details

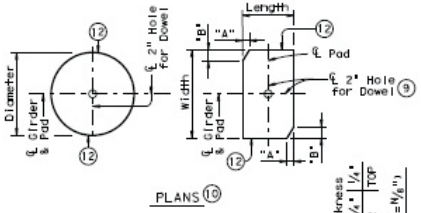

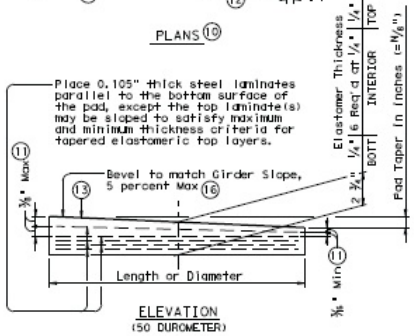

LAMINATED
ELASTOMERIC BEARING DETAILS (14)

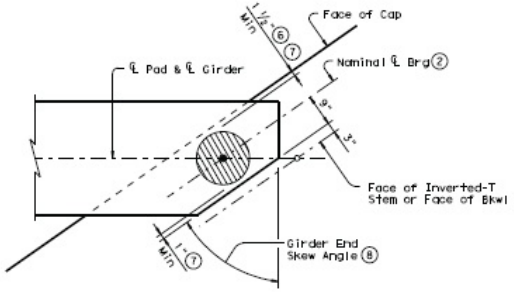

ROUND BEARINGS FOR
SKEWED GIRDER ENDS AT FACE OF
INVERTED-T STEM OR FACE OF BKWL

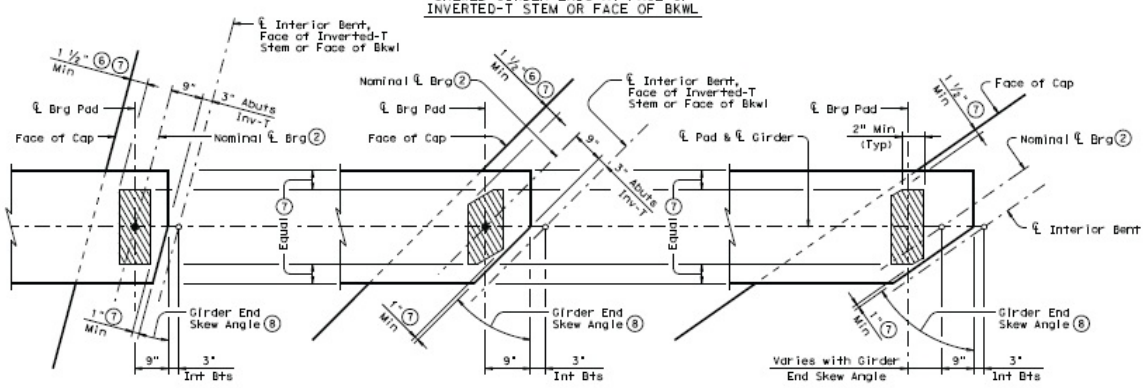

SKEWED GIRDER ENDS
AT INT BENTS, FACE OF
INVERTED-T STEM OR FACE OF BKWL

SKEWED GIRDER ENDS
AT CONVENTIONAL
INTERIOR BENTS (17)
(No Girder Dowels)

ELASTOMERIC BEARING PLACEMENT DIAGRAMS

TABLE OF MINIMUM SUBSTRUCTURE DIMENSIONS (15)			
Girder Type	Abutments	Int Bents	Inv-T Bents
	Face of Bkwl to Face of Cap	Overall Cap Width	Corbel Width
Tx28 thru Tx54	1'-9"	3'-6"	1'-10 ½"
Tx62 & Tx70	2'-0"	4'-0"	2'-1 ½"

ELASTOMERIC BEARING DATA TABLE						
Bent Type	Girder Type	Bearing Type (13)	Girder End Skew Angle Range	Pad Size Lgth x Width	Pad Clip Dimensions "A"	Pad Clip Dimensions "B"
ABUTMENTS, INVERTED-T AND TRANSITION BENTS WITH BACKWALLS	Tx28, Tx34, Tx40, Tx46 & Tx54	G-1-"N"	0° thru 21°	8" x 21"	---	---
		G-2-"N"	21°+ thru 30°	8" x 21"	1 ½"	2 ½"
		G-3-"N"	30°+ thru 45°	9" x 21"	4 ½"	4 ½"
		G-4-"N"	45°+ thru 60°	15" Dia	---	---
	Tx62 & Tx70	G-5-"N"	0° thru 21°	9" x 21"	---	---
		G-6-"N"	21°+ thru 30°	9" x 21"	1 ½"	2 ½"
		G-7-"N"	30°+ thru 45°	10" x 21"	4 ½"	4 ½"
		G-8-"N"	45°+ thru 60°	10" x 21"	7 ¼"	4 ¼"
CONVENTIONAL INTERIOR BENTS	Tx28, Tx34, Tx40, Tx46 & Tx54	---	---	---	---	---
		---	---	---	---	---
		G-1-"N"	0° thru 60°	8" x 21"	---	---
	Tx62 & Tx70	G-5-"N"	0° thru 60°	9" x 21"	---	---
CONVENTIONAL INTERIOR BENTS WITH SKEWED GIRDER ENDS (GIRDER CONFLICTS) (17)	Tx28, Tx34, Tx40, Tx46 & Tx54	G-1-"N"	0° thru 18°	8" x 21"	---	---
		G-2-"N"	18°+ thru 30°	8" x 21"	1 ½"	2 ½"
		G-9-"N"	30°+ thru 45°	8" x 21"	3"	3"
		G-10-"N"	45°+ thru 60°	9" x 21"	6"	3 ½"
	Tx62 & Tx70	G-5-"N"	0° thru 18°	9" x 21"	---	---
		G-5-"N"	18°+ thru 30°	9" x 21"	---	---
		G-11-"N"	30°+ thru 45°	9" x 21"	1 ½"	1 ½"
		G-12-"N"	45°+ thru 60°	9" x 21"	3"	1 ¾"

(2) For purposes of computing Bearing Seat Elevations, nominal centerline of bearing must be defined as shown. The actual center of bearing pad may vary from this line.

(6) 3" for Inverted-T.

(7) Factors controlling laminated bearing placement if no dowel is present. Place Centerline Pad as near Nominal Centerline Brg as possible between limits shown.

(8) Girder end skew angle is equal to 90° minus the girder angle except at some conflicting girders.

(9) Provide 2" Dia Hole only at locations required. See substructure details for location.

(10) See Elastomeric Bearing Data Table for dimensions.

(11) Maximum and minimum layer thicknesses shown are for elastomer only, on tapered layers.

(12) Locate Permanent Mark here.

(13) BEARING TYPE must be indicated on all pads. For tapered pads, BEARING TYPE must be located on the high side. The Fabricator must include the value of "N" (amount of taper in ⅛" increments) in this mark.
Examples: N=0, (for 0" taper)
N=1, (for ⅛" taper)
N=2, (for ¼" taper)
(etc.)
Fabricated pad top surface slope must not vary from plan girder slope by more than $\left(\frac{0.0625"}{\text{Length or Dia}}\right)$ IN/IN.

(14) The use of Polyisoprene (natural rubber), for the manufacture of bearing pads, is not permitted.

(15) Substructure dimensions must satisfy the minimums provided to accommodate the elastomeric bearings shown on this standard.

(16) See sheet 3 of 3 for beveled plate use when slopes exceed 5 percent.

(17) If girder end is skewed for a girder conflict at an interior bent and a beveled sole plate is required, use bearing type for abutments at this location. Location of bearing centerline is to be set as for abutments in this case.

HL93 LOADING SHEET 2 OF 3

Texas Department of Transportation
Bridge Division

ELASTOMERIC BEARING AND GIRDER END DETAILS
PRESTR CONCRETE I-GIRDERS

IGEB

FILE: igebstel.dgn	DN: AEE	CK: JMH	DW: JTR	CK: TxDOT
©TxDOT June 2007	DISTRICT	FEDERAL AID PROJECT		SHEET
REVISIONS 12/13: Added Sole Plate details.	COUNTY	CONTROL	SECT	JOB	HIGHWAY

PATH:

LEVEL DEFLUNG

APPENDIX C

Stressing Pressure Guide for Tx46

To properly fabricate the Tx46 and fail the beam in shear several design considerations had to be met. Initially, the prestressed strands had to be stressed f_p=202.5ksi. The spread sheet below shows the properties of the steel strands and the geometry of the rams and the required pressure to the top and bottom rams needed to achieve that stress and the expected displacement due to the stressing.

STRESSING PRESSURES GUIDE

Project:	6652	Specimen:	Tx46-Duct
Date:	19-Jan-12	Operator:	AMM

E_{wire}=	31500	ksi	effective wire modulus
E_{strand}=	28000	ksi	measured strand modulus
A_{ram}=	86.79	in^2	area of each ram
L=	50.0625	ft	length of strand
n=	48	--	number of strands
f_r=	270	ksi	stress of rupture
f_p=	202.5	ksi	final prestressing strand stress
A=	0.153	in^2	area of one strand
F_p=	31.0	kip	force on one strand
F_{all}=	1487	kip	total force on all strands
$A_{smallram}$=	4.5	in^2	area of single-strand stressing jack
x=	18.75	in	distance from BOTTOM rams to centroid
h=	41.5	in	distance between rams
F_{bot}=	**815**	kip	final force in bottom rams
F_{top}=	**672**	kip	final force in top rams
f_{bot}=	**4.70**	ksi	stress in bottom rams
f_{top}=	**3.87**	ksi	stress in top rams

f_{ram} ksi	Fract	$Force_{tot}$ kip	$Stress_{bot}$ psi	$Stress_{top}$ psi	f_{strand} ksi	ε_{strand} in./in.	Disp. in.	Check
0	0	0	0	0	0.0	0.00000	0.00	OK
700	10	149	500	400	20.3	0.00064	0.43	OK
1400	20	297	900	800	40.5	0.00129	0.87	OK
2100	30	446	1400	1200	60.8	0.00193	1.30	OK
2800	40	595	1900	1500	81.0	0.00257	1.74	OK
3400	50	744	2300	1900	101.3	0.00321	2.17	OK
4100	60	892	2800	2300	121.5	0.00386	2.61	OK
4800	70	1041	3300	2700	141.8	0.00450	3.04	OK
5500	80	1190	3800	3100	162.0	0.00514	3.48	OK
6200	90	1338	4200	3500	182.3	0.00579	3.91	OK
6900	100	**1487**	**4700**	**3900**	202.5	0.00643	4.34	OK

PX READ

Updated: May 22, 2010

APPENDIX D

Debonded Strand Elongations

Initial Jacking Load	4.5	k
E	29000	ksi
Strand Area	0.153	in^2
Prestress	202.5	ksi
Total Prestressing Force	30.983	k
Additional Force for Elongation	26.483	k
Bulkhead Width (N and S)	12	in
Space between bulkhead and beam end (S)	97.5	in
Space between bulkhead and beam end (N)	117.5	in
Beam Length	360	in
Debonding		
South End		
Termination Point From S End (in)	72	
		Termination From S End of Beam (in)
South End (Measured From Dead End)		
Final Debonding Location (in)	181.500	72
Initial Debonding Location (in)	180.423	70.923
Elongation Needed (in)	1.077	
Elongation Achieved (in)	1.077	
Goal Seek	0	
Termination Point From N End (in)	72	
		Termination From N End of Beam (in)
North End (Measured From Dead End)		
Final Debonding Location (in)	397.5	72
Initial Debonding Location (in)	395.142	74.358
Elongation Needed (in)	2.358	
Elongation Achieved (in)	2.358	
Goal Seek	0	

APPENDIX E

Tx46 control beam top and bottom stresses along half the length of the beam due to prestressing

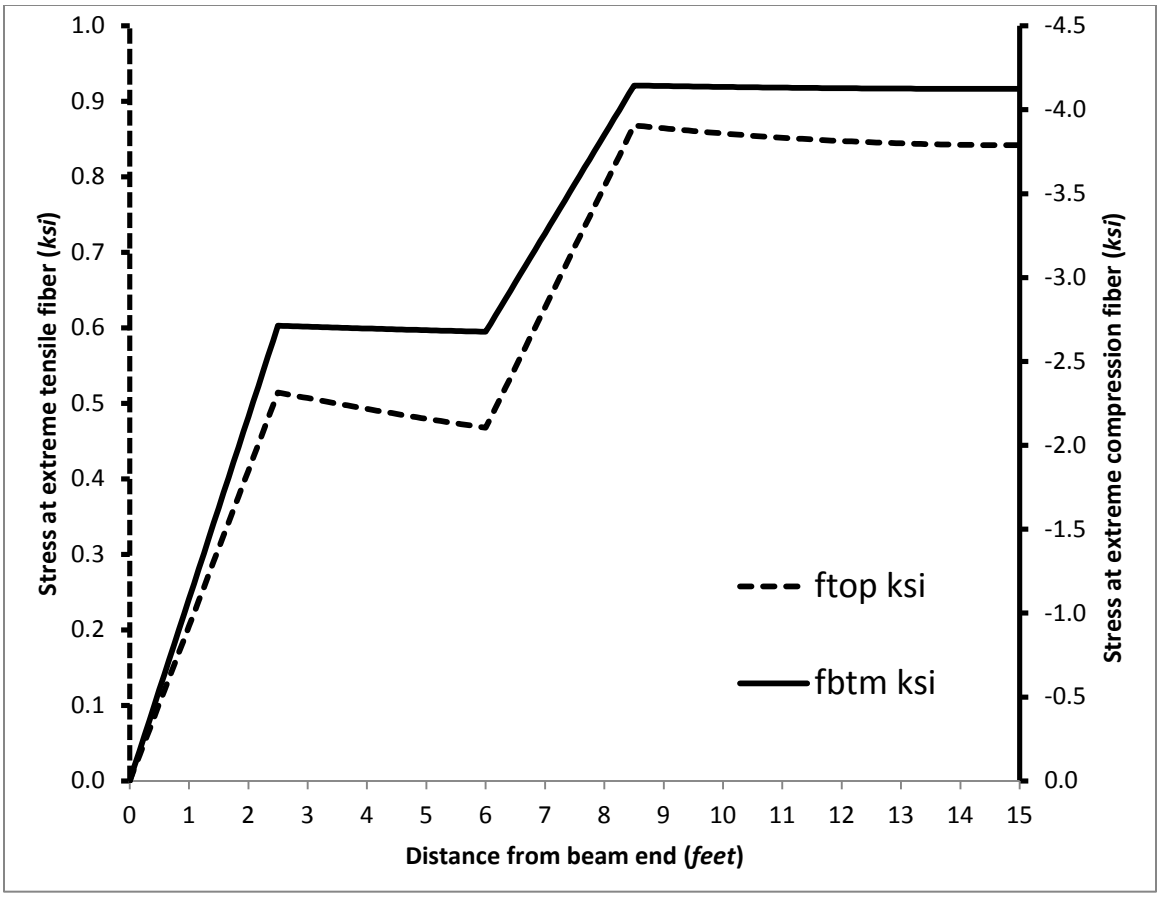

APPENDIX F

Flexure Capacity

This appendix provides calculated moment capacity of the Tx46 with a 6-feet wide 8-inch deck. The design includes 48 prestressed strands and its corresponding location and concrete strength of the beam and deck.

Concrete Properties

Type	fc' (psi)	εo	ϕ	εsh	$\alpha 1$	$\alpha 2$	εcu	Comments
1	9700	0.0025	2.5	0	0.00	0.00	0.003	Beam
2	9900	0.0025	2.5	0	0.00	0.00	0.003	Deck

Type	Ecs (ksi)	Ect (ksi)	εcr	Ec eff (ksi)	εo eff	ft'eff (ksi)	Comments
1	5613.8	7760	0.00008	2217.1	0.00875	0.169	Beam
2	5671.4	7920	0.00005	2262.9	0.00875	0.114	Deck

Reinforcement Bars Properties

Type	fy (ksi)	E (ksi)	εsth	εsu	fu (ksi)
1	61.1	29000	0	0.12	91.6

Strand Properties

Type	fpu (ksi)	Ep (ksi)	εpu	Relax (%)	Ramberg-Osgood			Epeff (ksi)
					A	B	C	
1PreTens	270.00	30000.00	0.040	0.05	0.025	118.00	10.00	28500
2PostTens	0.00	0.00	0.000	0.00	0.000	0.00	0.00	0

Section Geometry

Gross Section

Section Depth	54	[in.]
Moment Axis	31	[in.]
How many layers?	9	

Layer Number	y (in)	bottom width (in)	top width (in)	height (in)	Type Number
1	0	30.5	32	0.75	1
2	0.75	32	32	8	1
3	8.75	32	13	4.75	1
4	13.5	13	7	3	1
5	16.5	7	7	22	1
6	38.5	7	11	2	1
7	40.5	11	36	2	1
8	42.5	36	36	3.5	1
9	46	72	72	8	2

Prestressing Strands

How many layers? 4

Layer Number	y (in)	Area (in^2)	Prestrain	Type Number
1	2.5	2.142	0.006983	1
2	4.5	2.142	0.006983	1
3	6.5	2.142	0.006983	1
4	8.5	0.918	0.006983	1

Cross Section

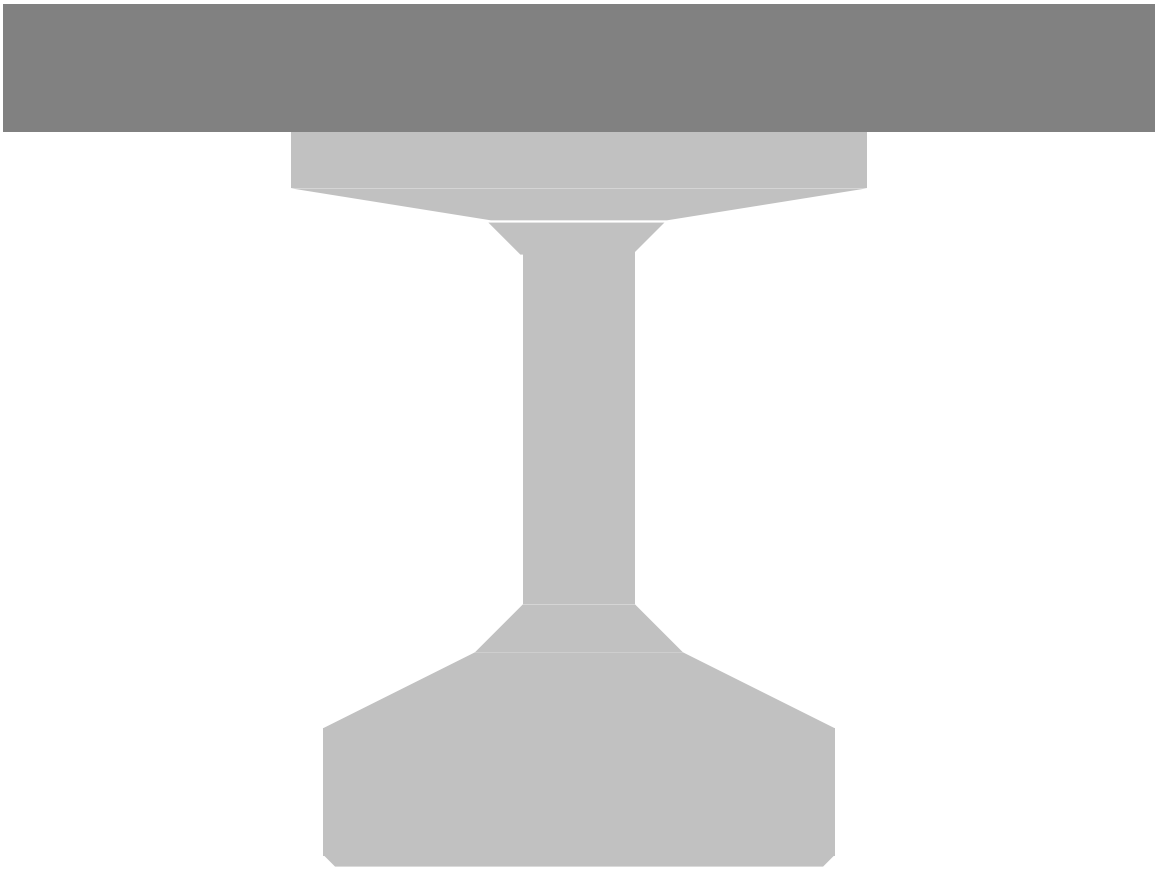

Area (in²)	yb (in)	yt (in)	Inertia (in^4)	Approx Area
1337.31	32.98	21.02	411294.41	1332.81

Moment Curvature Response

		Strains				
Curvature x 10^6	Moment (kips*ft)	εct	εcna	εcb	N (kips)	iter
-0.000514	-275.86	0.024516	0.012687	-0.003256	-0.225	17
-0.000486	-325.34	0.023291	0.012120	-0.002938	0.339	9
-0.000457	-324.16	0.021877	0.011363	-0.002809	-0.843	15
-0.000429	-318.54	0.020459	0.010602	-0.002684	-0.114	13
-0.000400	-312.16	0.019045	0.009845	-0.002555	0.190	13
-0.000371	-304.45	0.017628	0.009085	-0.002430	0.956	11
-0.000343	-301.32	0.016208	0.008322	-0.002307	-0.832	14
-0.000314	-290.27	0.014792	0.007563	-0.002180	0.373	10
-0.000286	-282.93	0.013376	0.006804	-0.002053	-0.855	15
-0.000257	-269.48	0.011964	0.006050	-0.001922	-0.217	10
-0.000229	-254.82	0.010552	0.005295	-0.001791	0.403	14
-0.000200	-240.77	0.009144	0.004544	-0.001656	-0.822	8
-0.000171	-217.64	0.007743	0.003801	-0.001514	-0.173	15
-0.000143	-189.25	0.006349	0.003063	-0.001365	0.306	13
-0.000114	-152.87	0.004962	0.002334	-0.001209	0.740	14
-0.000086	-102.05	0.003589	0.001617	-0.001040	0.703	19
-0.000057	-26.81	0.002230	0.000916	-0.000855	-0.105	13
-0.000029	108.45	0.000895	0.000238	-0.000647	0.193	16
0.000000	3315.98	-0.000140	-0.000140	-0.000140	0.414	20
0.000029	5937.99	-0.000446	0.000211	0.001097	0.877	18
0.000057	6501.20	-0.000628	0.000686	0.002458	-0.320	18
0.000086	6757.38	-0.000775	0.001197	0.003854	-0.335	16
0.000114	6879.77	-0.000903	0.001726	0.005269	0.779	17
0.000143	6958.84	-0.001021	0.002264	0.006693	0.734	14
0.000171	7019.77	-0.001132	0.002811	0.008125	-0.022	19
0.000200	7068.22	-0.001235	0.003365	0.009565	0.312	19
0.000229	7111.53	-0.001332	0.003926	0.011011	0.223	16
0.000257	7153.89	-0.001427	0.004488	0.012459	-0.636	16
0.000286	7190.12	-0.001518	0.005054	0.013911	0.656	16
0.000314	7227.91	-0.001606	0.005622	0.015365	-0.180	17
0.000343	7261.54	-0.001692	0.006193	0.016822	0.681	18
0.000371	7296.52	-0.001780	0.006763	0.018277	0.610	18
0.000400	7331.29	-0.001863	0.007337	0.019737	-0.619	16
0.000429	7364.44	-0.001949	0.007908	0.021194	-0.632	14
0.000457	7393.78	-0.002028	0.008486	0.022657	0.508	17
0.000486	7427.92	-0.002113	0.009058	0.024115	-0.974	14
0.000514	7456.88	-0.002192	0.009636	0.025579	-0.087	17
0.000543	7487.08	-0.002274	0.010211	0.027040	0.050	17
0.000571	7516.46	-0.002357	0.010785	0.028500	0.524	15
0.000600	7547.06	-0.002442	0.011358	0.029958	0.101	18
0.000629	7574.41	-0.002520	0.011938	0.031423	0.868	16
0.000657	7604.69	-0.002604	0.012511	0.032882	0.031	15
0.000686	**7631.93**	**-0.002688**	**0.013084**	**0.034341**	**0.840**	**8**

0.000714	3094.87	-0.001602	0.014827	0.036970	-0.534	12
0.000743	0.00	0.000500	0.017586	0.040614	0.000	3

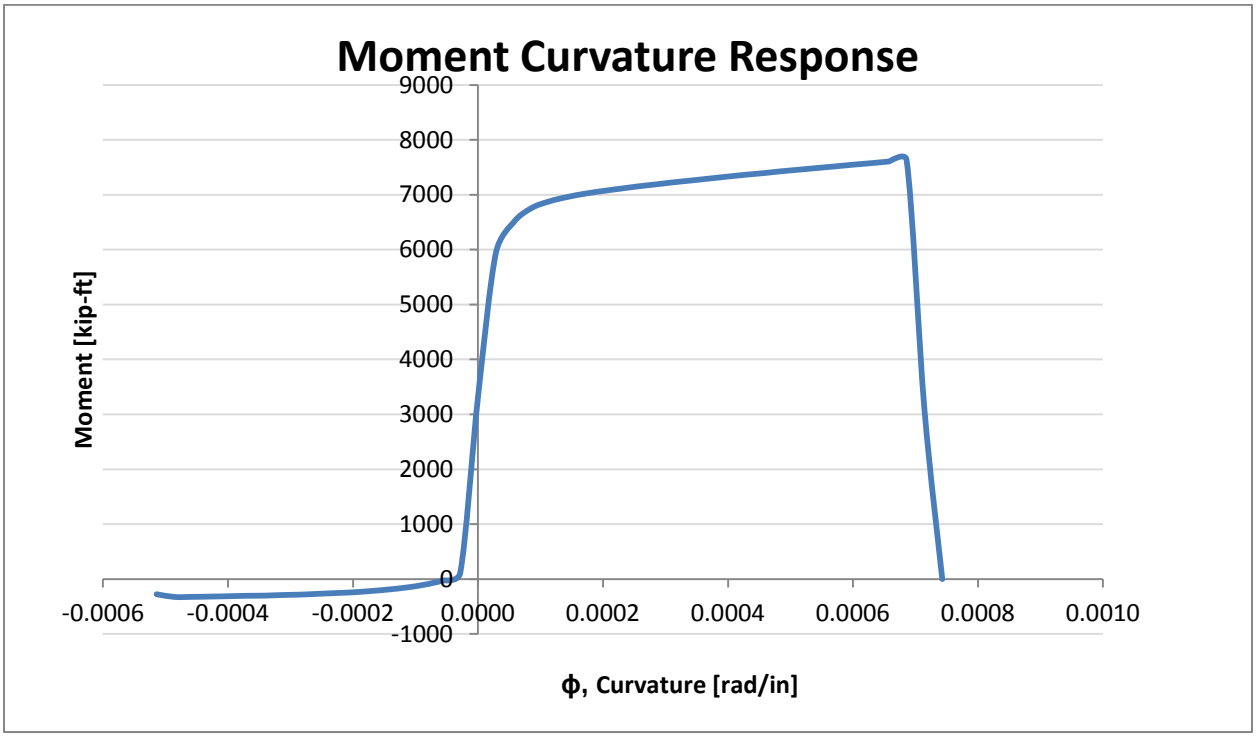

Max Moment Capacity **7631.93 k-ft** at $\phi=6.86x10^{-4}$

APPENDIX G

Tx46 Control Beam Dead Loads

This appendix provides tables of the self-weight to the Tx46 control beam and the load frame prior to applying load. The self-weight of the beam does include the 6-feet wide, 8-inch deck. In addition, from the self-weight, load frame and applied load, a moment and shear diagram was developed, which verified an exceeded flexure capacity.

Beam			
1	2	6	7
LC_SE	LC_SW	LC_NE	LC_NW
16.628	3.475	2.923	17.563
16.628	3.490	2.957	17.626
16.584	3.485	2.991	17.597
16.609	3.514	3.054	17.553
16.851	3.402	3.006	17.679
16.660	3.473	2.986	17.604

Load Frame			
1	2	6	7
LC_SE	LC_SW	LC_NE	LC_NW
5.298	3.988	1.482	7.602
5.288	3.954	1.496	7.593
5.288	4.026	1.525	7.593
5.085	4.268	1.589	7.603
5.399	3.944	1.671	7.661
5.271	4.036	1.553	7.610

Beam Self-Weight			
Total:	40.723		
South:	20.133	20.362	Avg
North:	20.590		

Load Frame		
Total:	18.470	
South:	9.307	
North:	9.163	
Average V:	9.235	Avg

LC-Load Cell
SE-South East NE-North East
SW-South West NW-North West

Failure point load			
	w/Plastic Duct	Control	Units
Self-Weight	1.3567	1.3567	Kips/ft
Test Frame & Rods	20.40	20.43	kips
Applied Point Load at Failure	886.39	1025.78	kips
Superimposed shear and moment (point load at failure, self-weight, load frame, rods)			
V	468.997	538.7	kips
M	5295.44	6097.11	k-ft

Results obtained from SAP2000

HIGHEST SHEAR AND MOMENT CASE - Tx46 Control Beam with self-weight, load frame, rods, applied point load at failure (shear & moment diagram)

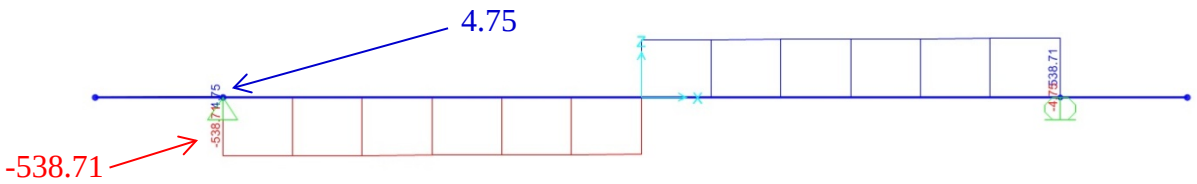

Tx46 control shear diagram(over-hang shear is due to self-weight)

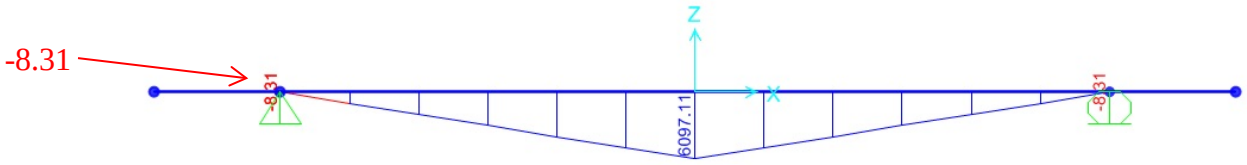

Tx46 Control moment diagram

Actual moment at failure 6097.11 k-ft < Calculated Moment Resistance 7631.93 k-ft **OK**

APPENDIX H

This appendix provides the stress vs. strain graph for the transverse reinforcement, R-bars used in the Tx46 beam with a plastic duct and the Tx46 control beam. The test followed ASTM A370 and A615 specifications. The calculated load rate was 0.72-kips per second as shown in Equation I-1 prior to yield. After yielding the load rate was changed to approximately 0.02" per second.

Equation I-1 $$\frac{1/_{16}*EA}{L*60}$$

Where: E = 29000, modulus of elasticity for steel [ksi]

A = 0.2, area of No. 4 bar [in^2]

L = 8, length of extensometer [in]

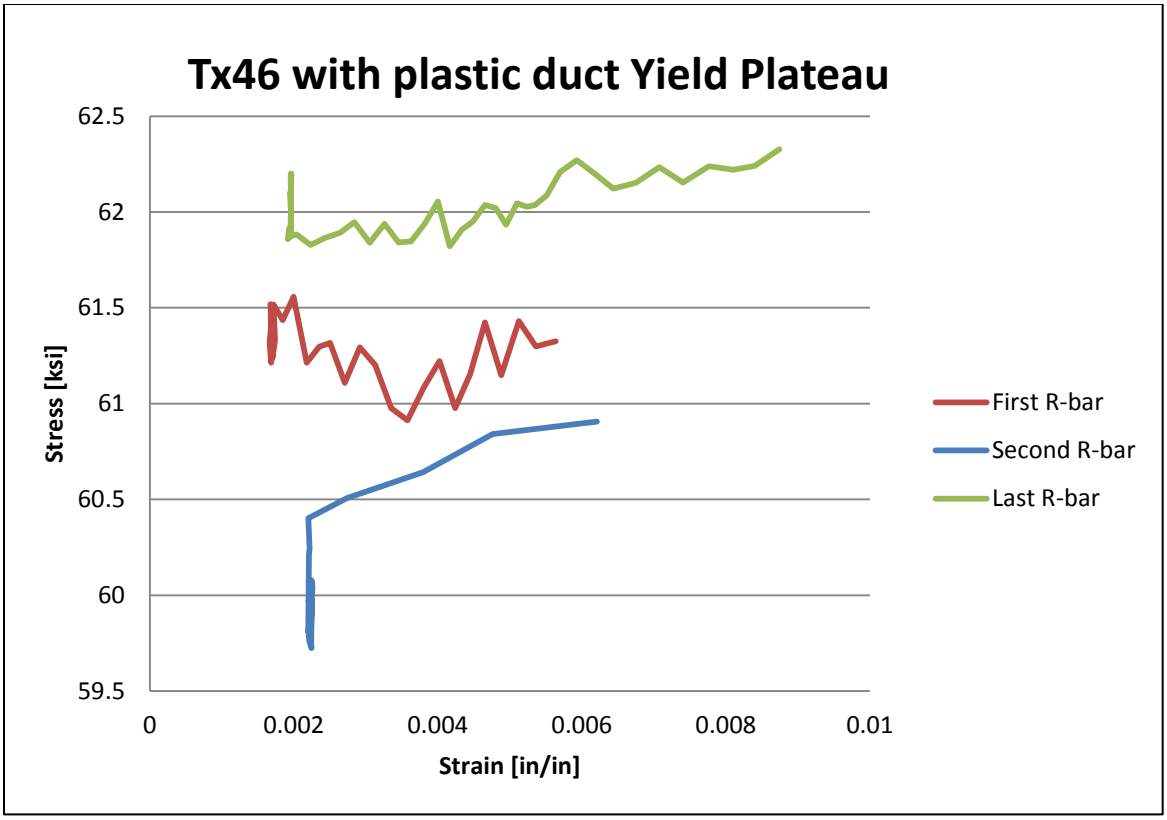

Stress vs. Strain graph yield plateau of the R-bars used in the Tx46 with plastic duct

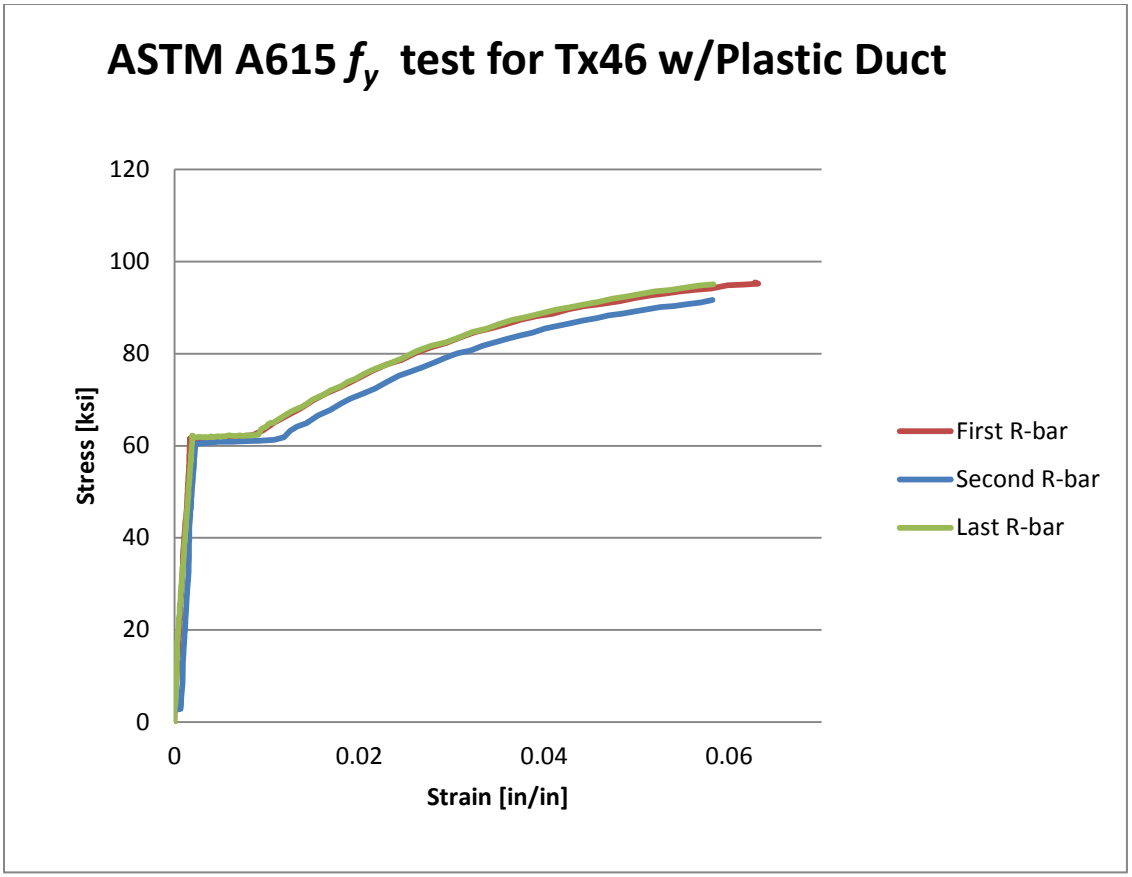

Stress vs. Strain graph of the R-bars used in the Tx46 beam with plastic duct

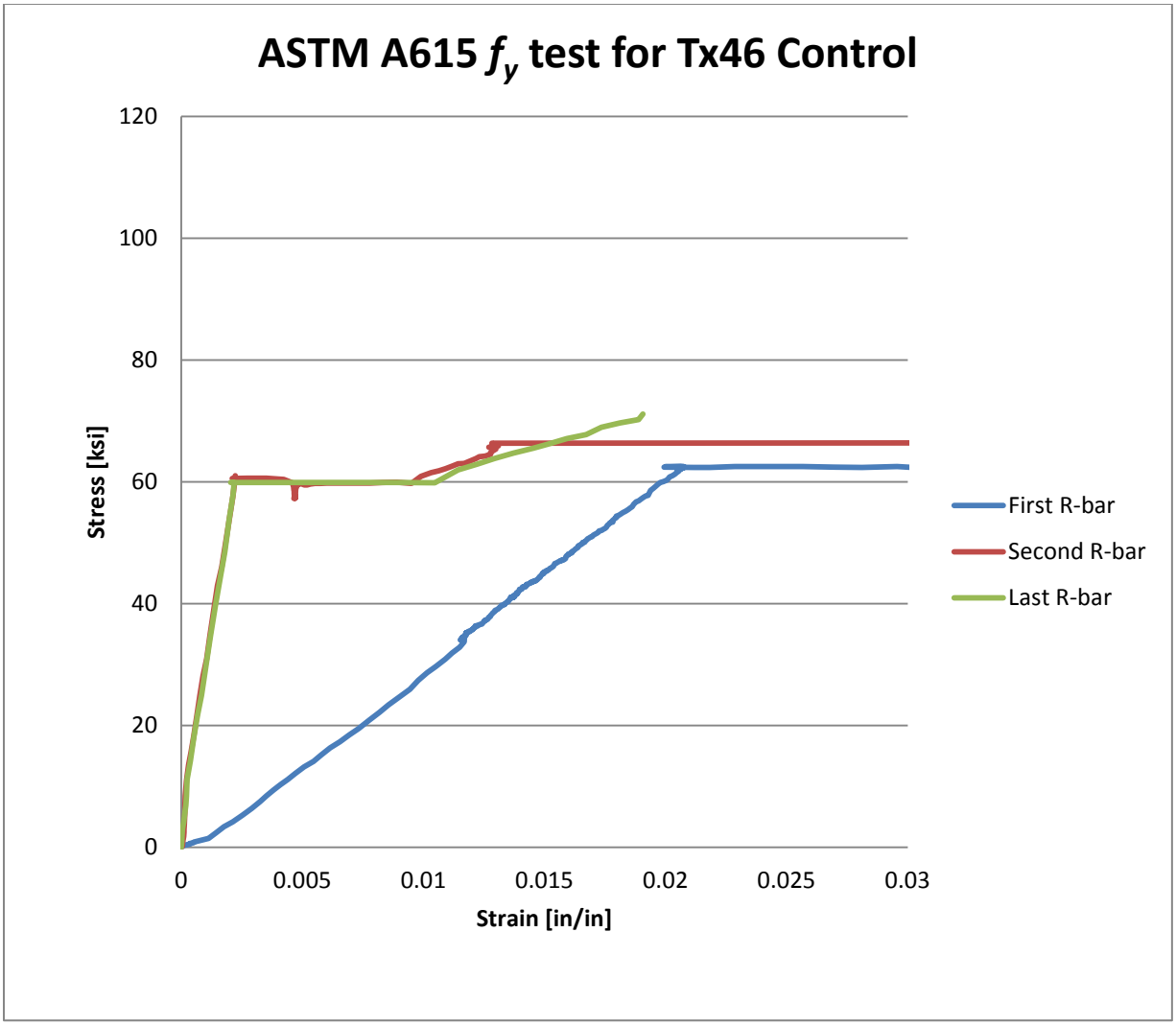

Stress vs. Strain graph of the R-bars used in the Tx46 Control

APPENDIX I

Tx46 Beam with a Plastic Duct Shear Capacity per AASHTO LFRD 2012 provisions

This appendix provides the input, equations and output used to calculate the shear capacity of the Tx46 beam with a plastic duct.

(Excel program written by Andrew Moore)

Geometry and Concrete Properties of Test Performed					
Beam			**Deck if No Deck Top Flange**		
h_{beam}	46	*inch*	h_{deck}	8	*inch*
$f'_{c\ beam}$	9.7	*ksi*	$f'_{c\ deck}$	9.9	*ksi*
b_v (k=1.4)	2.8	*inch*	$b_{eff\ deck}$ OR $b_{eff\ top\ flange}$	72	*in*
Web Width Gross	7	*inch*			
E_C	5614	*ksi*			
A_{ct}	490	in^2			

Steel Properties					
Prestressing Steel Properties			**Mild Steel Properties**		
Total # Strands	48	*unitless*	Compression Steel in Deck		
Area of Each Strand	0.153	in^2/ *strand*	A'_s	0	in^2
f_{Pu}	270	*ksi*	f'_s	60	*ksi*
$\bar{y}_P$ at critical sect.	5	*inch*	Tension Steel in Beam (if added then need mod.s)		
V_P at critical sect.	0	*kips*	A_s	0	in^2

f_{po}	189	*ksi*	f_y	60	*ksi*
Type of Strand	low lax	*text*	E_s	29000	*ksi*
E_P	28500	*ksi*	Transverse Steel in Beam		
$\bar{y}_P$ at beam end	5	*inch*	Minimum Shear Steel?	YES	*yes or no*
$\bar{y}_P$ at mid-span	5	*inch*	α	90	*degrees*
			A_v	0.4	in^2
			$f_{y\ v}$	61.06	*ksi*
			s	6	*inch*

Miscellaneous Properties

Load Properties			Other Properties		
M_u	15039.131	*kip-in*	φ	0.9	*unitless*
N_u	0	*kips*	Width of Bearing Pad	9	*inches*
V_u	290	*kips*	Shear Span	138	*inches*
			Total Span Length	276	*inches*

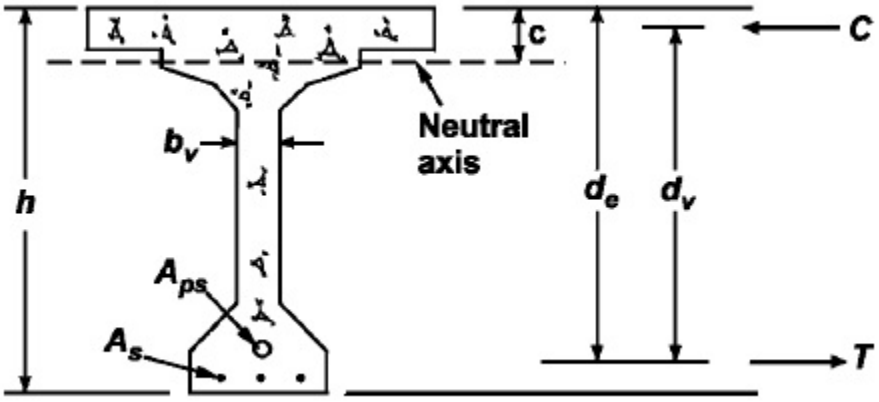

Figure F-1 Illustration of the terms b_v and d_v

2012 AASHTO LRFD BRIDGE DESIGN SPECIFICATIONS: CONCRETE STRUCTURES		
Code Provision	**Equation**	**Comments**
5.7.3.1.1-4	$C = \frac{A_{ps}f_{pu}+A_s f_y - A'_s f'_s}{0.85 f'_c \beta_1 b_{eff} + k A_{ps}\frac{f_{pu}}{d_p}}$	Rectangular Section
5.7.2.2	β_1 = 0.85-0.05(f'$_c$-4), β ≥0.65	Ratio of the depth of the of equiv. stressed comp. zone to the actual comp. zone
5.5.4.2	Φ = 0.9	Reduction factor for shear design
5.8.3.4.2-1	$\beta = \frac{4.8}{1+(750+\varepsilon_s)}$	Factor of diagonal cracked concrete to transmit tension
5.8.3.4.2-3	Θ = 29 + 3500ε_s	Angle of inclination of diagonal compressive stress
5.8.3.2-2	0.5d_v cotΘ	Critical section
5.8.2.9-2	$d_e = \frac{A_{ps}f_{ps}d_p + A_s f_y d_s}{f_{ps}A_{ps} + A_s f_y}$	Depth of the extreme comp. fiber to the centroid of tensile reinforcement
5.8.2.9	$d_v < \begin{matrix}0.9d_e \\ 0.72h\end{matrix}$	Effective shear depth
5.8.2.9-1	$V_u = \frac{\lvert V_u - \Phi V_p \rvert}{\Phi b_v d_v f'_c}$	Shear stress factor
5.8.2.5-1	$A_v \geq 0.0316\sqrt{f'_c}\frac{b_v S}{f_y}$	Minimum required shear reinforcement area
5.8.3.4.2-4	$\varepsilon_s = \frac{\frac{\lvert M_u \rvert}{d_v} + 0.5N_u + \lvert V_u - V_p \rvert - A_{ps}f_{po}}{E_s A_s + E_{ps}A_{ps}}$	Longitudinal strain
5.7.3.2.2-1	$M_n = A_{ps} f_{ps}(d_p + \frac{a}{2})$	Moment capacity from prestress strands
5.8.3.3-3	V_c =0.0316 $\beta\sqrt{f'_c}b_v d_v$	Concrete shear strength, 0.0316 conversion factor from sq. rt. of psi to ksi
5.8.3.3-4	$V_s = \frac{A_v f_y d_v (\cot\theta + \cot\alpha)\sin\alpha}{s}$	α – angle of transverse stirrups
	$V_s = \frac{A_v f_y d_v (\cot\theta)}{s}$	α = 90^o for transverse stirrups
5.8.3.3-1	$V_n = V_c + V_s + V_p$	Nominal shear resistance
5.8.3.3-2	$V_n = 0.25 f'_c b_v d_v + V_p$	The 0.25 is the upper limit intended to ensure the concrete in the web of the beam will not crush prior to yielding of the transverse reinforcement, “stirrups”

Figure F-2 Values ok* k *for Eq. 5.7.3.1.1-4 in determining the depth of the compression block, "c"

Type of Tendon	f_{py}/f_{pu}	Value of k
Low relaxation strand	0.90	0.28
Stress-relieved strand and Type 1 high-strength bar	0.85	0.38
Type 2 high-strength bar	0.80	0.48

Calculated Constants for MCFT from AASHTO LRFD 2012			
Constant	Value	Units	Description
A_{ps}	7.344	in^2	total area of prestressing steel
$h_{composite}$	54	*inch*	height of deck and girder
d_p	49	*inch*	dist. from extreme ten. to extreme comp
d_e	41	*inch* **	** not the same d_e reported in shear section
c	4.89	*inch*	distance from extreme comp fiber to neutral axis
k	0.28	*unitless*	
β_1	0.65	*unitless*	
a	3.18	*inch*	
f_{ps}	262.4	*ksi*	
M_n	91378	*kip * inch*	
M_U limit	13735	*kip * inch*	used in calculating ε
θ	28.08	*degrees*	
d_v	47.41	*inch*	d_v is calc. here as per AAHSTO specifications
critical section	51.9	*inch*	from the support
ε_s	0.00026387	*in / in*	
β	6.0	*unitless*	
V_C	78	*kips*	
V_S	362	*kips*	
Limited 0.25?	YES	yes/no	upper bound on shear strength met
Stress Factor	0.342	*unitless*	This is the value for comparison to AASHTO limit of 0.25
V_n	322	*kips*	

V_n unlimited	440	*kips*	
φ	0.9	*unitless*	
φV_n	290	*kips*	
critical section	51.9	*inch*	critical section for iteration from the support
difference in V	0.000E+00	*kips*	difference between the calculated and assumed shear
$V_U = V_n * \varphi$	290	*kips*	
Roots	27.7	*unitless*	this is the roots value of Vs when units are in psi

Tx46 Control Beam Shear Capacity per AASHTO LFRD 2012 provisions

This appendix provides the input to calculate the shear capacity of the Tx46 control beam. (Excel program written by Andrew Moore)

Geometry and Concrete Properties of Test Performed

Beam			Deck if No Deck Top Flange		
h_{beam}	46	*inch*	h_{deck}	8	*inch*
$f'_{c\ beam}$	8.69	*ksi*	$f'_{c\ deck}$	9.95	*ksi*
b_v	7	*inch*	$b_{eff\ deck}$ OR $b_{eff\ top\ flange}$	72	*in*
Web Width Gross	7	*inch*			
E_C	5314	*ksi*			
A_{ct}	490	in^2			

Steel Properties

Prestressing Steel Properties			Mild Steel Properties		
Total # Strands	32	*unitless*	Compression Steel in Deck		
Area of Each Strand	0.153	in^2 / *strand*	A'_s	0	in^2
f_{Pu}	270	*ksi*	f'_s	60	*ksi*
$\bar{y}_P$ at critical sect.	5.75	*inch*	Tension Steel in Beam (if added then need mod.s)		
V_P at critical sect.	0	*kips*	A_s	0	in^2
f_{po}	189	*ksi*	f_y	60	*ksi*
Type of Strand	low lax		E_s	29000	*ksi*
E_P	28500	*ksi*	Transverse Steel in Beam		

$\bar{y}_P$ at beam end	5.75	*inch*	Minimum Shear Steel?	YES	*yes or no*
$\bar{y}_P$ at mid-span	5.75	*inch*	α	90	*degrees*
			A_v	0.8	in^2
			$f_{y\ v}$	60.2	*ksi*
			s	3	*inch*

Miscellaneous Properties

Load Properties

M_u	33378.937	*kip * inch*
N_u	0	*kips*
V_u	646	*kips*

Other Properties

φ	0.9	*unitless*
Width of Bearing Pad	9	*inches*
Shear Span	138	*inches*
Total Span Length	276	*inches*

Calculated Constants for MCFT from AASHTO LRFD 2012

Constant	Value	Units	Description
A_{ps}	4.896	in^2	total area of prestressing steel
$h_{composite}$	54	*inch*	height of deck and girder
d_p	48.25	*inch*	dist. from extreme ten. to extreme comp
d_e	40.25	*inch* **	** not the same d_e reported in shear section
c	3.28	*inch*	distance from extreme comp fiber to neutral axis
k	0.28	*unitless*	if changed ps type CLICK INSIDE CELL!!!
β_1	0.65	*unitless*	
a	2.13	*inch*	
f_{ps}	264.9	*ksi*	

M_n	61189	*kip * inch*	
M_U limit	30473	*kip * inch*	used in calculating ε
θ	39.73	*degrees*	
d_v	47.19	*inch*	d_v is calc. here as per AAHSTO specifications
critical section	51.7	*inch*	
ε_s	0.00306638	*in / in*	
β	1.5	*unitless*	
V_C	45	*kips*	
V_S	911	*kips*	
Limited 0.25?	YES	yes/no	upper bound on shear strength met? Adj cell cont. value/
Stress Factor	0.333	*unitless*	This is the value for comparison to AASHTO limit of 0.25
V_n	718	*kips*	
V_n unlimited	956	*kips*	
φ	0.9	*unitless*	
φV_n	646	*kips*	
critical section	51.7	*inch*	critical section for iteration
difference in V	0.000E+00	*kips*	difference between the calculated and assumed shear
$V_U = V_n * \varphi$	646	*kips*	
Roots	29.6	*Unitless*	this is the roots value of Vs when units are in psi

REFERENCES

AASHTO. *LRFD Bridge Design Specifications*. Washington D.C.: American Association of State and Highway Transportation Officials, 2012.

AASHTO. *LRFD Bridge Construction Specifications*. Washington D.C.: American Association of State and Highway Transportation Officials, 2010.

ACI 318. *Building Code Requirements for Structural Concrete*. Farmington Hills: American Concrete Institute, 2011.

ACI-ASCE Joint Committee 445. *Recent Approaches to Shear Design of Structural Concrete*. Farmington Hills: American Concrete Institute, 2000.

Eurocode. 2 Design of concrete structures- Part 1: General rules and rules for buildings Ref. No. prEN 1992-1-1 (November 2002)

JSCE Guidelines for Concrete No. 3. Standard Specifications for Concrete Structures-2002 "Structural Performance Verification" Japan Society of Civil Engineers, 2005

Muttoni, A., Burdet, O. L., & Hars, E. (2006). "Effect of Duct Type on Shear Strength of Thin Webs." *ACI Structural Journal*, 103-S75, pp.729-735

Muttoni, A., & Ruiz, M.F. (2008). "Shear Strength of Thin-Webbed Post-Tensioned Beams." *ACI StructuralJournal*, 105-S30, pp. 308-317

Collins, M. P., Mitchell, D., Adebar, P., Vecchio, F.J. (1996) "A General Shear Design Method." *ACI Structural Journal*, 93-S5, pp. 36-45

Vecchio, F.J. and M.P. Collins. (1986). "The Modified Compression Field Theory for Reinforced Concrete Elements Subjected to Shear," *Journal of the American Concrete Institute*. American Concrete Institute, Farmington Hills, MI, Vol. 83, No. 2, pp. 219-231

Castrodale, Reid W. and White, Christopher, D., *NCHRP Report 517, Extending Span Ranges of Precast Prestressed Concrete Girders*, National Cooperative Highway Research Program Washington D.C.: Transportation Research Board, 2004.

Cox, William, R., American Segmental Bridge Institute 2012 Grouting Certification Training Manual, Buda, TX

Federal Highway Administration, *Post-Tensioning Tendon Installation and Grouting Manual*, Washington, D.C., 2004

Florida Department of Transportation, *Grouting of Bridge Post-Tensioning Tendons*, Training Manual, July 2002

2010 PCI Bridge Design Manual, Chapter 11 "*Extending Spans*" website: http://pci.org/view_file.cfm?file=MNL-133-97_ch11.pdf

Kansas Department of Transportation Design Manual, Vol. 3, Version 9/2009, US (LRFD) Section 3.5.2 Prestressed Concrete, pp. 3-5-2-4"Debonding"

Wald, David Michael. *Experimental Investigation of Crushing Capacity of I-Girder Webs Containing Post-Tensioning Ducts.* Austin: University of Texas At Austin, 2012

Massey, Josh. *Structural Implication of Post-Tensioned Ducts in Prestressed Concrete Girders.* Austin: University of Texas at Austin, 2012

Schmidt, Katherine Anne. *Development of a Testing Frame for Studying the Effects of Ducts on the Shear Capacity of Concrete Girders*. Austin: University of Texas at Austin, 2011

McKinstry Christopher Archer. *Frequency Response of Damaged External Post-Tensioned Tendons*. Austin: University of Texas at Austin, 2010

Avendaño, Alejandro Raul. *Shear Strength and Behavior of Prestressed Concrete Beams.* Austin: University of Texas at Austin, 2008

Moore, A., Wald, D., Schimdt, A., Nguyen, T., Felan, J., Bayrak, O., Jirsa, J., Ghannoum, W., Khaleghi, B., Seguirant, S., White, C., Spliced Tx-Girder Birdges Project Advisory Panel Meeting, Austin: University of Texas at Austin, 2011

Dr. Brown, Michael (2012, Spring) Adjunct Civil Engineer Professor at the University of Texas at Austin. CE 383P Lecture Notes: "Shear in Prestressed Concrete (AASHTO)

Castrodale, Reid W, *ASEC/NCDOT Spliced Girder Workshop*, Carolina Stalite Company Salisbury, NC, 2007

Schweitzer, Steve, HPC Bridge Views, Issue 67, "*HPC for Route 22 Bridge over the Kentucky River*", May/June 2011.

VITA

James Oscar Felan was born to Jim and Frances Felan on August 21, 1982 in San Jose, California. His family relocated to Austin, Texas in 1996, which then he attended and Graduated from Del Valle High School in 2000. Afterwards he studied at and received his Bachelors of Science in Architectural Engineering from the University of Texas at Austin.

After graduating James began his career for Texas Department of Transportation in the Design Division and then in the Bridge Division. Once obtaining his Professional License in Civil Engineering, he enrolled in the University of Texas at Austin and worked towards his Master's degree in Structural Engineering. He obtained his Masters of Science in Engineering in May of 2013 and returned to work for the Texas Department of Transportation in the Austin district.

Permanent address: 1164 Waller St.
Austin, TX 78702
jfelan1@gmail.com

This thesis was typed by the author.